

Clemson University

TigerPrints

All Dissertations

Dissertations

5-2023

Elucidating the Mechanical and Transport Properties of Lignin-Based Hydrogel Composites

Nicholas Gregorich
ngrego2@g.clemson.edu

Follow this and additional works at: https://tigerprints.clemson.edu/all_dissertations



Part of the [Biochemical and Biomolecular Engineering Commons](#), [Polymer and Organic Materials Commons](#), [Polymer Science Commons](#), and the [Transport Phenomena Commons](#)

Recommended Citation

Gregorich, Nicholas, "Elucidating the Mechanical and Transport Properties of Lignin-Based Hydrogel Composites" (2023). *All Dissertations*. 3309.

https://tigerprints.clemson.edu/all_dissertations/3309

This Dissertation is brought to you for free and open access by the Dissertations at TigerPrints. It has been accepted for inclusion in All Dissertations by an authorized administrator of TigerPrints. For more information, please contact kokeefe@clemson.edu.

ELUCIDATING THE MECHANICAL AND TRANSPORT PROPERTIES OF
LIGNIN-BASED HYDROGEL COMPOSITES

A Dissertation
Presented to
the Graduate School of
Clemson University

In Partial Fulfillment
of the Requirements for the Degree
Doctor of Philosophy
Chemical Engineering

by
Nicholas Ethan Gregorich
May 2023

Accepted by:
Eric M. Davis, Committee Chair
Mark C. Thies
Scott M. Husson
Igor Luzinov

ABSTRACT

The use of lignin in the fabrication of soft composites has become an emerging area of research in polymer science and polymer chemistry. These lignin-based materials present numerous benefits, notably, a reduction in the use of petroleum-based precursor, improved structural benefits to otherwise soft host polymers, as well as the inherent antimicrobial and antioxidant properties of lignin, making it suitable for biomaterials. Herein, we present two chemical reaction pathways of incorporating lignin that was fractionated and cleaned using the Aqueous Lignin Purification with Hot Agents (ALPHA) process into poly(vinyl alcohol) (PVA) hydrogel composites for aqueous-based separations. By leveraging the ALPHA process, we can obtain lignins of prescribed molecular weights (MWs) with narrow dispersity (\bar{D}) and low ash content – i.e., low concentrations of sodium and potassium.

In one reaction pathway, lignin was first functionalized with vinyl-containing acrylate groups that enabled free radical chemical crosslinking of lignin chains. Notably, both the lignin MW and chemical functionality had an impact on the permeability of methylene blue (MB), where the breakthrough time of the MB across the membrane was significantly longer for lignin with higher hydroxyl content. Further, the permeability of MB was seen to decrease by over two orders of magnitude with the introduction of just 20 wt % lignin. In addition, the importance of leveraging lignin of narrow \bar{D} in the development of structure–processing–property relationships for these materials was underscored by the consistent, repeatable permeation experiments obtained for these membranes versus their counterparts made with unfractionated lignins.

In the second reaction pathway, both the lignin and PVA chains were chemically crosslinked via a condensation reaction using glutaraldehyde (GA). In general, increases in the GA content and lignin MW resulted in improved mechanical properties, including increases in ultimate tensile strength, storage modulus, and Young's modulus, which was attributed to a tightening of the hydrated network structure and supported by decreases in equilibrium water uptake and molecular weight between crosslinks. Enhanced mechanical properties were also observed in hydrogel composites containing ALPHA-fractionated lignin as compared to unfractionated, stock lignin, underscoring the impact of the ALPHA process on the resulting properties.

DEDICATION

I dedicate this Dissertation to everyone who has supported me during this journey towards becoming a professor of chemical engineering. Eight years ago, in the fall of 2014, I was working the deli counter at Nino Salvaggio slicing cold cuts in the Detroit metropolitan area with no bachelor's degree and much uncertainty towards my future and what life had in store for me. I had just been placed on mandatory leave from The University of Michigan for the fourth time and struggled horribly with mental health. A few days before the start of the winter 2015 semester, I had a phone conversation with Dr. Susan Montgomery that ultimately influenced me to give chemical engineering one last chance and jumpstarted a turnaround. I went on to achieve A letter grades in both Thermodynamics and Fluid Mechanics and somehow landed an internship at Grid Logic, founded by Dr. Matt Holcomb, despite my overall GPA being a 2.0. My experiences at Grid Logic led me to pursue a research-based, academic career path, bringing me to where I am now.

I am so incredibly grateful for my family, friends, and mentors who have been there with me every step of the way. I want to thank my late grandma, Shirley Gregorich, for being my biggest supporter and molding me into the person that I am today. Although you are longer with us, I can only imagine how proud you would be. I also want to thank my grandpa, Al Gregorich, along with my parents, Michael and Marianne Gregorich, and my late grandma Dorothy Prizgint, for supporting and encouraging me in so many ways. In no order, I want to thank a few close friends that are family to me: Will Timmer, Casey D'Angelo, Jay Morse, Abigail Teitelbaum, Adam Schumaier, and Adam Smith. Thank you

to my cat Molson for being such a great companion. Lastly, I want to thank Josh Osuofa and Caleb Arp for making my time as a Clemson student so special. I am appreciative of all the great times we had together as roommates and lifelong friends. I will forever cherish my time as a doctoral student and am so proud to be a part of the Clemson Tigers family.

ACKNOWLEDGMENTS

I want to give a huge thank you to my PhD advisor, Prof. Eric M. Davis, for his phenomenal support, guidance, and mentorship throughout my time as a doctoral student in his research group at Clemson University the last five years. As a result of his outstanding mentorship, I have profoundly grown into a stronger researcher, critical thinker, public speaker, and ultimately a confident, well-rounded scientist. The decision I made in coming down to Clemson University and joining the Davis Research Group was one of the best decisions I ever made. Although my time in the group has come to an end, I am looking forward to remaining in the academic landscape and establishing potential research collaboration within the hydrogel research field in the future.

I would also like to thank and acknowledge the other members of the lab group, those being Xueting Wang, Keturah Bethel, and Missouri Wolff. I would like to give a special thank you to undergraduate researcher Jaden Stutts. Mentoring Jaden on my research project and watching her grow as a researcher the past few years has been one of the most memorable experiences during my time at Clemson. A big thank you to the graduate students in Drs. Thies and Ogale groups that I collaborate with, those being Graham Tindall and Sagar Kanhere. Thank you to my committee members, Dr. Scott Husson, Dr. Marc Thies, and Dr. Igor Luzinov. I also want to thank Dr. Tyler Martin from NIST NCNR for all his help performing, analyzing, and discussing SANS data.

I want to thank and acknowledge Dr. Tia Dumas for her guidance, support, and mentorship during my time as a 3MT® competitor and molding me into a stronger leader while serving as the Director of Research Initiatives for Graduate Student Government.

Lastly, thank you to the Department of Education GAANN Fellowship (P200A180076 and P200A210105), and the National Science Foundation under Grant Nos. CBET-1915787 and CBET-1403873 for the funding of my project.

TABLE OF CONTENTS

	Page
TITLE PAGE	i
ABSTRACT	ii
DEDICATION	iv
ACKNOWLEDGMENTS	vi
LIST OF TABLES	xii
LIST OF FIGURES	xiv
CHAPTER	
I. INTRODUCTION	1
1.1 Introduction.....	1
1.1.1 Hydrogels.....	1
1.1.2 Fabrication Routes for Hydrogels.....	2
1.1.3 Characterizing Hydrogel Network Structures.....	5
1.1.4 Lignin – The Movement Towards Biopolymers.....	9
1.1.5 Lignin-Based Materials.....	15
1.1.6 Lignin-Based Hydrogels	17
1.1.7 Incorporating Fractionated, ALPHA Lignin into Hydrogels.....	21
II. METHODS AND BACKGROUND	26
2.1 Lignin Modification Techniques.....	26
2.1.1 Lignin Acrylation Process.....	26
2.2 Lignin-Hydrogel Characterization Techniques.....	27
2.2.1 Dynamic Mechanical Analysis of PVA- Lignin Hydrogel Composites	27
2.2.2 Young’s Modulus of PVA-Lignin Hydrogel Composites via Mechanical Indentation.....	30
2.2.3 Calculating Permeability through PVA-Lignin Hydrogel Composites.....	34

III.	NOVEL COMPOSITE HYDROGELS CONTAINING FRACTIONATED, PURIFIED LIGNINS FOR AQUEOUS-BASED SEPARATIONS	41
	3.1 Introduction.....	41
	3.2 Experimental Section	46
	3.2.1 Materials	46
	3.2.2 Characterization of Molecular Weight of Lignin.....	47
	3.2.3 Lignin Acrylation Procedure.....	47
	3.2.4 Characterization of lignin using infrared spectroscopy	48
	3.2.5 Lignin Hydrogel Synthesis	48
	3.2.6 Mechanical Indentation Experiments	49
	3.2.7 Nuclear Magnetic Resonance Spectroscopy	50
	3.2.8 Methylene Blue Permeation.....	51
	3.2.9 Equilibrium Liquid Water Uptake	53
	3.2.10 Characterization of Molecular Weight Between Crosslinks.....	53
	3.3 Results.....	55
	3.3.1. Lignin Characterization and Composite Hydrogel Fabrication ...	55
	3.3.2 Separation Performance of the Composite Hydrogels.....	60
	3.3.3 Young’s Modulus and Equilibrium Water Uptake	68
	3.3.4 Network Structure of the Composite Hydrogels.....	71
	3.4 Conclusions.....	74
IV.	ENHANCED MECHANICAL PROPERTIES OF COMPOSITE HYDROGELS CONTAINING FRACTIONATED AND PURIFIED LIGNIN	76
	4.1 Introduction.....	76
	4.2 Experimental Section	81
	4.2.1 Materials	81
	4.2.2 Characterization of Molecular Weight of Lignin.....	83
	4.2.3 Nuclear Magnetic Resonance Spectroscopy	84
	4.2.4 Lignin Hydrogel Synthesis	85
	4.2.5 Characterization of Ultimate Tensile Strength (UTS)	86
	4.2.6 Dynamic Mechanical Analysis (DMA) Experiments	86
	4.2.7 Characterization of Molecular Weight Between Crosslinks.....	87
	4.2.8 Mechanical Indentation Experiments	88
	4.2.9 Equilibrium Liquid Water Uptake	89
	4.2.10 Scanning electron microscopy (SEM) imaging	89

4.3 Results and Discussion	91
4.3.1 Soft Composite Nomenclature and Fabrication.....	91
4.3.2 Ultimate tensile strength (UTS), dynamic mechanical analysis (DMA), and Young's modulus.....	94
4.3.3 Equilibrium Water Uptake.....	106
4.3.4 Scanning Electron Microscopy (SEM) Imaging.....	108
4.4 Conclusions.....	114
V. CONCLUSIONS AND FUTURE WORK.....	116
5.1 Conclusions.....	116
5.2 Future Work.....	118
5.2.1 General Future Work	118
5.2.2 Elucidating the Impact of Lignin Dispersity on PVA–Lignin Hydrogel Composites Containing Lignin of Constant Molecular Weight.....	117
5.2.3 Elucidating PVA-Lignin Hydrogel Composites for the Removal of Hexavalent Chromium.....	120
5.2.4 Characterizing Lignin Hydrogel Composites Crosslinked with Chitosan or Cellulose.....	120
5.2.5 Characterizing Methylene Blue Solubility into Lignin Hydrogel Composites.....	120
5.2.6 Characterizing the Mesh Size Lignin Hydrogel Composites Saturated with Methylene Blue	121
APPENDICES	122
A: Appendix A.....	123
A.1 ¹ H NMR Spectroscopy.....	123
A.2 Hydroxyl (–OH) Content of Crude Bulk and Ultraclean Lignins.....	123
A.3 Infrared Characterization of UCLs and CBLs	124
A.4 Thermal Stability of Composite Hydrogels	125
B: Appendix B.....	128

B.1 Solubility Investigation of Crosslinked and Uncrosslinked Lignin.....	128
B.2 Hydroxyl (–OH) Content of BioChoice™ and ALPHA-Fractionated Lignin	130
B.3 Dynamic Mechanical Analysis (DMA) of Lignin Soft Composites	130
B.4 Molecular Weight Between Crosslinks versus Other Properties	135
C: Appendix C	140
C.1 All Properties of Lignin Hydrogels Containing SLRP and BCL Lignin.....	140
D: Appendix D.....	144
D.1 Inductive Coupled Plasma Analysis and Ash Content for SLRP and BCL Lignin	144
REFERENCES	145

LIST OF TABLES

Table		Page
3.1	Nomenclature for PVA–lignin composite hydrogels.....	55
4.1	Nomenclature for neat PVA and PVA–lignin composite hydrogels	91
A.1	Aliphatic and aromatic hydroxyl (–OH) content for both unfunctionalized (UF) and functionalized (F) crude bulk lignins (CBLs) and ultraclean lignins (UCLs)	124
A.2	The following table contains images of the two series PVA–lignin hydrogel composite membranes under hydration at temperatures ranging from room temperature (~25 °C) to 80 °C. Note, the first column shows the membranes that have been under hydration for >120 days.....	126
B.1	Quantitative hydroxyl (–OH) content for BCL, Low MW lignin, and High MW lignin used in the synthesis of the PVA–lignin hydrogels. All values are reported in mmol OH/g lignin Nomenclature for PVA–lignin composite hydrogels	130
C.1	Number average molecular weight and dispersity for CBL lignin acquired from the SLRP process and fractionated, UCL lignin	140
C.2	MB permeability, hydrated Young’s modulus, and equilibrium water uptake for hydrogels containing UCL and CBL lignin.....	140
C.3	Molecular weight between crosslinks values for hydrogels containing UCL and CBL lignin.....	141
C.4	Weight average molecular weight and dispersity for BCL, Low, and High MW lignin.....	141
C.5	Ultimate tensile strength, storage modulus, molecular weight between crosslinks, and hydrated Young’s modulus values for samples containing BCL, Low, and High lignin.....	142

C.6	Equilibrium water uptake values for samples containing BCL, Low, and High MW lignin.....	143
D.1	ICP values for SLRP and BCL lignin.....	144
D.2	Ash content values for BCL, Low and High MW lignin.....	144

LIST OF FIGURES

Figure	Page
1.1	Reaction schematic for chemically crosslinked N-isopropylacrylamide (NIPAM) and N-N'-methylenebisacrylamide (MBA) chains via free radical polymerization and crosslinking.....3
1.2	Idealized network structure of chemically crosslinked polymer chains in a hydrogel.....4
1.3	Reaction schematic for chemically crosslinked poly(vinyl alcohol) (PVA) chains via condensation reaction.....5
1.4	Depiction of the hydrogel network structure at nanometer scale. Mesh size is the end-to-end distance between crosslinks (blue arrows, ξ), and molecular weight between crosslinks is the molecular weight of polymer between crosslinks (red oval, M_C)6
1.5	Total generation of municipal solid waste (in metric tons) in the United States from 1960 to 20189
1.6	A feedstock renewability/polymer degradability matrix for various common plastics and bioplastics 11
1.7	Proposed chemical structure of lignin containing a high abundance of phenolic rings and hydroxyl groups 12
1.8	Depiction of the three main components (lignin, hemicellulose, and cellulose) found in plant cell walls 14
1.9	(a) Aqueous Lignin Purification with Hot Agents (ALPHA) process (US Patent No. 10,053,482; August 2018). (b) Molecular weight distribution before and after lignin is recovered from the ALPHA process22

1.10	Homogenizing the network structure of lignin-based hydrogel composites via incorporation of controlled, narrow dispersity fractions of lignin	23
2.1	Reaction schematic and proposed chemical structure for functionalized lignin with vinyl-containing acrylate groups that replaced once present hydroxyl groups along lignin chains	27
2.2	Dynamic mechanical analysis spectra from 0.1 to 100 rad s ⁻¹ for Low molecular weight lignin-based PVA hydrogel composites. Note, the error bars in the figure represent the standard deviation of the average, which was calculated from repeat measurements on at least three separate membranes	29
2.3	Experimental setup for a Young's modulus measurement via mechanical indentation	32
2.4	Indentation load versus contact area times representative strain data. Slope of data is indicative of Young's modulus for hydrogel sample	33
2.5	Illustrative schematic of permeation cell used for methylene blue (MB) permeability experiments	34
2.6	Illustrative schematic of permeation cell used for methylene blue (MB) permeability experiments	36
3.1	Illustrative schematic of permeation cell used for methylene blue (MB) permeation experiments.....	52
3.2	(a) Reaction schematic and proposed network structure for thermally-crosslinked, as well as thermally- and chemically-crosslinked PVA–lignin composite hydrogels using both unfunctionalized and functionalized lignin. (b) Picture of free-standing neat PVA and PVA–lignin hydrogels containing 0 wt % to 50 wt % unfunctionalized and functionalized UCLs and CBLs	57

3.3	³¹ P NMR spectra of unfunctionalized (dashed blue line) and functionalized (solid red line) (a) ultraclean lignins (UCLs) and (b) crude bulk lignins (CBLs)	59
3.4	Concentration of methylene blue (MB) in the receiving cell as a function of time for neat PVA and PVA membranes containing various amounts of unfunctionalized and functionalized (a) ultraclean lignins (UCLs) and (b) crude bulk lignins (CBLs). Note, the data have been normalized by the square of the membrane thickness. (c) Concentration of MB in the receiving cell as a function of time for PVA membranes containing 10 wt % UCLs (closed green symbols) and CBLs (open black symbols), both unfunctionalized. Each data set is a unique MB permeation experiment on an individual hydrogel sample. Note, some of the data displayed in Figs. 3.4a & 3.4b was reshown in 3.4c, as part of a collection of multiple experiments. (d) Summary of the calculated MB permeabilities for neat PVA and PVA–lignin composite hydrogels. The dashed black line indicates the average MB permeability for neat (or pristine) PVA (i.e., PVA containing no lignin). Note, the error bars in the figure represent the standard deviation of (at least three) repeat experiments	62
3.5	(a) Hydrated Young’s modulus (that is, Young’s modulus of the hydrogel equilibrated in liquid water) and (b) equilibrium liquid water uptake of neat PVA and PVA–lignin composite membranes containing various concentrations of unfunctionalized (light blue bars) and functionalized (solid red bars) UCLs and CBLs. The dashed black lines in (a) and (b) represent the average hydrated Young’s modulus and equilibrium water uptake of neat (or pristine) PVA (i.e., PVA containing no lignin), respectively. Prior to both measurements, all hydrogels were hydrated in liquid water for at least 48 hours. Note, the error bars in the figure represent the standard deviation of (at least three) repeat experiments	69

3.6	The molecular weight between crosslinks, M_c , of pristine PVA and PVA–lignin composite membranes containing various concentrations of unfunctionalized (light blue bars) and functionalized (solid red bars) UCLs and CBLs. The dashed black line represents the average M_c of neat (or pristine) PVA (i.e., PVA containing no lignin). Note, the error bars in the figure represent the standard deviation of (at least three) repeat experiments	72
4.1	(a) Reaction schematic and proposed network structure for chemically crosslinked neat PVA and PVA–lignin composite hydrogels via condensation reaction. (b) Picture of free-standing, robust membranes of varying lignin concentration, lignin MW, and crosslinker content	93
4.2	Ultimate tensile strength values for neat PVA (solid black bars) and PVA–lignin composites containing BCL (solid green bars), Low MW (solid red bars), and High MW (solid blue bars). Note, the error bars in the figure represent the standard deviation of the average, which was calculated from repeat measurements on at least three separate membranes	95
4.3	Storage modulus values for neat PVA (solid black bars) and PVA–lignin composites containing BCL (solid green bars), Low MW (solid red bars), and High MW (solid blue bars). All experiments were measured in tensile mode. Note, the error bars in the figure represent the standard deviation of the average, which was calculated from repeat measurements on at least three separate membranes. Also note, stars denote samples whose storage moduli could not be measured as these samples were too soft to be mounted in the apparatus	98

4.4	The molecular weight between crosslinks values for neat PVA (solid black bars) and PVA–lignin composites containing BCL (solid green bars), Low MW (solid red bars), and High MW (solid blue bars). Note, the error bars in the figure represent the standard deviation of (at least three) repeat experiments. Also note, stars denote samples whose storage moduli could not be measured, and consequently M_C , as these samples were too soft to be mounted in the apparatus	101
4.5	Hydrated Young’s modulus results for neat PVA (solid black bars) and PVA–lignin composites containing BCL (solid green bars), Low MW (solid red bars), and High MW (solid blue bars). Note, the error bars in the figure represent the standard deviation of (at least three) repeat experiments.....	104
4.6	Equilibrium water uptake results for results for neat PVA (solid black bars) and PVA–lignin composites containing BCL (solid green bars), Low MW (solid red bars), and High MW (solid blue bars). Note, the error bars in the figure represent the standard deviation of (at least three) repeat experiments	107
4.7	SEM images for (a,d) neat PVA and (b,c,e,f) PVA–lignin composites containing unfractionated BCL lignin. Specific labels, following the nomenclature listed in Table 4.1, are provided below each SEM image. Also note, the scale bar in all the images is 5 μm	110
4.8	SEM images for (a,d) neat PVA and (b,c,e,f) PVA–lignin composites containing unfractionated Low lignin. Specific labels, following the nomenclature listed in Table 4.1, are provided below each SEM image. Also note, the scale bar in all the images is 5 μm	111

4.9	SEM images for (a,d) neat PVA and (b,c,e,f) PVA– lignin composites containing unfractionated High lignin. Specific labels, following the nomenclature listed in Table 4.1, are provided below each SEM image. Also note, the scale bar in all the images is 5 μm	113
A.1	^1H NMR spectra of unfunctionalized (dotted blue line) and functionalized (solid red line) (a) ultraclean lignin (UCL) and (b) crude bulk lignin (CBL)	123
A.2	FTIR spectra of unfunctionalized (dashed blue line) and functionalized (solid red line) for (a) ultraclean lignin and (b) crude bulk lignin	125
B.1	Scintillation vials containing DMSO and (a) unmodified High MW lignin, (b) heat-treated High MW lignin + glutaraldehyde (fabricated with no acid), and (c) heat-treated High MW lignin + glutaraldehyde (fabricated in a solution with $\text{pH} \approx 3$)	129
B.2	Dynamic mechanical analysis spectra from 0.1 to 100 rad s^{-1} for BCL molecular weight lignin-based PVA hydrogel composites. Note, the error bars in the figure represent the standard deviation of the average, which was calculated from repeat measurements on at least three separate membranes	131
B.3	Dynamic mechanical analysis spectra from 0.1 to 100 rad s^{-1} for High molecular weight lignin-based PVA hydrogel composites. Note, the error bars in the figure represent the standard deviation of the average, which was calculated from repeat measurements on at least three separate membranes	132
B.4	Dynamic mechanical analysis spectra from 0.1 to 100 rad s^{-1} for Low molecular weight lignin-based PVA hydrogel composites. Note, the error bars in the figure represent the standard deviation of the average, which was calculated from repeat measurements on at least three separate membranes	134

B.5	<p>Dynamic mechanical analysis spectra from 0.1 to 100 rad s⁻¹ for neat PVA hydrogel composites. Note, the error bars in the figure represent the standard deviation of the average, which was calculated from repeat measurements on at least three separate membranes</p>	135
B.6	<p>Ultimate tensile strength values for neat PVA (solid black bars) and PVA–lignin composites containing BCL (solid green bars), Low MW (solid red bars), and High MW (solid blue bars). The molecular weight between crosslinks values for neat PVA (open black circles) and PVA–lignin composites containing BCL (open green squares), Low MW (open red diamonds), and High MW (open blue triangles). Note, the error bars in the figure represent the standard deviation of the average, which was calculated from repeat measurements on at least three separate membranes. Also note, stars denote samples whose storage moduli could not be measured as these samples were too soft to be mounted in the apparatus</p>	136
B.7	<p>Storage modulus values for neat PVA (solid black bars) and PVA–lignin composites containing BCL (solid green bars), Low MW (solid red bars), and High MW (solid blue bars). The molecular weight between crosslinks values for neat PVA (open black circles) and PVA–lignin composites containing BCL (open green squares), Low MW (open red diamonds), and High MW (open blue triangles). Note, the error bars in the figure represent the standard deviation of the average, which was calculated from repeat measurements on at least three separate membranes. Also note, stars denote samples whose storage moduli could not be measured as these samples were too soft to be mounted in the apparatus</p>	137

B.8	<p>Hydrated Young's modulus values for neat PVA (solid black bars) and PVA–lignin composites containing BCL (solid green bars), Low MW (solid red bars), and High MW (solid blue bars). The molecular weight between crosslinks values for neat PVA (open black circles) and PVA–lignin composites containing BCL (open green squares), Low MW (open red diamonds), and High MW (open blue triangles). Note, the error bars in the figure represent the standard deviation of the average, which was calculated from repeat measurements on at least three separate membranes. Also note, stars denote samples whose storage moduli could not be measured as these samples were too soft to be mounted in the apparatus</p>	138
B.9	<p>Equilibrium water uptake values for neat PVA (solid black bars) and PVA–lignin composites containing BCL (solid green bars), Low MW (solid red bars), and High MW (solid blue bars). The molecular weight between crosslinks values for neat PVA (open black circles) and PVA–lignin composites containing BCL (open green squares), Low MW (open red diamonds), and High MW (open blue triangles). Note, the error bars in the figure represent the standard deviation of the average, which was calculated from repeat measurements on at least three separate membranes. Also note, stars denote samples whose storage moduli could not be measured as these samples were too soft to be mounted in the apparatus.....</p>	139

CHAPTER ONE

INTRODUCTION

1.1 Introduction

1.1.1 Hydrogels

Polymers are long-chain molecules assembled from many smaller, repeating molecules called monomers. Polymers can be natural or synthetic, along with hydrophobic or hydrophilic. Hydrogels are crosslinked hydrophilic polymers that form tunable three-dimensional network structures. The presence of hydrophilic functional groups such as hydroxyls ($-\text{OH}$), carbonyls ($\text{C}=\text{O}$), carboxyls ($-\text{COOH}$), and aminos ($-\text{NH}_2$) in the monomer unit provides these materials with the unique capability of absorbing a high amount of water, which can range anywhere from ≈ 150 wt %¹ to as high as ≈ 1200 wt % (relative to the dry mass) equilibrium water uptake,² or greater). Common polymers utilized in hydrogels include poly(vinyl alcohol) (PVA),³ poly(2-hydroxyethyl methacrylate) (pHEMA),⁴ poly(N-isopropylacrylamide) (PNIPAM),⁵ polyvinylpyrrolidone (PVP),⁶ polyethylene glycol (PEG),^{7,8} polyethylene glycol diacrylate (PEGDA).^{9,10}

Due to their high hydrophilicity, rubbery-like behavior, and tunable mechanical and transport properties, hydrogels have shown promise in a broad range of fields. Some of these fields include separations,^{11–18} drug delivery,^{19–24} tissue engineering,^{25–29} wound healing,^{30–32} and medical device coatings.³³ Some of these separations include removal of oil from water/oil emulsions,¹⁷ organic dyes (e.g., methylene blue) from water,³⁴ and toxic, heavy metal ions (e.g., Cu^{2+} , Pb^{2+})¹⁴ that find their way into our water sources.

Additionally, hydrogels have been investigated as materials for controlled adsorption and release of model drugs, such as salicylic acid²² and diclofenac sodium,³⁵ along with model proteins, such as bovine serum albumin,³⁶⁻³⁹ and polypeptides such as insulin-like growth factor-1.²⁰ Such investigations highlight how the characteristic properties for these soft polymer composites can be tuned and optimized to function in a wide range of separations, as well as a variety of controlled adsorption and release applications. Hydrogels that respond to stimuli changes in the environment (e.g., pH, heat, light) are attractive for controlled drug release as they allow for *in situ* gelation and are commonly referred to as smart hydrogels. Much research has investigated biocompatible, thermoresponsive PNIPAM hydrogels that undergo a sol-gel transition at a lower critical solution temperature (LCST) of 32 °C, an attractive characteristic for designing efficient drug delivery systems as this is close to and below the human body temperature (37 °C).²⁴ Due to their similarities in structure and composition to that of the extracellular matrix (ECM), many studies have investigated pHEMA hydrogels for tissue engineering applications, particularly urethral tissues.²⁷

1.1.2 Fabrication Routes for Hydrogels

Optimizing these soft materials for specific applications oftentimes involves fine-tuning the characteristic mechanical and transport properties, which are ultimately governed by the network structure of the hydrated hydrogel. The hydrogel network structure is defined as the three-dimensional architecture of crosslinked hydrophilic polymers at the molecular level. Many different approaches have been employed to alter the network structure of hydrogels. Some of these approaches include manipulation of the

reaction pathway,^{40,41} crosslinker/initiator concentration,^{19,42–46} molecular weight of host polymer,⁴⁷ and synthesis temperature.^{21,48,49} When considering PNIPAM hydrogels, these can be chemically crosslinked via a combination of free-radical polymerization of NIPAM monomer chains, along with crosslinking via N,N'-methylenebisacrylamide (MBA). In other words, the NIPAM monomers free-radically polymerize with themselves to form PNIPAM, while MBA chains are simultaneously crosslinking PNIPAM chains together to form a chemically crosslinked network structure. A reaction schematic detailing this reaction of NIPAM and MBA chains is shown in Figure 1.1. Note, this fabrication route is

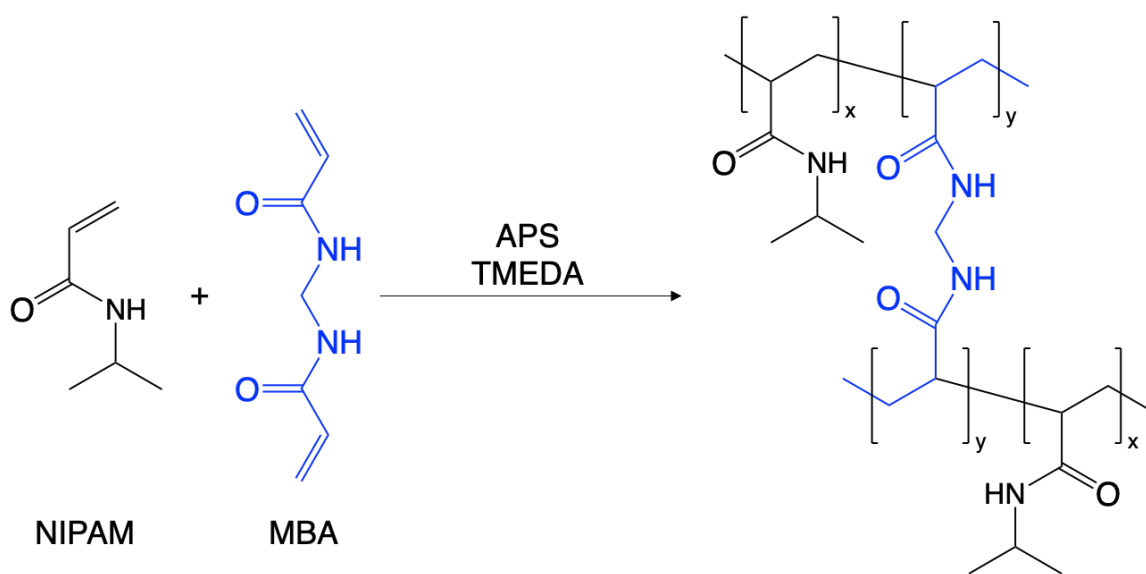


Figure 1.1. Reaction schematic for chemically crosslinked N-isopropylacrylamide (NIPAM) and N,N'-methylenebisacrylamide (MBA) chains via free radical polymerization and crosslinking.

also present in PEGDA^{50–52} and pHEMA^{53–55} hydrogel systems. Upon crosslinking, a chemically crosslinked network structure is formed. An idealized version of homogeneously crosslinked polymer chains is shown in Figure 1.2.

When considering PVA-based hydrogels that are commonly utilized in biomedical and water purification applications, these can be synthesized several ways. Some of these include thermal crosslinking,^{56,57} chemical crosslinking,^{45,47,58-66} or a combination of

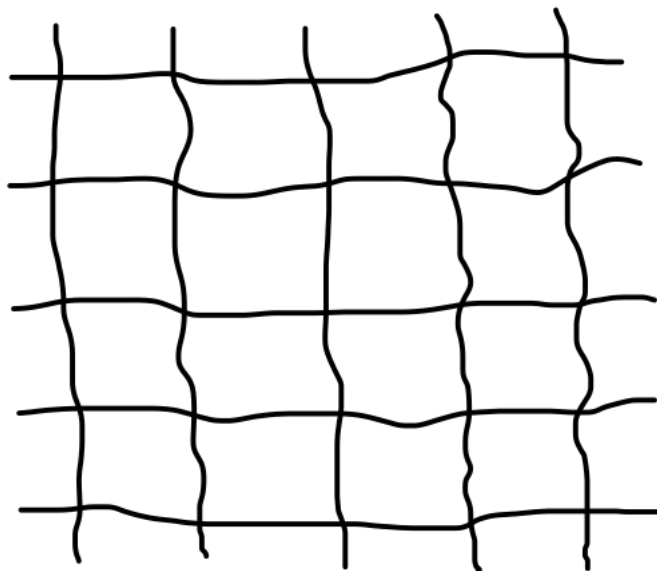


Figure 1.2. Idealized network structure of chemically crosslinked polymer chains in a hydrogel.

both.^{60,67} Another common, less chemically invasive fabrication method for PVA hydrogels is referred to as the “freeze-thaw method”, which induces physical crosslinks between PVA chains through sequential cycles between temperatures of $<273\text{K}$ and $>293\text{K}$.⁶⁸⁻⁷¹ For chemically-crosslinked PVA films, covalent crosslinks between chains are achieved through the use of crosslinking agents such as glutaraldehyde (GA)^{47,58,61,63} or various acids (e.g., citric acid).^{45,65,66} When GA is used to fabricate chemically-crosslinked PVA membranes, hydroxyl ($-\text{OH}$) groups along the PVA chains are consumed during the crosslinking process (i.e., condensation reaction). The reaction schematic for PVA hydrogels chemically crosslinked via GA is shown in Figure 1.3. Further, the consumption

of -OH groups during fabrication can be leveraged as a means of altering the hydrophilicity of the resulting crosslinked membrane.⁶⁴

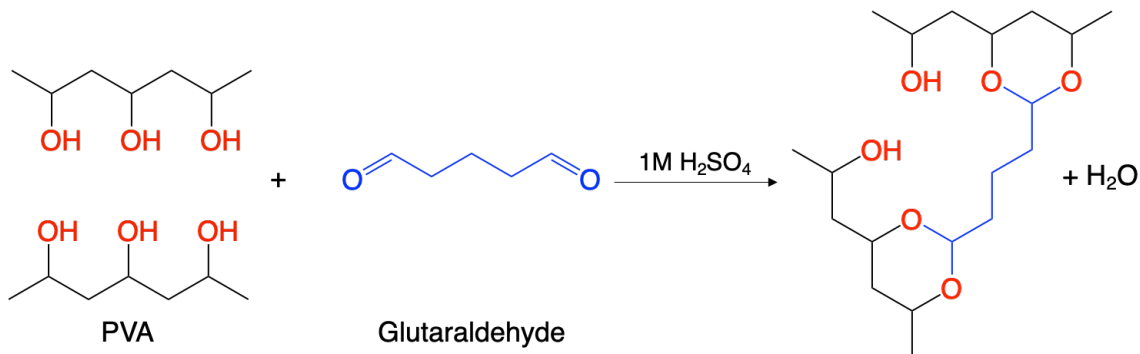


Figure 1.3. Reaction schematic for chemically crosslinked poly(vinyl alcohol) (PVA) chains via condensation reaction.

1.1.3 Characterizing Hydrogel Network Structures

There are many properties to consider when characterizing hydrogel network structures, with the parameter of merit being the mesh size. The mesh size (ξ) is the end-to-end distance between crosslinks in the network structure (note, this is analogous to how the size of a television or computer screen is measured) and is depicted in the schematic of a crosslinked hydrogel network shown in Figure 1.4. The mesh size ultimately governs several transport properties characteristic of soft polymer materials, those including the diffusion coefficient (D) and intrinsic permeability (k). The diffusion coefficient is defined as the speed of a molecule moving within a material, while the intrinsic permeability is the ability for a fluid to flow through the pores of a swollen material, or the ease at which a molecule moves through a system. The intrinsic permeability is not time dependent, and calculating its square root provides a pore (mesh) size measurement. The diffusion coefficient is a major factor in the calculation of penetrant permeability (P), the overall

mass transport of a particular penetrant through a material. Increases in D , k , and P generally correlate with increases in the mesh size for a hydrogel system. For a deeper understanding of permeability and its mathematical derivation, please refer to Chapter 2.2.3.

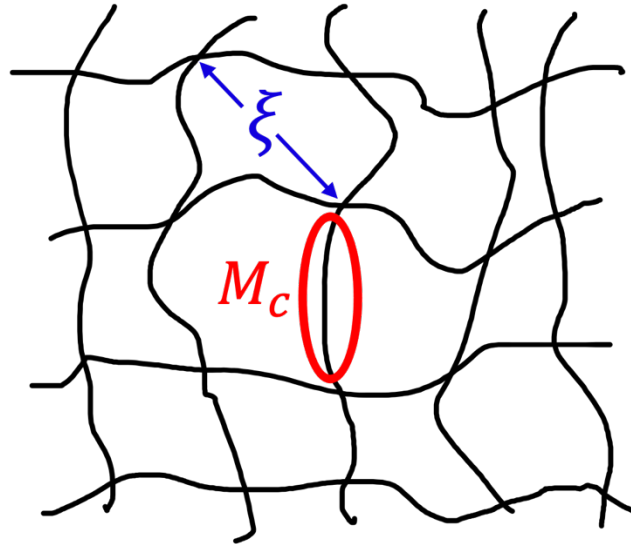


Figure 1.4. Depiction of the hydrogel network structure at nanometer scale. Mesh size is the end-to-end distance between crosslinks (blue arrows, ξ), and molecular weight between crosslinks is the molecular weight of polymer between crosslinks (red oval, M_c).

Another parameter similar to the mesh size that is used to characterize the network structure of crosslinked materials is the molecular weight between crosslinks (M_c), representing the total molecular weight of polymer between two crosslinks. An illustration depicting both the mesh size and M_c is shown in Figure 1.4.

When characterizing the network structure of a crosslinked hydrogel, it is critical to understand the average ξ or M_c in developing fundamental structure–property–processing

relationships that correlate changes in network structure with changes in mechanical and transport properties.

One experimental method employed to acquire the mesh size of crosslinked hydrogels is small-angle neutron scattering (SANS). SANS can be used to characterize structures at length scales ranging from a couple to 10s of nanometers. Inhomogeneities in scattering length density result in small-angle scattering that are fitted to models depicting structures in reciprocal space. For the simplest case – a material that exhibits a single scattering peak in the SANS curve – the most common model used to analyze the scattering data and extract a correlation length is referred to as the correlation-length model, where the measured intensity can be related to the scattering vector via the following equation:

$$I(Q) = \frac{C}{1 + (Q\Omega)^m} + \text{Bkg} \quad (1.1)$$

where $I(Q)$ is scattering intensity, Q is scattering vector, Ω is correlation length, C is Lorentz scale, m is Porod exponent, and Bkg is the incoherent background. Solving for Ω gives an indication of the mesh size in a hydrogel network structure⁷² as shown in the following modified equation:

$$\Omega = \left(\frac{1}{Q}\right) \left(\frac{C}{I(Q) - \text{Bkg}} - 1\right)^{1/m} \quad (1.2)$$

In addition to the correlation length model, some other common models employed in fitting scattering data include Broad Peak Model,⁷³ Debye-Beuche,⁷⁴ and Ornstein-Zerniche.⁷⁵

Many studies have explored correlations between fabrication parameters of hydrogels and their resulting mechanical properties in correlation with the mesh size. For example, work by Zander et al.⁷³ investigated a PEG-based hydrogel system where the mesh size was inversely proportional to storage modulus, a material's ability to store energy elastically. In another study by Papagiannopoulos et al.,⁷⁶ polyethylene oxide hydrogels were fabricated for the controlled release of bovine serum albumin and lysozyme. Mesh sizes for the hydrogels were extracted from scattering data, where release profiles of both proteins correlated with mesh size.

There are many processes for characterizing the M_C of a hydrogel network structure, with two common methods being application of the Peppas-Merrill equation to hydrogel swelling data and dynamic mechanical analysis (DMA). The Peppas-Merrill equation combines thermodynamic and rubber elasticity theories to predict an average molecular weight of polymer between two crosslinks in the network structure. The equation is dependent on the swelling behavior of the hydrogel system, taking into account the mass at swollen, relaxed, and dry states.¹ For a crosslinked polymer, M_C is directly correlated with the storage modulus in the rubbery plateau region of a DMA measurement. DMA experiments can be performed in various setups, with the two most common being shear and tensile mode. Upon acquiring a storage modulus, these measurements can be taken one step further to calculate an M_C by simply knowing the density of the polymer and the measurement temperature. A more detailed description of DMA is provided in Section 4.2.6.

1.1.4 Lignin – The Movement Towards Biopolymers

Synthetic plastics have dominated many materials-based markets since their invention in the 1950s due to their ability to be molded into numerous shapes, high mechanical strength, and light weight.⁷⁷ According to a 2018 report by the United States Environmental Protection Agency, *National Overview: Facts and Figures on Materials, Wastes and Recycling*, 35.7 million tons of plastic products were generated in the US.⁷⁸ This 35.7 million tons of plastic encompasses 292 million tons of total waste generated in 2018, as

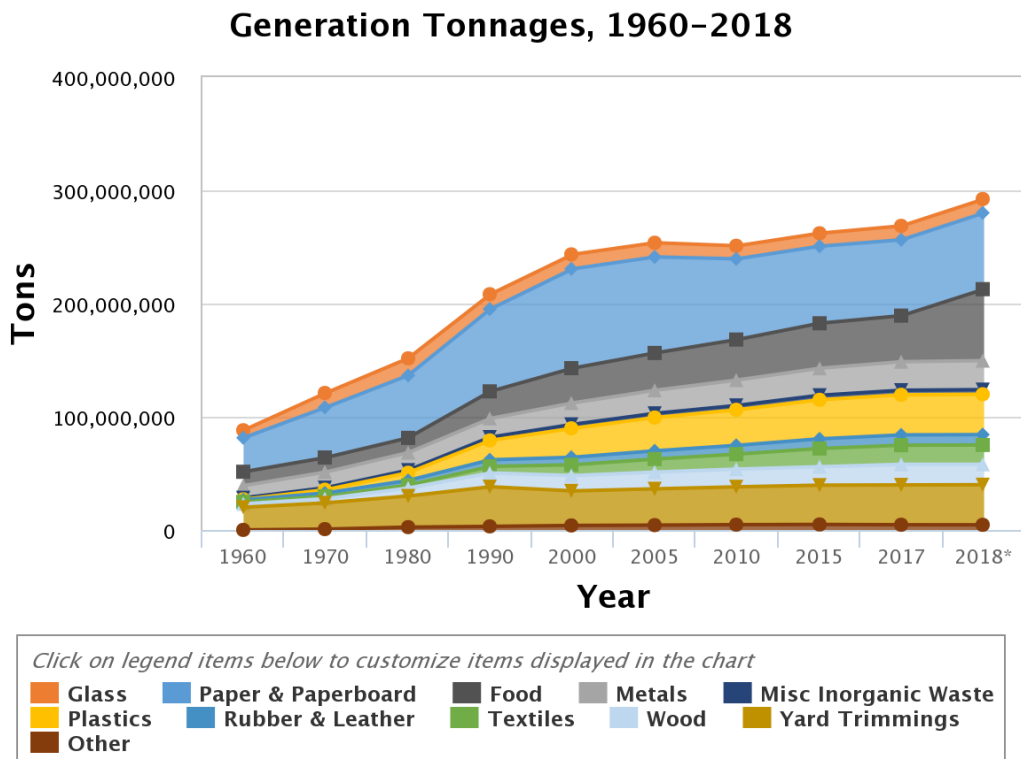


Figure 1.5. Total generation of municipal solid waste (in metric tons) in the United States from 1960 to 2018. Image taken from: US Environmental Protection Agency. *National Overview: Facts and Figures on Materials, Wastes and Recycling* [internet database] available via <https://www.epa.gov/facts-and-figures-about-materials-waste-and-recycling/national-overview-facts-and-figures-materials>. Accessed November 18, 2022.

shown in Figure 1.5. Of mention, the amount of plastic waste entering the ocean worldwide in 2010 was approximately 4.8 to 12.7 million metric tons, with that number expected to increase by an order of magnitude by 2025.⁷⁹ In addition to polluting water sources, microplastics can contaminate air and soil. Many studies have shown that aquatic fauna and terrestrial flora are contaminated by microplastics, which humans can easily consume, leading to potential digestive issues and even colon cancer.⁷⁷ As such, the movement towards biopolymers replacing plastics has vastly grown due to their accelerated biodegradability when compared to synthetic polymers – some biopolymers degrade within 2 months as compared to synthetic polymers that can take >100 years to degrade (>500 years in some cases).⁸⁰ This long-standing issue of biodegradability has pushed polymer chemists towards engineering degradation pathways for sustainable polymers that are decades long instead of millennia.⁸¹ These efforts towards renewable, plant-based polymers with shorter degradation times are visualized in Figure 1.6. In addition to faster degradability timeframes, biopolymers do not carry any toxins (i.e., carbon monoxide release during combustion) that synthetic polymers traditionally have.

Another big drawback to traditional synthetic polymers is they require the use of petroleum-based precursors (e.g., ethylene, propylene, benzene), commonly referred to as petrochemicals. According to a report by the U.S. Energy Information Administration, the United States consumed 72.9 quadrillion British thermal units (Btu) of fossil fuels in 2020. Our reliance on fossil fuels and the movement towards renewable, sustainable energy has further increased interest in fabricating soft polymer composites from environmentally friendly, renewable biopolymers.

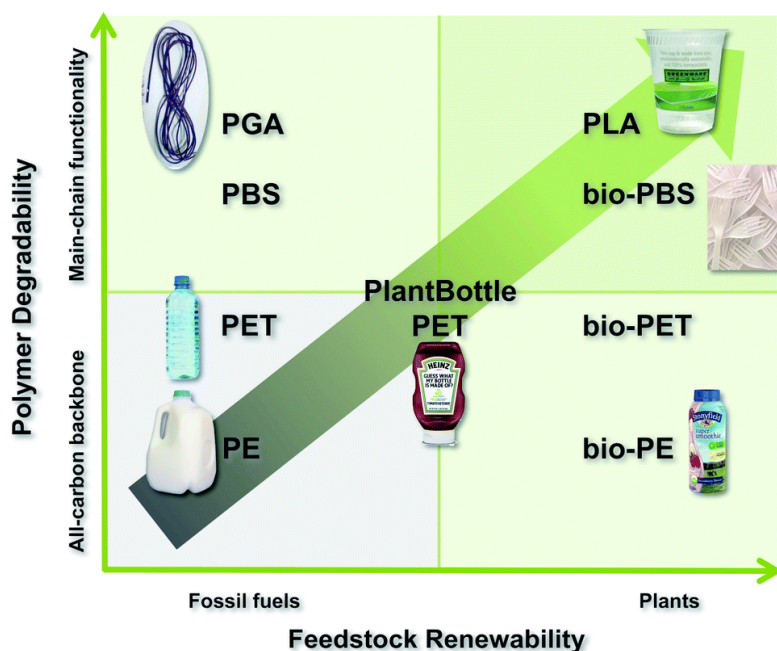


Figure 1.6. A feedstock renewability/polymer degradability matrix for various common plastics and bioplastics. Reproduced from Ref. *Polym. Chem.*, **2014**, *5*, 3117-3118 with permission from the Royal Society of Chemistry.

Coinciding with the movement towards “greener,” sustainable polymers, much materials research has moved towards the usage of composites employing renewable biopolymers. Specifically, some of the most common green additives utilized in the fabrication of next-generation hydrogel materials are chitosan,^{38,82,83} cellulose,^{84,85} and lignin.^{33,86–100} Much research has been conducted with chitosan-based hydrogels due to their high biocompatibility, low toxicity, and their degradation by human enzymes.¹⁰¹ Cellulose-based hydrogels also present good biocompatibility, along with mechanical strength, and being the most abundant natural material on Earth.¹⁰² When considering the relatively low cost (\approx \$0.40 per pound), high abundance, and appealing chemical structure, lignin has emerged as a popular greener alternative in hydrogel-based, materials research. Lignin exhibits numerous inherent properties, including high ultra-violet (UV) light

absorption,^{67,68} high thermal stability,¹⁰⁵ and antioxidant^{106,107} and antimicrobial properties.^{108,109} Further, lignin contains an abundance of hydroxyl (–OH) groups that creates avenues for various chemical functionalizations¹¹⁰ and direct crosslinking, although access to these groups is not straightforward as a result of a highly complex and obfuscated structure.^{105,111,112} A proposed chemical structure for lignin is shown in Figure 1.7.¹¹³

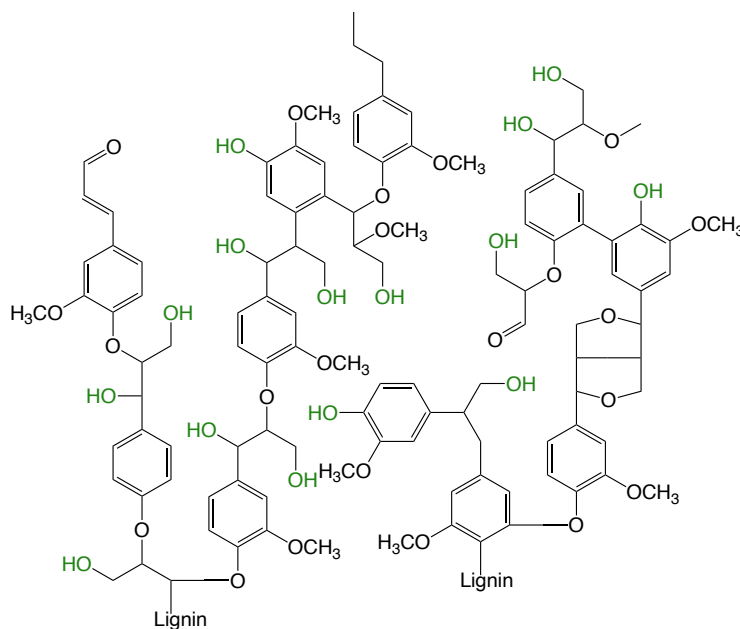


Figure 1.7. Proposed chemical structure of lignin containing a high abundance of phenolic rings and hydroxyl groups. Image adapted from Adler. *Wood Sci. Technol.* **1977**, *11*, 169-218.

According to the report, Global Lignin Market – Industry Analysis, Size, Growth, Trends, Statistics, Segment and Forecast 2014-2020, the market for lignin and lignin-based products was valued at USD 775 million in 2014¹¹⁴ and is expected to continue growing to USD 1.54 billion globally by the end of 2026.¹¹⁵ In line with the increasingly growing lignin market, the volume of research publications focused on lignin and lignin-based materials has also increased. In 2000, there were approximately 100 lignin-based research

publications, though that number rapidly increased to nearly 600 by 2016.¹¹⁴ Additionally, there were 10 patents dedicated to lignin in 2000 with that amount increasing to nearly 40 in 2016.¹¹⁶

Lignin is the second most abundant biopolymer on earth, behind only cellulose. It composes roughly 30 wt % of the mass in softwood trees, and 20–25 wt % of hardwood trees. Plants generate lignin via photosynthesis with carbon dioxide being utilized for the aromatization and polymerization of carbohydrates. It is found naturally in vascular plant cell walls and serves as the glue that holds together cellulose and hemicellulose. A depiction of the three main components found in plant cell walls is shown in Figure 1.8.¹¹⁷ When considering separation processes for recovering cellulose, lignin is a byproduct of both pulp-and-paper mill and biorefineries. Overall, the Kraft pulping process is used by 95% of the pulp-and-paper mill industry. The Kraft process involves immersing wood fibers in a hot (170 °C) aqueous solution of sodium sulfide and sodium hydroxide, referred to as white liquor, breaking most of the bonds that link lignin and cellulose.¹¹⁸ It is during this process that most lignin dissolves into the solution, freeing cellulose from the wood matrix as a pulp that is utilized in the paper-making process. The resulting, lignin-based solution is commonly referred to as black liquor, which is mostly burned (>99%) for its heating value in a recovery boiler. Approximately ~50 million tons of lignin are readily available a year,^{119,120} with only 0.2% of lignin recovered for nonfuel uses. Approximately 90% of the lignin that is recovered (~150,000 tons) is lignin from Kraft pulp mills,^{105,118} and is used in materials applications. The Kraft processes has many advantages over other recovery processes, including a surprisingly low sulfur content (~2-3%) despite being

exposed to a high sulfur environment, low waste generation, and high purity (low metals content).¹¹⁴ There are several proposed commercial processes for recovering lignin from black liquor solution, including LignoBoost™, LignoForce System™, and Sequential Liquid-Lignin Recovery and Purification (SLRP).¹²¹

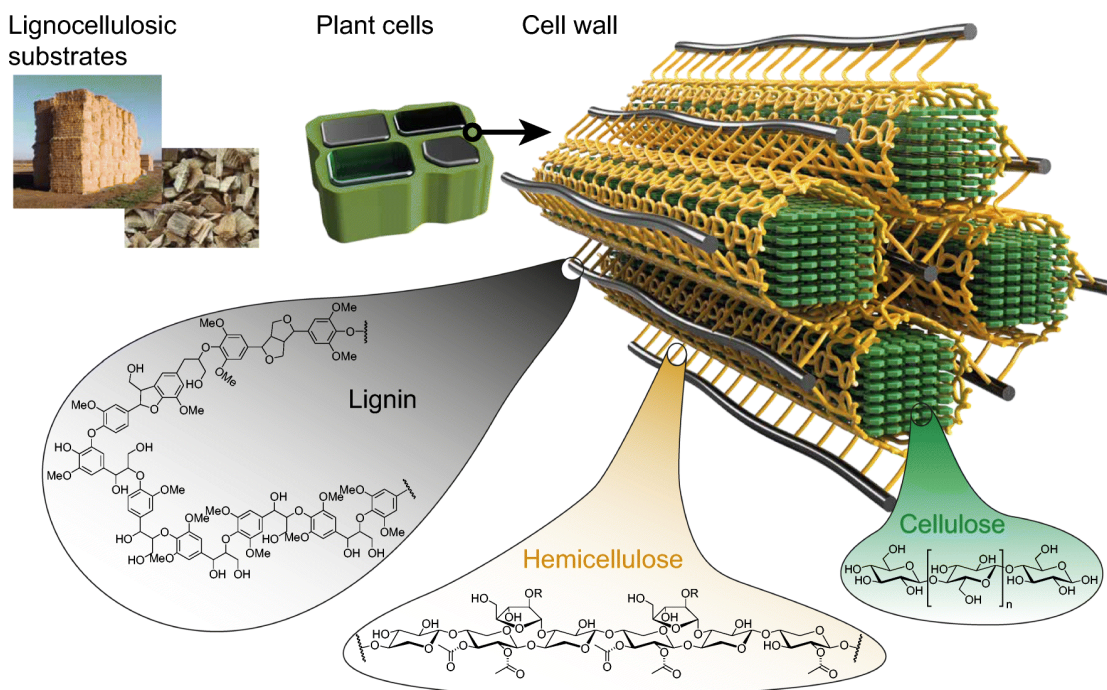


Figure 1.8. Depiction of the three main components (lignin, hemicellulose, and cellulose) found in plant cell walls. Image taken from: Brethauer et al. *Appl. Microbiol. Biotechnol.* **2020**, *104*, 5201–5212. (Creative Commons License)

In addition to the Kraft process, there is another, older sulfur-bearing lignin recovery process in practice whereby liginosulfate lignin is recovered from sulfite pulping mills. When considering sulfur-free extraction processes, the two most common extraction methods are soda lignin via alkaline pulping and the Organosolv process via solvent pulping. The Organosolv process is an attractive extraction method as there are no inorganic solvents utilized in the process. In addition, the final lignin product has low ash

content (~1.75 wt %) and molecular weight values can be less than 1000 kg mol⁻¹. While the Organosolv process exhibits many attractive qualities, the major drawback is that it is rather expensive.¹²² Lignin obtained from Kraft processes has a market value of 50 to 280 USD per metric ton (MT), while Organosolv lignin has much higher prices ranging from 280 to 520 USD/MT.¹¹⁶ Of mention, the Kraft process is the dominant pulping process in the world, and neither the Organosolv nor alkaline process are commercially practiced in North America today.

While not of direct relevance to this project, it is worth mentioning that recovered lignin can be broken down into small molecule, oligomeric products, through processes such as catalytic depolymerization^{123–125} or pyrolysis^{126–128}. However, use of such materials was not a focus of this project as these methods completely destroy the unique polymeric nature of lignin.¹²⁹

1.1.5 Lignin-Based Materials

When properly recovered, there are many valuable uses for lignin, including concrete additives,^{130–133} pesticides,^{134–136} binders,^{137–139} adhesives,^{140–142} activated carbon,^{143–145} and adsorbents.^{146,147} For instance, work by Wei et al.¹³² demonstrated that the water resistance and bending strength of botanical concrete, a sustainable material that simultaneously recycles concrete and wood waste in absence of cement, can be enhanced by the addition of Kraft lignin, at loadings of up to 20 wt %. Another study by Huang et al.¹³⁰ produced lignosulfates from alkaline lignin that were incorporated into concrete admixtures for improved compressive strength. Experimental results indicated that these lignosulfates can be used as a dispersant for improving the fluidity of cement paste, along

with meeting the industrial standards as water reducers for concrete admixtures. From an agricultural standpoint, the reliance on copper compounds in plant protection products for more than 100 years has created movements towards reducing usage of copper due to its negative environmental impact. As a result, work by Gazzurelli et al.¹³⁶ highlighted the fabrication of lignin-copper materials that can be used for efficient pathogen control. Another investigation by Lin et al.¹³⁴ showed that lignin can be utilized in the controlled release of pesticides where drug-loaded microspheres were deemed to be temperature-responsive.

When considering the pavement industry, bitumen is commonly used as a gluing binder for loose aggregates during pavement construction. To reduce our reliance on bitumen, a byproduct of crude oil, work by Xu et al.¹³⁷ investigated the feasibility of lignin in modified bituminous binders with improved performance and lower construction costs. Studies done by Xie et al.¹³⁸ created new avenues for lignin to serve as an asphalt binder modifier with improved high and low temperature performance. In a similar area of research, lignin has been investigated for incorporation into bio-based adhesives for wood bonding. In particular, work by Chen et al.¹⁴² showed that lignin adhesives can have acceptable dry shear strength when used in wood bonding applications. Another lignin-based adhesive studied by Henn et al.¹⁴¹ demonstrated that epoxidized Kraft lignin combined with biocolloids (in the form of lignin nanoparticles) resulted in the formation of a strong adhesive comparable to commercially used adhesives, along with high wet strength, great thermal stability, and free of fossil fuel such as phenol or formaldehyde.

Porous carbon materials have been extensively researched for the removal of volatile organic compounds from air such as benzene, halomethanes, and aldehydes. Lignin has shown promise as a precursor for activated carbon, as noted in a recent study by He et al.¹⁴³ where lignin-based pitch was used as a precursor for activated carbon in the removal of gaseous benzene. In another study by Wu et al.,¹⁴⁵ lignin-based magnetic activated carbon material demonstrated a higher adsorption of p-arsanilic acid from water, creating a new avenue for organic arsenic compound adsorbents.

1.1.6 Lignin-Based Hydrogels

When considering hydrogels, there are many studies investigating lignin-based hydrogels for an array of applications. Some of these applications include adsorbents/separations,^{13,86,148–152} stimuli-responsive materials,^{95,153,154} controlled-release,^{91,154} biomedical materials,^{33,92,155} and energy storage devices.^{156–158} Since lignin is a fairly ill-defined polymer, much research involving lignin-based hydrogels was performed without a specific application in mind and had a focus on strictly tuning the swelling and mechanical properties of those well-defined host polymers seen in traditional hydrogel research.^{49,89,159} Specifically, work done by Rajan et al.⁸⁹ investigated crosslinking 2-hydroxyethyl methacrylate-lignin hydrogels with 39% increase in water retention, a three-order magnitude increase in storage modulus, and 20% increase in thermostability. These properties were all tunable via modification of lignin content in the fabrication process.

Many lignin-based hydrogels have been synthesized for adsorbent and/or separation applications. In general, almost all lignin used in hydrogels is unfractionated, with the main

source being pine wood and recovered from the Kraft process. For example, work by Wu et al.¹⁴⁸ studied lignin-based hydrogels containing unfractionated, alkali lignin from pine and eucalyptus soda pulping, with super-adsorbent capacities of rhodamine 6G (196 mg g⁻¹), crystal violet (169 mg g⁻¹), and methylene blue (179 mg g⁻¹), presenting opportunities for these materials in soil water retention, agricultural seed cultivation, and dye pollutant removal from water. Additional studies involving lignin-based hydrogels for methylene blue removal were carried out by Yu et al.¹⁴⁹ where a lignosulfate-g-acrylic acid hydrogel was capable of adsorbing 2013 mg g⁻¹ of methylene blue. The lignosulfonate utilized was unfractionated and supplied by Sunson (China). It was discovered that pH and initial concentration of methylene blue in solution had a profound impact on adsorption capacity. Shifting from dyes to heavy metal ion removal, work by Mengyu Liu et al.¹⁵⁰ investigated polyacrylic acid lignin-based hydrogels with adsorption capacities of Pb²⁺ (1.076 mmol g⁻¹), Cu²⁺ (0.3233 mmol g⁻¹), and Cd²⁺ (0.059 mmol g⁻¹). The lignin employed here was unfractionated, alkali lignin from a paper mill. These lignin-containing materials show promise for treatment of water with a mixture of heavy metal ions, with a focus on selective removal of Pb²⁺. Further examining the potential for usage in water purification applications, work by Yuan et al.¹⁵¹ examined lignin-based hydrogels (again containing unfractionated, alkali lignin) with cellulose nanofibers and carbon dots for the adsorption and removal of hexavalent chromium, a highly toxic and carcinogenic compound.

One of the biggest drawbacks to stimuli-responsive hydrogels employing traditional polymers is the difficulty in achieving fast pH-response in combination with low cost and high mechanical performance. To address this concern, work done by Dai et al.⁹⁵

investigated poly(ethylene glycol) diglycidyl ether lignin-based hydrogels with fast pH-stimuli-response, reversibility, and good mechanical properties, which was attributed to the incorporation of unfractionated, Kraft lignin. These smart materials could create a new field for lignin-based hydrogel actuators. In another study of stimuli-responsive, lignin-based hydrogels, work by Parvathy et al.¹⁵³ examined N-isopropylacrylamide, acrylic acid, lignin hydrogels with temperature and pH responsive behavior that ultimately impacted equilibrium swelling capacity. These hydrogels again contained unfractionated, Kraft lignin, but showed improved cell viability and could find usage in possible biomedical applications.

Lignin-based hydrogels can potentially serve as controlled release systems, with work by Ciolacu et al.⁹¹ highlighting cellulose–lignin hydrogels for the controlled release of polyphenols. The lignin employed in this study was unfractionated, stream explosion lignin from aspen wood. The swelling and release profiles of these materials is tunable via hydrogel composition and could find potential in various biomedical applications. In another study by Jin et al.,¹⁵⁴ lignosulfate-based hydrogels were synthesized containing unfractionated, lignosulfate from Borregaard LignoTech USA. The resulting hydrogels had stimuli-responsive behaviors that present great potential for the controlled release of pesticides or drugs.

When considering lignin hydrogels as biomedical materials, work done by Larrañeta et al.³³ involved the fabrication of lignin-based hydrogels with resistance to infection and ability to release drugs over several days with high potential for medical material coatings. Specifically, these materials showed reduction in adherence to *Staphylococcus aureus* and

Proteus mirabilis. Of mention, the lignin utilized was unfractionated, and purchased from Cambridge Bioscience. In a similar line of work, an investigation by Kai et al.⁹² studied poly(ethylene glycol) methyl ether methacrylate, grafted lignin hyperbranched copolymers with high biocompatibility, tunable mechanical response, and self-healing capability suitable for smart biomaterials in biomedical applications. The lignin used in this study was unfractionated, Kraft lignin with a \bar{M}_w of 5.6. Additional work done by You et al.¹⁵⁵ involved a multi-energy dissipative lignin-based hydrogel that exhibited effectual antioxidant properties and nontoxicity, properties desirable for further exploration in biomedical hydrogel applications. Of mention, the lignin used in these hydrogels was unfractionated, acetic acid lignin from bamboo.

When focusing on lignin-hydrogels for energy storage applications, work by Liu et al.¹⁵⁶ studied a hybrid double-crosslinked lignin hydrogel that possessed high specific capacitance after 500 cycles and high energy density, paving way for a new area of lignin-based materials that are compression-resistant, foldable energy storage devices. The lignin used in this investigation was derived from the corncob, with no mention of fractionation or a recovery process. Similarly, work by Cui et al.¹⁵⁷ also investigated a flexible supercapacitor containing unfractionated, corncob-lignin-based nitrogen-doped carbon dots, suitable for portable/wearable electronic products.

Overall, incorporating lignin into composite materials has been demonstrated as a viable means of altering both the mechanical and permselective properties of resulting composite materials.^{89,155,159–161} Specifically, improvements to the Young's^{159,160} and storage moduli,^{89,155,160} as well as the ultimate tensile strength¹⁵⁵ and toughness¹⁶¹ have

been observed with the introduction of lignin, even at small lignin contents. In general, the majority of these studies do not mention a \bar{M}_w , and oftentimes do not mention a molecular weight either.

1.1.7 Incorporating Fractionated, ALPHA Lignin into Hydrogels

While the introduction of lignin has led to improved mechanical and permselective properties in many different hydrogel materials, to date, the majority of studies involving the synthesis of lignin-based hydrogels involve fabrication methods that utilize unfractionated lignin with high \bar{M}_w , anywhere from ~ 5 to as high as 10 and beyond.^{86,89,92,162–}

172

Current recovery methods, those being Kraft and Organosolv, indiscriminately precipitate lignin out of solution, leading to a final product with broad molecular weight (MW) distributions (i.e., high \bar{M}_w)¹⁰⁵ and high metals content (~ 1 – 2 wt %, primarily composed of sodium and potassium salts). These impurities can pose a risk for health or product contamination as these salts can leach out of the lignin-containing composite into an expensive product stream or the human body.¹¹⁸ Consequently, the development of lignin-based hydrogels for various applications is hindered by our limited understanding surrounding the role of lignin molecular weight (MW) and purity in the formation of the network structure of the resulting hydrogel composite. Fortunately, recent work by Thies and co-workers^{118,173,174} involving the fractionation and purification of lignin presents a viable avenue for obtaining lignin of well-defined and controlled MWs of lower \bar{M}_w . Specifically, they have developed the Aqueous Lignin Purification with Hot Agents (ALPHA) process,¹⁷⁵ which can be used to continuously clean, fractionate, and solvate

lignin. Some of these fractions can have prescribed MWs of narrow dispersity as low as $\bar{D} \approx 2$ and metals contents as low as 50 ppm (referred to as ultraclean lignin (UCL)).¹¹⁸ For a full inductively coupled plasma (ICP) analysis, along with ash content of all lignin used in this Dissertation, please refer to Appendix D. The uniqueness of the patented ALPHA process is that the lignin–solvent mixture forms two liquid phases, enabling separation of the lignin by molecular weight and purity by tuning the composition of the aqueous renewable solvent.¹⁷⁵ The ALPHA process operates in liquid-liquid equilibrium, which allows for better fractionation due to diffusion coefficients in liquid being much faster than in solid phase diffusion, along with potential for higher purity. A schematic of the ALPHA

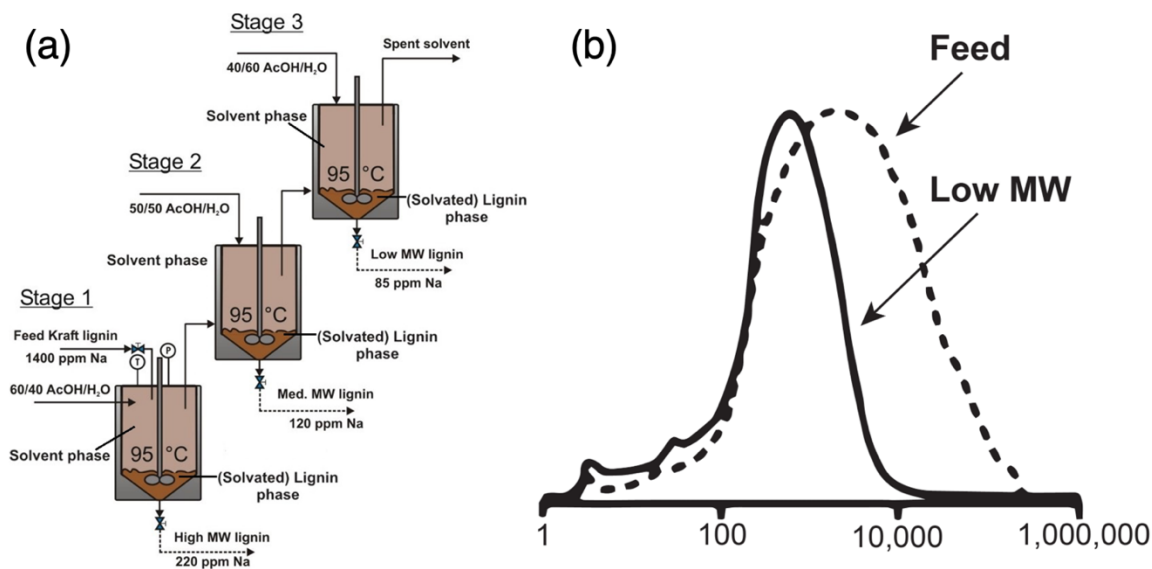


Figure 1.9. (a) Aqueous Lignin Purification with Hot Agents (ALPHA) process (US Patent No. 10,053,482; August 2018). (b) Molecular weight distribution before and after lignin is recovered from the ALPHA process

process, along with an illustration comparing the molecular weight distribution of feed lignin and ALPHA-fractionated lignin is shown in Figure 1.9.

When considering the importance of the mesh size in the network structure of a hydrogel composite, this present work supports the hypothesis that ALPHA-fractionated lignin of low \mathcal{D} homogenizes the resulting hydrogel network structure by potentially increasing the repeatability of mesh size distributions during the fabrication process. This homogenization of the network structure provides better tailored control of opening and closing the effective mesh size and allows for the establishment of fundamental structure-

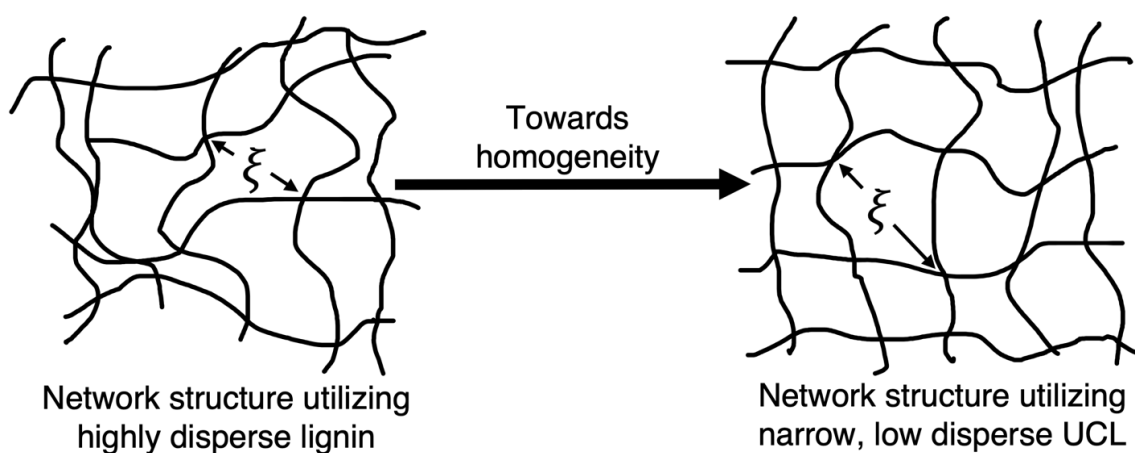


Figure 1.10. Homogenizing the network structure of lignin-based hydrogel composites via incorporation of controlled, narrow dispersity fractions of lignin.

process-property relationships in this emerging class of green hydrogel composites. A depiction of the network structure with both high and low \mathcal{D} lignin chains is shown in Figure 1.10.

In this Dissertation, much of the work has focused on elucidating the structure-processing-property relationships of lignin-based hydrogel composites that utilize lignin of narrow \mathcal{D} and a range of molecular weights. For detailed tables describing all types of lignin, their MW and \mathcal{D} , along with the characteristic mechanical and transport properties for all hydrogels in this Dissertation, please refer to Appendix C. The first study (Chapter

3) investigates the impact of lignin \bar{M}_w , functionalization, and loading on both mechanical and transport properties. Specifically, the \bar{M}_w of lignin had a profound impact on the repeatability of methylene blue permeability in hydrogel composites containing lignin of high \bar{M}_w , where repeatable measurements were difficult to attain. An avenue for direct chemical functionalization of ALPHA-fractionated lignin was demonstrated and verified via proton and phosphorus nuclear magnetic resonance (^1H NMR and ^{31}P NMR, respectively). Results from the ^{31}P NMR concluded that ALPHA-fractionated lignin possessed a higher hydroxyl content and higher yield of hydroxyl groups removed during functionalization than unfractionated SLRP lignin containing a higher molecular weight and \bar{M}_w . These results support the hypothesis that access to hydroxyl groups is hindered by heterogeneous lignin of high \bar{M}_w and higher molecular weight. It was concluded that lignin-containing samples had the capability of reducing methylene blue permeability by over two magnitudes.

The second investigation (Chapter 4) expands upon the work of Chapter 3, investigating the impact of lignin MW, loading, and crosslinker concentration on the mechanical properties of PVA-lignin composites. Lignin was crosslinked with PVA via glutaraldehyde through a condensation reaction along the hydroxyl groups of both lignin and PVA chains. Substantial increases in ultimate tensile strength, Young's modulus, and storage modulus were observed when lignin content was increased, along with increases in crosslinker concentration in most cases. Results from the dynamic mechanical analysis were utilized in calculating a molecular weight between crosslinks that showed correlations between stiffer and stronger composites having smaller M_c values. This decrease in M_c

demonstrated a tightening of the network structure that was visualized from scanning electron microscopy images of the hydrogel composites.

CHAPTER TWO

METHODS AND BACKGROUND

This section will cover the experimental details and general methods utilized in this Dissertation. Specifically, this includes background information related to experimental techniques used, as well as employed equations and their respective derivations, some which may be somewhat esoteric. Note, every chapter that follows will include a methods section that specifically pertains to all experiments performed in that Chapter.

2.1 Lignin Modification Techniques

2.1.1 Lignin Acrylation Process

A functionalization process was performed on lignin whereby hydroxyl groups along lignin chains were replaced with vinyl-containing acrylate groups. When considering the high abundance of hydroxyl groups along lignin chains, this creates avenues for direct chemical functionalization. As such, much research has investigated different chemical functionalizations of lignin, with a common one being methacrylation.^{89,154,176} To perform free radical crosslinking of the lignin chains, vinyl-containing acrylate groups need to be present in the chemical structure. To achieve this, a chemistry approach utilized in PEG-based hydrogels^{177,178} was exercised on lignin chains where hydroxyl groups were functionalized with acrylate monomers. A proposed reaction schematic and chemical structure for this functionalization process is shown in Figure 2.1. By tuning the molar quantities of triethylamine and acryloyl chloride with respect to lignin, optimum functionalization can be achieved and confirmed via ¹H NMR and ³¹P NMR techniques.

These acrylate-containing functional groups can now perform in free radical crosslinking as seen in Chapter 3.

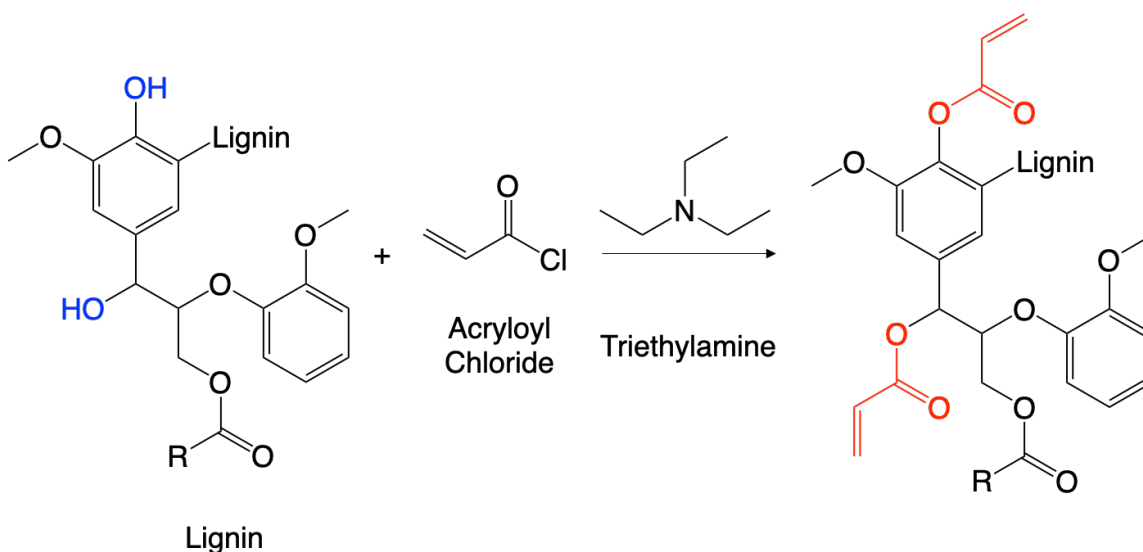


Figure 2.1. Reaction schematic and proposed chemical structure for functionalized lignin with **vinyl-containing acrylate groups** that replaced once present **hydroxyl groups** along lignin chains.

2.2 Lignin-Hydrogel Characterization Techniques

2.2.1 Dynamic Mechanical Analysis of PVA-Lignin Hydrogel Composites

Measuring the elasticity of a material via Dynamic Mechanical Analysis (DMA) is a common technique of rheological characterization. The utilization of oscillatory experiments to measure elasticity in a material was first performed by Poynting in 1909 and was further mainstreamed in the 1980s with the progression of technology. One way to describe DMA analysis is the application of an oscillating force to a material and analyzing its response to that applied force.¹⁷⁹ DMA experiments can be performed in a

number of ways, those being shear, torsion, compression, three point bending, and tension.¹⁸⁰ Applying an oscillatory strain to a viscoelastic material induces elastic and viscous stresses that are referred to as the in-phase and out-of-phase stresses. The elastic stress is a measure of the degree to which a sample behaves as an elastic solid, with the ratio of elastic stress to strain representing a material's ability to store energy elastically and is commonly referred to as the storage modulus (E'). The viscous stress is the measure of the degree to which a sample behaves as an ideal fluid, with the ratio of viscous stress to strain representing the material's ability to dissipate energy and is commonly referred to as the loss modulus (E'').¹⁸¹ When performed in linear geometry, storage and loss modulus are represented by E' and E'' , however, when performed in shear geometry they are represented by G' and G'' .

DMA can be performed on a sample across a temperature or frequency range. Performing a temperature sweep provides information about the glass transition temperature (T_g) and melting temperature (T_m). Performing a frequency sweep above the T_g and below the T_m is known as the rubbery plateau, whereby storage modulus is independent of frequency and remains approximately constant.¹⁷⁹ When considering the high-water content of hydrogels, and the T_g of PVA being ≈ 85 °C, it is safe to assume the T_g of all hydrogels utilized in this Dissertation are below room temperature (25 °C). An illustrative example of a DMA frequency sweep performed on PVA-lignin hydrogel composites is shown in Figure 2.2. Note, this figure is explained in further detail in Figure B.4 of Appendix B.

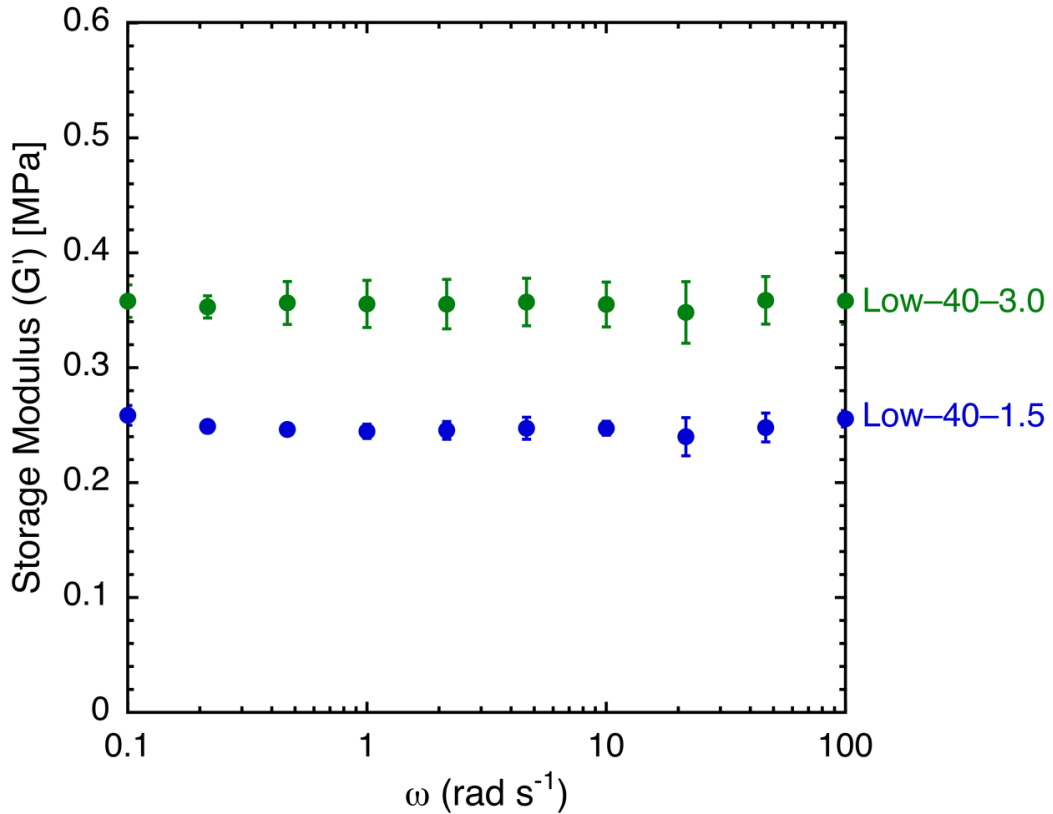


Figure 2.2. Dynamic mechanical analysis spectra from 0.1 to 100 rad s⁻¹ for Low molecular weight lignin-based PVA hydrogel composites. Note, the error bars in the figure represent the standard deviation of the average, which was calculated from repeat measurements on at least three separate membranes.

A major takeaway from Figure 2.2 is the relatively constant storage modulus across the entire frequency sweep, demonstrating these experiments being performed in the rubbery plateau. It is in this rubbery plateau where the storage modulus is proportional to the molecular weight between crosslinks (M_c) of the network structure. By using principles from the theory of rubber elasticity that explain relationships between stress and deformation,¹⁸² we are able to employ the following equation¹⁸³

$$M_c = \frac{\rho RT}{G'} \quad (2.1)$$

where ρ is the density of the hydrogel measured via mass in its dry state, and volume in hydrated state. R is the universal gas constant, T is temperature of the DMA measurements (room temperature, ≈ 25 °C), and G' is the shear modulus of the hydrogels. Note, when doing these measurements in tension mode, an equation is needed to convert linear storage modulus to shear modulus. The shear modulus of each hydrogel was calculated from the following equation^{179,180,184}

$$G' = \frac{E'}{2(1 + \nu)} \quad (2.2)$$

where E' is the storage modulus and ν is the Poisson's ratio, which was assumed to be 0.5 for all hydrogels used in this Dissertation.¹⁸⁵

2.2.2 Young's Modulus of PVA-Lignin Hydrogel Composites via Mechanical Indentation

Measuring the compression Young's modulus of PVA-lignin hydrogel composites was utilized in all investigations of this Dissertation. Much research has been done investigating the Young's modulus of soft hydrogel materials.¹⁸⁶⁻¹⁸⁹ The utilization of mechanical indentation can be used acquire a compression Young's modulus.¹⁹⁰

When considering mechanical indentation on soft materials, inhomogeneous deformations result in complex stress fields creates difficulty in describing the fundamental relations of applied load, P , to internal stresses and penetration depth, h , to the adjoint strains. Fortunately, Meyer's principle of geometrical similarity supports the notion of a representative stress, commonly referred to as the mean contact pressure, σ^* . This contact pressure is calculated from the following equation

$$\sigma^* = \frac{P}{A_c} \quad (2.3)$$

where P is indentation load, and A_c is to the contact area of impression. When considering stress-strain relationships, Hooke's law is commonly employed, which is given by the following equation:

$$d\sigma^* = \frac{E}{1 - \nu^2} d\varepsilon^* \quad (2.4)$$

where $d\sigma^*$ is representative stress, E is Young's modulus, ν is poisson's ratio, and $d\varepsilon^*$ is representative strain. For experiments employing a spherical indenter, the following equations are used for $d\sigma^*$ and $d\varepsilon^*$

$$d\sigma^* = \frac{\gamma P}{2\pi R h} = \frac{P}{2\pi} \quad (2.5)$$

$$d\varepsilon^* = k_s \left(\frac{dr}{R} \right) \quad (2.6)$$

where γ is the geometrical factor, R is radius of the indenter, h is total penetration depth, k_s is frontal coefficient, r is radius of contact, and d is diameter of the spherical indenter. Upon further examination of the geometrical factor for spherical indentation and purely elastic indentations, we can say that $\gamma = 2$ (Hertz's solution). When considering total penetration depth, h , the contact depth, $h = \gamma h_c$. The frontal coefficient, $k_s = \frac{4}{\pi}$, for Sneddon's elastic solutions. Compiling all of these substitutions and assumptions brings us

to a modified version of Hooke's law in calculating a Young's modulus via spherical indentation given by the following equation¹⁹¹

$$E = \frac{(1 - \nu^2) \Delta(P/h)}{\pi \Delta r} \quad (2.7)$$

where r is the contact radius of the indenter contacting the membrane. A substitution for contact radius is shown in the following equation:

$$r^2 = Rh \quad (2.8)$$

When considering a spherical indenter, the following equation applies for Hertz contact mechanics¹⁹⁰

$$P = \frac{E}{(1 - \nu^2)} \frac{4r^3}{3R} \quad (2.9)$$

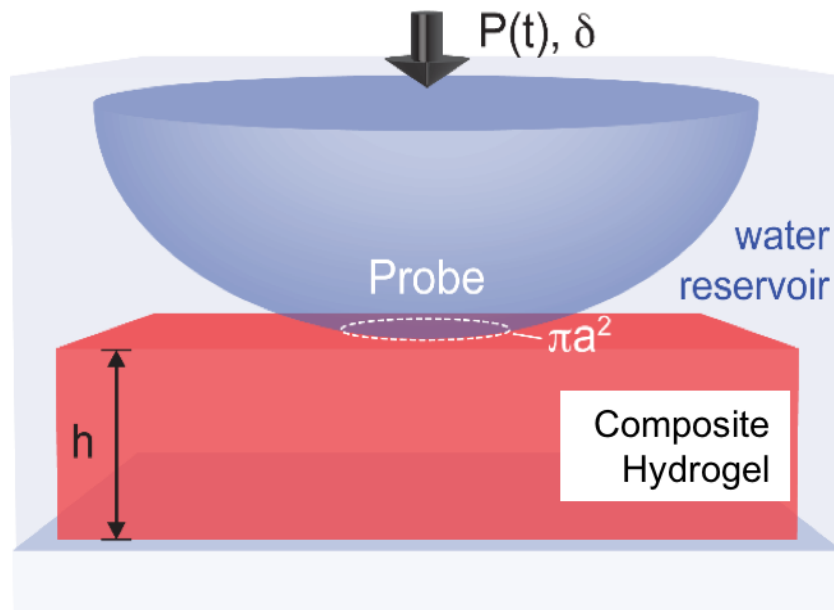


Figure 2.3. Experimental setup for a Young's modulus measurement via mechanical indentation.

Performing these Young's modulus measurements involves placing a hydrogel membrane into a water bath directly located under the indenter. A depiction of this experimental setup is shown in Figure 2.3. A LabVIEW software program was created to measure load applied to the sample versus time. Manipulation of the load versus time data, while taking equation 2.9 into consideration, leads us to a plot of indentation load versus contact area times representative strain as shown in Figure 2.4. Fitting a linear model to this data allows one to calculate a Young's modulus value as it is directly related to the slope of the fitted line.

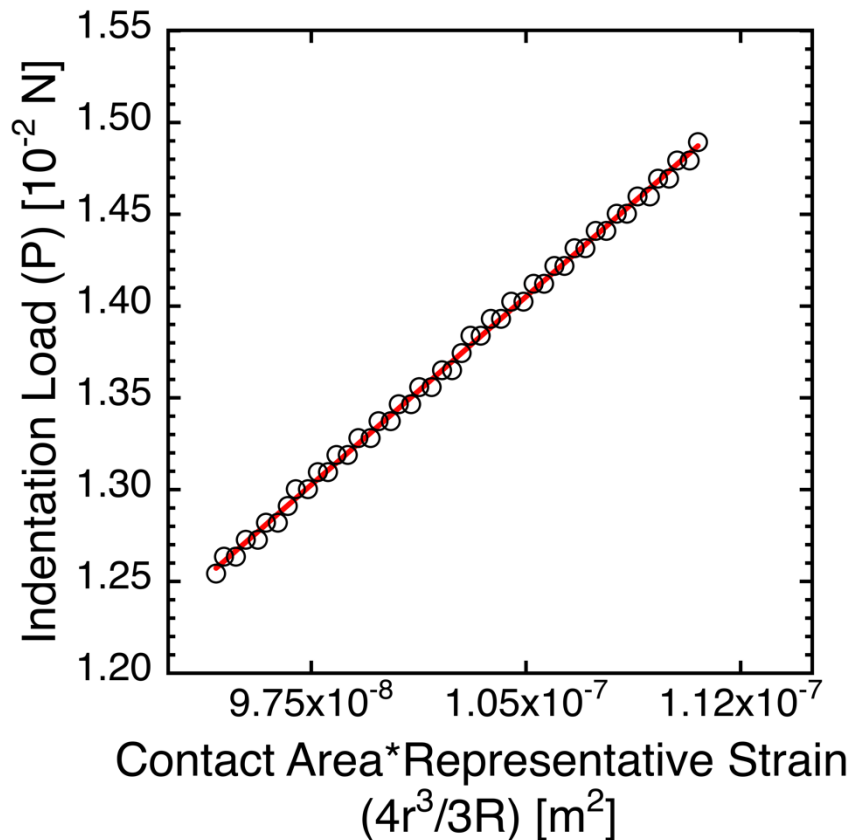


Figure 2.4. Indentation load versus contact area times representative strain data. Slope of data is indicative of Young's modulus for hydrogel sample.

2.2.3 Calculating Permeability through PVA-Lignin Hydrogel Composites

Methylene blue (MB) permeability experiments were utilized in Chapter 3 to analyze transport performance of PVA-lignin hydrogel composites. Methylene blue is a cationic dye that serves as a common model pollutant in water filtration research. Much work has investigated the adsorption of MB from water,^{12,13,34,192–194} along with permeability experimentation of MB^{195–197} and other various permeates.^{198–203} Permeability is defined as the overall mass transport through a material.

A schematic of the static permeation cell utilized in these experiments is shown in Figure 2.5. The hydrogel membrane is mounted in between the donating and receiving

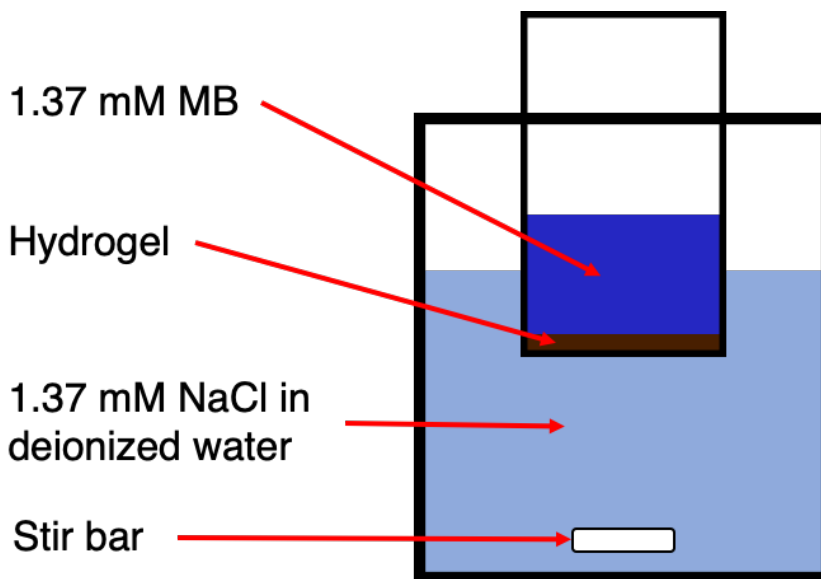


Figure 2.5. Illustrative schematic of permeation cell used for methylene blue (MB) permeability experiments.

reservoirs, making sure the hydrogel stays hydrated for the entirety of the experiment to prevent it from drying out and cracking. Above the hydrogel is a high concentration (1.37 mM) of MB in reverse osmosis (RO) water. To minimize osmotic drag of the permeation

setup, an equimolar concentration (1.37 mM) of NaCl in RO water was placed in the receiving reservoir.

There are a few assumptions that must be taken into consideration when obtaining the final equation to calculate MB permeability through PVA-lignin hydrogel composites. Specifically:

1. Methylene blue permeability is independent of its concentration.
2. The permeation through the membrane has reached pseudo-steady state.
3. The concentration of methylene blue concentration in the donating reservoir is assumed to be constant and is much greater than the methylene blue concentration in the receiving reservoir for the entirety of the experiment.
4. The reduction in the concentration of the donating reservoir over the length of the experiment is negligible.

Taking these assumptions into consideration, the permeability equation derivation starts at Fick's second law of diffusion as shown in the following equation²⁰⁴

$$\frac{dC_i}{dt} = D_{ij}\nabla^2 C_i \quad (2.9)$$

where C_i is the concentration of the diffusing species and D_{ij} is the diffusion coefficient which is assumed to be constant here. The diffusion for these permeation experiments is assumed to be in one direction, that being the z-direction. An illustration of this z-direction diffusion from donating reservoir through the hydrogel membrane to the receiving reservoir is shown in Figure 2.6 where V_1 is the donating reservoir volume, $C_1(t)$ is the concentration of MB in the donating reservoir at time t , A is the cross sectional area of the

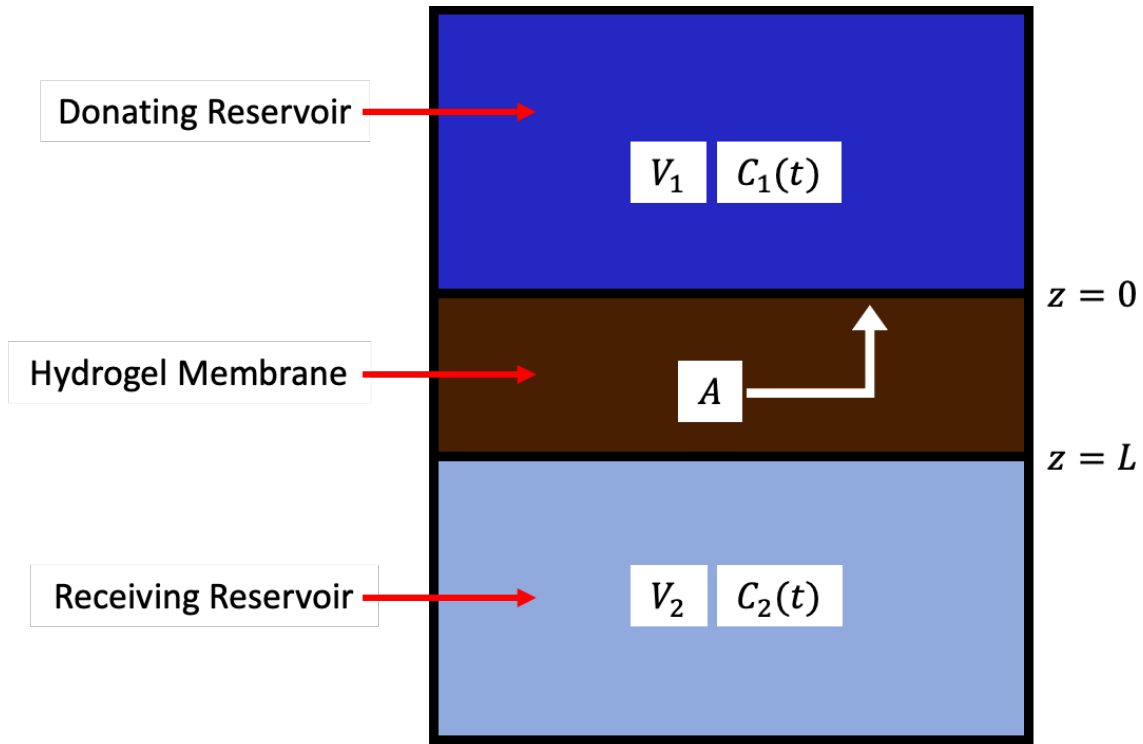


Figure 2.6. Illustrative schematic of permeation cell used for methylene blue (MB) permeability experiments.

exposed hydrogel to MB, L is thickness of the hydrogel membrane, V_2 is the receiving reservoir volume, and $C_2(t)$ is the concentration of permeated MB in the receiving reservoir at time t . The representative equations for MB concentration with respect to position and time ($C(z, t)$), along with both boundary conditions are shown in the following equations

$$\frac{d^2C}{dz^2} = 0 \quad (2.10)$$

$$C(0, t) = KC_1(t) \quad (2.11)$$

$$C(L, t) = KC_2(t) \quad (2.12)$$

where K is the partition coefficient, or the ratio of MB concentrations inside and outside of the membrane. It is an indication of MB solubility into the medium (hydrogel membrane in this case). Beginning with Fick's second law of diffusion

$$D \frac{d^2C}{dz^2} = \frac{dC}{dt} \quad (2.13)$$

and taking into consideration pseudo-steady state conditions leads to the following equation.

$$\frac{d^2C}{dz^2} = 0 \quad (2.14)$$

Integrating equation 2.14 and applying both boundary conditions in equations 2.11 and 2.12 leads to the following equation representative of a concentration profile.

$$C(z, t) = \left(\frac{z}{L}\right) K(C_2(t) - C_1(t)) + KC_1(t) \quad (2.15)$$

The concentration profile for permeated MB into the receiving reservoir can then be modeled with respect to the fluxes on both sides of the membrane facing the donating and receiving reservoirs. Beginning with the following flux equations

$$N_z(0, t) = -D \frac{dC}{dz}(0) \quad (2.15)$$

$$N_z(L, t) = -D \frac{dC}{dz}(L) \quad (2.16)$$

and substituting in the first derivation of equation 2.15 with respect to dz leads to the following equations.

$$N_z(0, t) = \frac{D}{KL} (C_1(t) - C_2(t)) \quad (2.17)$$

$$N_z(L, t) = \frac{D}{KL} (C_1(t) - C_2(t)) \quad (2.18)$$

where $N_z(0, t)$ and $N_z(L, t)$ are the z -direction fluxes. As seen in equations 2.17 and 2.18, these fluxes happen to be equal. This means there is zero accumulation of MB in the membrane during the entirety of the experiment.

Taking a closer look at the integral balances for each compartment, we begin with the following integral equation and boundary conditions

$$V \frac{d}{dt} \int_V C dV = - \int_S \underline{n} * \underline{N} dS \quad (2.19)$$

$$C_1(0) = C_0 \quad (2.20)$$

$$C_2(0) = 0 \quad (2.21)$$

where \underline{N} is the flux vector, \underline{n} is the unit vector normal to the surface, and C_0 is the starting concentration in the donating reservoir at time 0. Integration, derivation, and substitution of appropriate boundary conditions is shown in the following equations

$$\frac{d}{dt}(C_1V_1) = -AN_z(0, t) \quad (2.22)$$

$$V_1 \frac{dC_1}{dt} + C_1 \frac{dV_1}{dt} = -AN_z(0, t) \quad (2.23)$$

$$V_1 \frac{dC_1}{dt} = -AN_z(0, t) \quad (2.24)$$

$$\frac{d}{dt}(C_2V_2) = AN_z(L, t) \quad (2.25)$$

$$V_2 \frac{dC_2}{dt} + C_2 \frac{dV_2}{dt} = AN_z(L, t) \quad (2.26)$$

$$V_2 \frac{dC_2}{dt} = AN_z(L, t) \quad (2.27)$$

where equations 2.24 and 2.27 are flux entering and exiting the membrane. Focusing on equation 2.27, and substituting in equation 2.18 leads to the following equation

$$\frac{dC_2}{dt} = \frac{ADK}{V_2L} (C_1(t) - C_2(t)) \quad (2.28)$$

If we recall that the concentration in the donating reservoir is much greater than in the receiving reservoir, this presents the following equation.

$$\frac{dC_2}{dt} = \frac{ADK}{V_2L} C_0 \quad (2.29)$$

We can correlate diffusion coefficient and partition coefficient with permeability in the following equation.

$$P = DK \quad (2.30)$$

Lastly, substituting equation 2.30 into 2.29 brings us to the following final permeability equation²⁰⁵ that is utilized in Chapter 3 of this Dissertation.

$$P = \frac{dC_2}{dt} \frac{V_2 L}{AC_0} \quad (2.31)$$

CHAPTER THREE

NOVEL COMPOSITE HYDROGELS CONTAINING FRACTIONATED, PURIFIED LIGNINS FOR AQUEOUS-BASED SEPARATIONS

Gregorich, N.; Ding, J.; Thies, M. C.; Davis, E. M. Novel Composite Hydrogels Containing Fractionated, Purified Lignins for Aqueous-Based Separations. *J. Mater. Chem. A* **2021**, *9*, 1025-1038.

3.1 Introduction

Hydrogels are attractive materials for aqueous-based separations as the selectivity of the membrane can be altered through manipulation of its network structure (i.e., mesh size) and chemical composition (or functionality). As such, these soft materials have been used to separate oil from water/oil emulsions,²⁰⁶ organic dyes (e.g., methylene blue)^{34,86} and heavy metal ions (e.g., Cu²⁺, Pb²⁺) from aqueous solutions,^{207,208} as well as controlled adsorption and release of model drugs²⁰⁹ and model proteins, such as bovine serum albumin.^{38,82,210} However, the use of petroleum-based precursors in the fabrication of traditional synthetic hydrogels – e.g., poly(acrylic acid), poly(acrylamide), poly(vinyl alcohol) – has resulted in increased interest in the use of environmentally friendly, renewable biopolymers for these membrane-based separations. As such, the use of renewable biopolymers, such as chitosan,^{38,82,83} cellulose,^{84,85} and lignin,^{33,86–100} in the fabrication of next-generation materials has been extensively researched.

Of particular interest to the current work is the use of lignin in the fabrication of soft composites. As an additive for composite hydrogels, lignin possesses several beneficial attributes, including antioxidant^{106,107} and antimicrobial properties,^{108,109} high ultra-violet (UV) light absorption,^{103,104} and high thermal stability.¹⁰⁵ In addition, the abundance of

hydroxyl (–OH) groups and chemical linkages allow for the potential of a wide variety of chemical functionalizations,¹¹⁰ although access to these groups is not straightforward due to the complex and heterogeneous structure of the lignins.^{105,111,112} Lastly, as lignin is the world's second most abundant natural polymer (behind only cellulose),^{105,173,211,212} lignin-based composite membranes present an opportunity to substantially reduce the use of petroleum-based products.^{213,214}

Lignin holds significant potential for added value in the fabrication of advanced soft composites,^{215,216} with ~50 million tons per year readily available as a by-product of biomass processing. However, today, >99% of that lignin is simply burned as fuel or sent to waste treatment.¹¹⁸ Approximately 90% of the lignin that is recovered (~150,000 tons) is Kraft lignin from pulp mills,^{105,118} and is used in materials applications. However, all of the recovery methods in use today indiscriminately precipitate and isolate crude bulk lignins (CBLs), which have broad molecular weight (MW) distributions (i.e. high dispersity (\mathcal{D})), complex and heterogeneous chemical architectures, and low purities.¹⁰⁵ Furthermore, the recovered CBLs possess a high metals content (~10,000 ppm total metals, primarily sodium and potassium), which is of particular concern for bioseparations,¹¹⁸ as metals can leach out of the composite material into the human body or into an expensive product stream, presenting risks for both health and product contamination. Note, lignin can be further broken down into small molecule, oligomeric products, through processes such as catalytic depolymerization^{123–125} or pyrolysis^{126–128}. However, use of such materials was not the focus of the current study, as these methods completely destroy the unique polymeric nature of lignin.¹²⁹

The addition of lignin to hydrogels has been demonstrated as a viable means of altering both the mechanical and permselective properties of composite lignin hydrogels.^{93–95,105,106,110,162,217,218} However, starting with early work in the late 1970s and early 1980s by Lindström and Westman,^{219–221} to date, the vast majority of studies regarding lignin-based hydrogels involve fabrication methods that utilize heterogeneous, ill-defined lignins (i.e., CBLs with high \mathfrak{D}).^{146,147,149,159,162–169,171,172,222–231} Furthermore, developing lignin-based hydrogels for targeted separations is hindered by our lack of understanding as to how the addition of lignins to these soft composites alters the crosslinked network structure of the resulting hydrogel. When used in the fabrication of composite hydrogels, the heterogeneity of the lignins results in composites with ill-defined network structures, obfuscating the molecular-scale interactions and fundamental mechanism governing transport in these ‘green’ materials. Fortunately, recent work by Thies and co-workers^{118,173,174} involving the fractionation and purification of CBLs has presented a feasible avenue for obtaining lignins of well-defined MWs and low \mathfrak{D} . Specifically, they have developed the Aqueous Lignin Purification with Hot Agents (ALPHA) process,¹⁷⁵ which can be used to continuously and simultaneously clean, fractionate, and solvate lignins into prescribed MWs of narrow dispersity ($\mathfrak{D} \approx 2$), having metals contents lower than 50 ppm (referred to as ultraclean lignins (UCLs)).¹¹⁸ Incorporating UCLs of prescribed MWs and low dispersity into hydrogels should, in principle, result in a more homogeneous network structure of the composite hydrogel. Moving forward, such materials systems will allow us to more accurately elucidate the fundamental relationships between lignin molecular weight, soft

composite network structure, and membrane separation performance for this emerging class of ‘green’ materials.

Traditionally, poly(vinyl alcohol) (PVA) hydrogels have been synthesized via thermal crosslinking,^{56,57} chemical crosslinking,^{45,47,58–66} or a combination of both^{60,67}. They have also been synthesized via freeze-thaw methods inducing physical crosslinks.^{68–71,232–236} In the case of thermal crosslinking, physical crosslinks are formed in the PVA hydrogels through the formation of crystallites. This has proven to be a viable method for creating free-standing PVA membranes that are stable when re-immersed in water (i.e., they do not redissolve when placed in water). As the crosslinks formed in this case are not permanent crosslinks, thermally-crosslinked PVA films are susceptible to dissolution if placed in water at elevated temperatures (> 60 °C). In the case of chemically-crosslinked PVA films, permanent crosslinks between chains are achieved through the use of a crosslinking agent. For example, stable chemical crosslinking of PVA hydrogels has been achieved with glutaraldehyde,^{47,58–64} and various acids,^{45,65,66} to name a few. As hydroxyl groups along the backbone of the hydrogel are consumed during the crosslinking process, the resulting membranes are much less hydrophilic than neat PVA. While this can be leveraged as a means to alter the hydrophilicity of the crosslinked membrane, it may also be beneficial to retain the high hydrophilicity of the neat PVA in the resulting membrane, especially for lower temperature applications, where the stability of the PVA membrane is not in question.

In this work, two series of PVA composite hydrogels containing unfunctionalized and functionalized lignins at concentrations ranging from 0 to 50 wt % were synthesized. These

soft composites were fabricated using both crude bulk lignins (CBLs; apparent number-average molecular weight, $M_{N,app} \approx 4170 \text{ g mol}^{-1}$, dispersity, $\mathcal{D} \approx 3.9$) that were recovered from a Southeastern pine black liquor via the Sequential Liquid-Lignin Recovery and Purification (SLRP) process,¹²¹ and ultraclean lignins (UCLs; apparent number-average molecular weight, $M_{N,app} \approx 1250 \text{ g mol}^{-1}$, dispersity, $\mathcal{D} \approx 2.2$), which were isolated from the aforementioned CBLs via the ALPHA process. Detailed descriptions of the SLRP and ALPHA techniques are given elsewhere.¹⁷⁴ The chemical functionality of the lignins was altered via an acrylation process, where a portion of the $-\text{OH}$ groups were replaced with vinyl groups (i.e., $\text{C}=\text{C}$). This functionalization allows for the formation of an interpenetrated network (IPN)^{48,237–243} containing chemically-crosslinked lignin and thermally-crosslinked PVA. Successful functionalization of $-\text{OH}$ groups was confirmed by both proton and phosphorus nuclear magnetic resonance (^1H NMR and ^{31}P NMR, respectively), as well as via infrared spectroscopy. The mechanical and transport properties of the soft composites were also measured. Specifically, the Young's moduli of the hydrated composites were characterized using mechanical indentation, while the permeability of methylene blue (MB) across the membranes was captured by ultraviolet-visible (UV-vis) spectroscopy. Note, as a 'proof of concept' regarding the fabrication of composite hydrogels with high lignin content, composite hydrogels containing 50 wt % unfunctionalized CBL and UCL were also fabricated.

3.2 Experimental Section

3.2.1 Materials

Dimethyl sulfoxide (DMSO) (ACS reagent, $\geq 99.9\%$), dimethylformamide (DMF) (anhydrous, 99.8%), diethyl ether (ACS reagent, $\geq 98.0\%$, contains $\sim 2\%$ ethanol and ~ 10 ppm BHT as inhibitor), ammonium persulfate (APS) (ACS Reagent, $\geq 98.0\%$), methylenebisacrylamide (MBA) (99%), N,N,N',N'-tetramethylethylenediamine (TMEDA) (ReagentPlus®, 99%), acryoyl chloride (97.0%, contains < 210 ppm MEHQ as stabilizer), triethylamine ($\geq 99\%$), DMSO- d_6 (99.9 atom %D, contains 0.03 % (v/v) TMS) were purchased from Sigma Aldrich. Methylene blue (MB) was purchased from VWR Analytical. Poly(vinyl alcohol) ($M_w = 78,000$ g mol $^{-1}$, 99+% hydrolyzed) (PVA) was purchased from Polysciences, Inc. Kraft lignin ($M_N \approx 4170$ g/mol, $D \approx 3.9$), produced from the Sequential Liquid Lignin Recovery and Purification (SLRP) process,²⁴⁴ were obtained from Liquid Lignin, LLC. From these Kraft lignin, ultraclean lignins ($M_N \approx 1250$ g mol $^{-1}$, $D \approx 2.2$), were produced from the Aqueous Lignin Purification with Hot Agents (ALPHA) process,¹¹⁸ developed by the Thies Group at Clemson University. Briefly, the UCLs were isolated from the CBLs using a 50/50 (by volume) acetic acid–water solution at 70 °C, with the low MW lignin of interest being isolated in the solvent-rich phase. The UCL was then precipitated from the solvent-rich phase as a solid by adding deionized (DI) water in a 1:1 (v/v) ratio. Reverse osmosis (RO) water (resistivity ≈ 18 M Ω ·cm) was used for all experiments.

3.2.2 Characterization of Molecular Weight of Lignin

The molecular weight of the unfunctionalized UCLs and CBLs was determined using gel permeation chromatography (GPC). Specifically, the lignins were analyzed using an Alliance GPCV 2000 instrument. Two columns were used in series: (1) a Waters Styragel HT5 column (10 mm, 4.6 mm × 300 mm) and (2) an Agilent PolarGel-L column (8 mm, 7.5 mm × 300 mm). In this case, the mobile phase consisted of 0.05 mol L⁻¹ lithium bromide in DMF at a flow rate of 1 mL min⁻¹. Poly(ethylene glycol) (PEG) calibration standards were used for the estimation of the apparent molecular weight of the lignins. Samples were dissolved in the mobile phase at a concentration of 1 mg mL⁻¹ and were filtered using a 0.2 mm nylon membrane syringe filter prior to injection into the column. Detection of the PEG standards was carried out via a Waters differential refractometer, while the detection of lignins was carried out via ultraviolet-visible light (UV-vis) with a Waters 2487 detector at 280 nm.²⁴⁵ The molecular weight for a given sample were generally reproducible within +/- 50 g mol⁻¹.¹⁷³

3.2.3 Lignin Acrylation Procedure

After the aforementioned drying procedure, for example, 1 g of ultraclean lignin was immediately added to 5 mL of DMF in a RBF, and the solution was brought into a nitrogen atmosphere (i.e., nitrogen glove box). Based on a previously developed method,¹⁷⁸ 786 µL of triethylamine, followed by 986 µL of acryloyl chloride, were added to the solution. The RBF was then capped with a rubber stopper and removed from the glove box. Next, the solution was left to stir for 24 h, after which it was vacuum filtered to remove unwanted salts. Precipitation and dissolution were performed three times using diethyl ether and

DMF. This solution was then placed into a vacuum oven at room temperature under dynamic vacuum until all DMF was removed.

3.2.4 Characterization of lignin using infrared spectroscopy

Successful functionalization of the lignins was analyzed by FTIR spectroscopy using a Thermo Scientific Nicolet iS50R FT-IR equipped with Specac Golden Gate attenuated total reflectance (ATR) attachment. All spectra were collected using a liquid nitrogen-cooled mercury-cadmium-telluride detector with 64 scans per spectrum at a resolution of 4 cm^{-1} .

3.2.5 Lignin Hydrogel Synthesis

(1) *Thermally-crosslinked hydrogels:* A solution of PVA and DMSO was produced by dissolving PVA in DMSO at 9% w/w for 6 h at 120 °C. After cooling to room temperature, high-purity nitrogen gas was bubbled through the PVA–DMSO solution for 1 h at room temperature. Additionally, pure DMSO was placed in a separate round bottom flask (RBF), and high-purity nitrogen gas was bubbled through the DMSO for 1 h at room temperature. The lignins (both crude bulk and ultraclean lignins) were dried in a room temperature oven under dynamic vacuum for 24 h. Note, to prevent thermal crosslinking of the lignins prior to their use in the fabrication procedure, the lignins were not dried at elevated temperatures (i.e., were not dried above 60 °C). After drying, a prescribed amount of lignin (unfunctionalized or functionalized – see next section) was added to the purged DMSO and mixed until the lignin was fully dissolved, creating a dark black solution. The lignin–DMSO solution was then added to the PVA–DMSO solution, creating PVA–lignin–DMSO solutions at various lignin loadings (10 wt %, 20 wt %, and 50 wt %, relative to the mass

of PVA) and was stirred for 10 min to ensure homogeneous mixing of the two solutions. After 10 min of stirring, the solution was cast onto a polytetrafluoroethylene (PTFE) dish and placed into an oven under partial static vacuum at 60 °C for 36 hours or until all DMSO was removed, creating a robust, free-standing film. To remove any residual DMSO, the hydrogels were subjected to multiple rinse-soak cycles with DI water. (2) *Thermally- and chemically-crosslinked hydrogels*: For these composite hydrogels, everything in the aforementioned fabrication process remains the same except that we start with functionalized lignins (both UCLs and CBLs). Next, 1.5 wt % APS (relative to the mass of PVA) was dissolved in purged DMSO (< 1 g) and added to the PVA–lignin–DMSO solution. After 1 min of stirring, 0.5 wt % MBA (relative to the mass of PVA) was dissolved in purged DMSO (< 1 g) and added to the PVA–lignin–DMSO solution. After 1 min of stirring, 0.75 wt % TMEDA (relative to the mass of PVA) was added to the PVA–lignin–DMSO solution. After 5 min of stirring, the solution was cast onto a polytetrafluoroethylene (PTFE) dish and placed into an oven under partial static vacuum at 60°C for 36 hours or until all DMSO was removed, creating a robust, free-standing film. To remove any residual DMSO, the hydrogels were subjected to multiple rinse-soak cycles with DI water. Once fabricated, all composite hydrogels were stored in DI water at room temperature (~20 °C) until they were used in experiments.

3.2.6 Mechanical Indentation Experiments

Hydrated Young's modulus measurements, based on the JKR (Johnson-Kendall-Roberts) theory of adhesion,²⁴⁶ were conducted using a custom-built mechanical indentation apparatus. The setup consisted of a high-resolution linear actuator (M-230.25,

Physike Intrumente) and mercury servo controller (C-863.11, Physike Intrumente) connected to a S-beam load cell (Futek LSB200, FUTEK Advanced Sensor Technology, Inc) with a rigid glass indenter of radius of curvature $R = 3.308$ mm. The linear actuator was mounted to a high-performance linear stage with 46 mm of travel range (M433, Newport). A custom program designed in LabVIEW was used to acquire load and indenter height data as a function of time from the S-beam load cell and the linear actuator, respectively, during all indentation experiments. For these experiments, the indenter was lowered at a speed of $2 \mu\text{m s}^{-1}$ until the indenter came in contact with the swollen hydrogel. Upon contact, the indenter velocity increased to $4 \mu\text{m s}^{-1}$ until a prescribed load of 29.4 mN was reached, after which the indenter was retracted from the sample. Using Hertz's solution for spherical indentation, a solution to Hooke's law was used to acquire Young's modulus.¹⁹¹ Note, prior to beginning all indentation experiments, the membranes were equilibrated in liquid water for at least 48 h. Also, the Poisson's ratio (ν) of the hydrated composite hydrogels was assumed to be $\nu = 0.5$.

3.2.7 Nuclear Magnetic Resonance Spectroscopy

Characterization of the lignins, before and after acrylation, was performed using ^1H nuclear magnetic resonance (NMR) spectroscopy on a Bruker 300 MHz. The lignin was dissolved in DMSO- d_6 at a concentration of ~ 4 mg/mL and placed into an NMR tube. Measurements were performed at 16 scans/spectrum. All spectra were Fourier-transformed, baseline corrected, and phased using SpinWorks. Of interest to this investigation were NMR peaks corresponding to the aromatic ($\delta = 6.7$ ppm) and aliphatic

($\delta = 3.7$ ppm) hydroxyl ($-\text{OH}$) groups,²⁴⁷ as well as the peak corresponding to protons on a vinyl group ($\delta = 6.2$ ppm)²⁴⁸.

Additional characterization of the hydroxyl content of the lignins, before and after acrylation, was performed using ^{31}P NMR spectroscopy on a Bruker Neo 500 MHz (with cryoprobe). The solutions for dissolving lignin were prepared from the following: (1) 1 mL of chloroform-d and 1.6 mL of pyridine, and (2) 1 mL of chloroform-d, 1.6 mL of pyridine, 100 mg of cyclohexanol (internal standard), and 90 mg of chromium acetylacetonate. 20 mg of vacuum dried lignin were added to a solution containing 400 μL of (1) and 150 μL of (2). 50 μL of 2-Chloro-4,4,5,5-tetramethyl-1,3,2-dioxaphospholane (TMDP) was added to this solution and transferred into an NMR tube. Measurements were performed within 30 minutes of sample prep and at 32 scans/spectrum. All spectra were Fourier-transformed, baseline corrected, and phased using TopSpin. Of interest to this investigation were NMR peaks corresponding to the aromatic ($\delta = 144.6\text{--}137.3$ ppm) and aliphatic ($\delta = 149.1\text{--}145.4$ ppm) hydroxyl ($-\text{OH}$) groups.²⁴⁹

3.2.8 Methylene Blue Permeation

A custom-built diffusion cell was used for MB permeation experiments. As depicted in Figure 3.1, the hydrated hydrogel was sandwiched between a receiving reservoir filled with 25 mL of 1.37 mmol L^{-1} NaCl in RO water and a donating reservoir filled with 2 mL of 1.37 mmol L^{-1} MB in RO water. To measure the concentration of MB in the receiving reservoir, aliquots were taken at fixed time intervals. The concentration of MB ions in each aliquot was measured via ultraviolet-visible light (UV-vis) spectroscopy (VWR, UV-3100PV), scanning from wavelengths of 700 nm to 600 nm. Following the scan, the aliquot

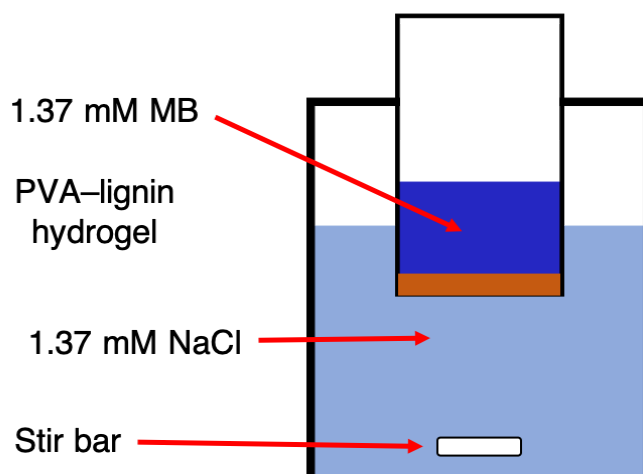


Figure 3.1. Illustrative schematic of permeation cell used for methylene blue (MB) permeation experiments.

was immediately returned to the receiving reservoir. Observed in the UV-vis spectrum, the prominent peak at 662 nm is attributed to MB ions.²⁵⁰ From these data, the permeability of MB ions can be calculated from the following equation:²⁰⁵

$$V_R \frac{dC_R(t)}{dt} = A \frac{P}{L} C_D \quad (3.1)$$

where C_D and $C_R(t)$ are the MB ion concentrations (mol L^{-1}) in the donating and receiving reservoirs, respectively, A and L are the area (cm^2) and thickness (cm) of the membrane, respectively, P is the permeability of MB ions ($\text{cm}^2 \text{s}^{-1}$), and V_R is the volume (L) of the receiving cell. The following assumptions were made in use of this expression: (1) MB permeability is independent of ion concentration; (2) permeation in the membrane is at pseudo-steady state; and (3) the concentration of MB in the donating reservoir remains constant and $C_D \gg C_R(t)$.

3.2.9 Equilibrium Liquid Water Uptake

The equilibrium liquid water uptake of the membranes was determined for each hydrogel by first immersing the hydrogel in RO water for at least 48 h. After 48 h, the hydrogels were removed from the RO water, quickly patted with a KimWipe to remove any liquid water on the membrane surface, and then weighed using an analytical balance (Mettler Toledo ME204E) to obtain the hydrated mass of the hydrogel. To measure the dry weight, the hydrogels were dried at 90 °C for 24 h under dynamic vacuum. After 24 h, the membranes were removed from the oven and quickly weighed using an analytical balance. The equilibrium liquid water uptake for each membrane was calculated using the following equation:

$$\text{Water Uptake} = \left(\frac{W_{\text{wet}} - W_{\text{dry}}}{W_{\text{dry}}} \right) \times 100\% \quad (3.2)$$

where W_{wet} and W_{dry} are the hydrated and dry mass of the hydrogel, respectively.

3.2.10 Characterization of Molecular Weight Between Crosslinks

The molecular weight between crosslinks of the membranes was calculated based on the Peppas-Merrill equation.²⁵¹ The swollen, wet mass of the membranes was determined by first immersing the hydrogel in RO water for at least 48 h. After 48 h, the hydrogels were removed from the RO water, quickly patted with a KimWipe to remove any liquid water on the membrane surface, and then weighed using an analytical balance (Mettler Toledo ME204E) to obtain the hydrated (swollen) mass of the hydrogel. To weigh the

hydrogel in the relaxed state, the hydrogels were dried at 60 °C for 3.75 h under 10 inHg vacuum. After 3.75 h, the hydrogels were quickly weighed to acquire a relaxed membrane mass. Note, due to the fact that the hydrogels were fabricated in DMSO, and not water, this step of the procedure is slightly different than the traditional method reported in literature. The hydrogels were then put back into the oven at 100 °C for 24 h under dynamic vacuum to acquire a mass in the dried state. The following equations were then used to acquire the polymer volume fractions in the swollen ($v_{2,s}$) and relaxed ($v_{2,r}$) state:¹⁹⁸

$$Q = \left(\frac{W_{\text{wet}} - W_{\text{dry}}}{W_{\text{dry}}} \right) \quad (3.3)$$

$$v_{2,s} = \frac{1}{Q \frac{\rho}{\rho_{H_2O}} + 1} \quad (3.4)$$

where Q is the mass swelling ratio, ρ is polymer density, and ρ_{H_2O} is the density of water.

These values were then used in the following Peppas-Merril equation:

$$\frac{1}{M_c} = \frac{1}{M_n} - \frac{\frac{1}{V_1} [\ln(1 - v_{2,s}) + v_{2,s} + \chi v_{2,s}^2]}{\rho v_{2,r} \left[\left(\frac{v_{2,s}}{v_{2,r}} \right)^{\frac{1}{3}} - \frac{1}{2} \left(\frac{v_{2,s}}{v_{2,r}} \right) \right]} \quad (3.5)$$

where M_n is the number average molecular weight of the polymer, χ is the Flory-Huggins parameter and was taken from previous work on PVA–water systems,²⁵² and V_1 is the molar volume of water ($\approx 18 \text{ cm}^3 \text{ mol}^{-1}$).

3.3 Results

3.3.1. Lignin Characterization and Composite Hydrogel Fabrication

The nomenclature for each of the composite hydrogels is summarized in Table 3.1.

Table 3.1. Nomenclature for PVA–lignin composite hydrogels.

Type of lignin	Lignin content	Unfunctionalized (UF) or Functionalized (F)	Nomenclature
UCLs	10 wt %	UF	PVA–UCL–10UF
		F	PVA–UCL–10F
	20 wt %	UF	PVA–UCL–20UF
		F	PVA–UCL–20F
	50 wt %	UF	PVA–UCL–50UF
CBLs	10 wt %	UF	PVA–CBL–10UF
		F	PVA–CBL–10F
	20 wt %	UF	PVA–CBL–20UF
		F	PVA–CBL–20F
	50 wt %	UF	PVA–CBL–50UF

Figure 3.2 shows the proposed reaction schemes and an image of free-standing membranes for neat (or pristine) PVA and the two series of hydrogel composites synthesized in this work. Specifically, Reaction Schematic No. 1 in Figure 3.2a shows the proposed reaction scheme for neat PVA and PVA–lignin composite hydrogels synthesized via thermal crosslinking. As previously mentioned, thermal crosslinking is one route by which dense, free-standing PVA hydrogels can be fabricated.^{56,57} In the schematic of the proposed network structure for these neat PVA hydrogels, the green dots represent the physical

crosslinks between PVA chains created during the thermal crosslinking process. In addition to neat PVA hydrogels, Reaction Schematic No. 1 shows the proposed network structure of the thermally-crosslinked PVA–lignin hydrogels, whereby the unfunctionalized lignins (shown as curved blue lines) remain in the hydrogel via physical entanglements with thermally-crosslinked network of PVA chains. Next, Reaction Schematic No. 2 in Figure 3.2a shows the proposed reaction scheme for PVA–lignin composite hydrogels synthesized via combined thermal and chemical crosslinking with functionalized CBLs and UCLs.^{45,47,58–66} In the schematic, the –OH groups on lignin are colored in blue and the reactive vinyl groups, containing a C=C bond that undergoes free radicalization, are colored in red. Prior to synthesis of the composite hydrogel, the CBLs and UCLs are first functionalized, undergoing an acrylation process that replaces some of the –OH groups on lignin with vinyl groups containing a C=C bond, allowing the functionalized lignins to act as an additional crosslinker in the reaction scheme. In the schematic for the proposed network structure for these PVA–lignin hydrogels, the red dots represent the chemical crosslinks between functionalized lignin chains (shown as curved purple lines). As shown

in the schematic, these composite hydrogels form an IPN of thermally-crosslinked PVA chains and chemically-crosslinked lignin chains.

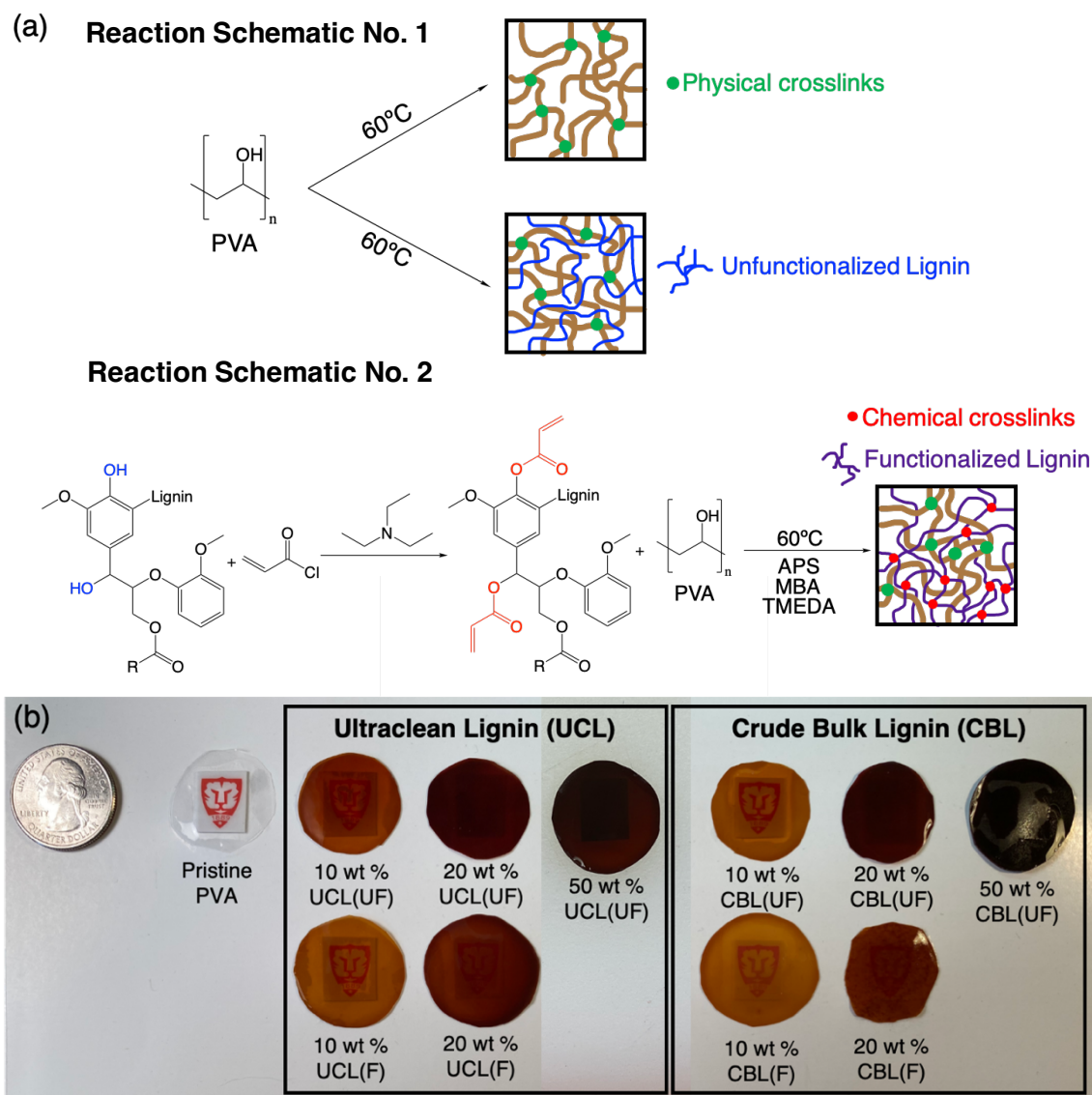


Figure 3.2. (a) Reaction schematic and proposed network structure for thermally-crosslinked, as well as thermally- and chemically-crosslinked PVA–lignin composite hydrogels using both unfunctionalized and functionalized lignin. (b) Picture of free-standing neat PVA and PVA–lignin hydrogels containing 0 wt % to 50 wt % unfunctionalized and functionalized UCLs and CBLs.

As seen in Figure 3.2b, successful fabrication of stable, free-standing, crosslinked PVA hydrogels via both reaction schemes was achieved. Figure 3.2b contains an image of the free-standing hydrogel composite membranes with lignin concentrations ranging from 0 wt % (i.e., neat PVA) to 50 wt % CBLs and UCLs. As seen in Figure 3.2b, the optical properties of the hydrogels change significantly with the introduction of lignin, with membranes becoming less transparent as the lignin content was increased from 10 wt % to 50 wt %. This lack of transparency is most noticeable for PVA–CBL–50UF, where these membranes are almost completely opaque. Note, as shown in Table A.2 in Appendix A, all of the membranes were stable in room temperature water ($\sim 20\text{ }^{\circ}\text{C}$) for >120 days. Further, all membranes remained stable up to a temperature of $40\text{ }^{\circ}\text{C}$ for 4 hours. Above $40\text{ }^{\circ}\text{C}$, for both series of composite hydrogels, the thermal stability of the membranes varied with both functionalization and lignin content. Interestingly, the hydrogels containing unfunctionalized CBL at 20 wt % and 50 wt % remained stable (i.e., did not dissolve or break down) up to temperatures of $80\text{ }^{\circ}\text{C}$ for 24 hours. While degradation (or lack thereof) for these membranes at higher temperatures presents an area of interest, full thermal characterization of these membranes is outside the scope of this investigation, as all mechanical and transport properties were characterized for composite membranes at room temperature ($\sim 20\text{ }^{\circ}\text{C}$).

To ensure the CBLs and UCLs were properly acrylated, both ^1H and ^{31}P NMR were performed on the lignins before and after functionalization. For the sake of conciseness, only the ^{31}P NMR spectra have been presented in this chapter (see Figure A.1 in Appendix A for ^1H NMR data). Figures 3.3a and 3.3b show the ^{31}P NMR spectra of the UCLs and CBLs, respectively, before (dashed blue line) and after (solid red line) acrylation. While the use of ^{31}P NMR may not seem intuitive given the lack of phosphorous groups in lignin, phosphorylation of the $-\text{OH}$ groups in lignin, by reagents such as 2-chloro-4,4,5,5-tetramethyl-1,3,2-dioxaphospholane, is carried out prior to conducting ^{31}P NMR experiments. This process is commonly utilized to quantify the type and amount of hydroxyl groups present in lignins,^{249,253–256} and was therefore employed in our current

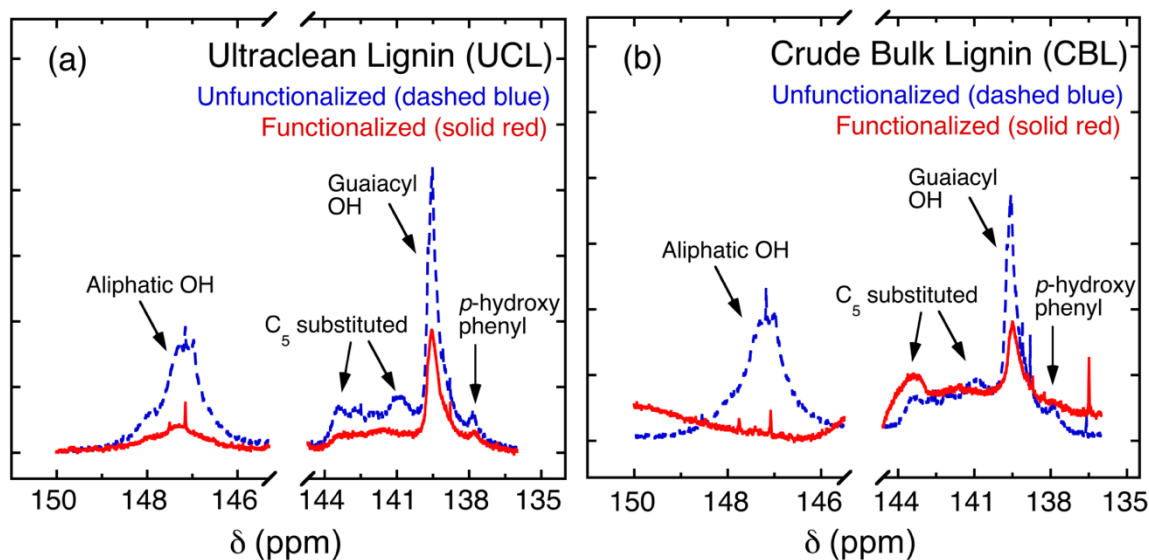


Figure 3.3. ^{31}P NMR spectra of unfunctionalized (dashed blue line) and functionalized (solid red line) (a) ultraclean lignins (UCLs) and (b) crude bulk lignins (CBLs).

work. The broad peak on the left-hand side of each figure is associated with the aliphatic $-\text{OH}$ groups, while the collection of peaks on the right-hand side are associated with the

aromatic –OH groups of the lignins.²⁴⁹ As seen from these two figures, the decrease in height of the NMR spectral peaks indicates that the concentrations of –OH groups on both the UCLs and CBLs have decreased after the lignins underwent acrylation. This is quantitatively shown in Table A.1 of Appendix A, where it can be seen that for both the CBLs and UCLs, the –OH content (mmol OH/g lignin) is lower post functionalization. Further, if we take a deeper look at the –OH contents pre- and post-functionalization, it is apparent that, collectively, a higher degree of functionalization occurred in the UCLs as compared to CBLs. That is, a higher concentration of –OH groups were consumed during acrylation. Specifically, post functionalization, an ~60% decrease in the total –OH content (aliphatic + aromatic) of the UCLs was observed, while only a ~45% decrease was observed for the CBLs. The reactivity difference between these two lignins highlights the lower steric hinderance for the –OH groups in the ultraclean, fractionated UCLs (i.e., there is better access to the –OH groups in the UCLs). Interestingly, relative reactivity of the aliphatic and aromatic –OH groups varied between the CBLs than UCLs, where a higher reactivity of the aromatic –OH groups was observed for the UCLs. To further verify successful functionalization of the lignins, the addition of the C=C bond to the functionalized lignin was confirmed via ¹H NMR (see Figure A.1 in Appendix A).

3.3.2 Separation Performance of the Composite Hydrogels

The aqueous-separation properties of the PVA–lignin composite hydrogels were characterized by performing methylene blue (MB) permeability experiments. For these experiments, the hydrogels were challenged with a high concentration of MB on one side of the membrane, and the concentration of permeated MB in the receiving reservoir – i.e.,

the reservoir on the side of the membrane opposite the MB solution – was measured as a function of time. Figures 3.4a and 3.4b show the results of the MB permeation experiments performed on neat PVA, as well as PVA–lignin hydrogel composites containing both unfunctionalized and functionalized UCLs and CBLs, respectively. More specifically, these two figures show the concentration of MB in the receiving reservoir as a function of time. Note, the time data have been normalized by the square of the thicknesses of the hydrogels so direct comparisons between membranes of different thicknesses can be made. Also note that MB permeation data for PVA–UCL–50UF and PVA–CBL–50UF is not shown in Figure 3.4, as there was never a detectable concentration of MB in the receiving reservoir. That is, membranes with 50 wt % UCL and CBL adsorbed the entire amount of MB loaded in the donating reservoir. Therefore, no permeation analysis was performed on these membranes. In general, a visual inspection of the slopes of these normalized data provide qualitative insight into the relative changes in the MB permeability, where reductions in MB permeability manifest as reductions in the slopes of these data. Interestingly, as seen in Figures 3.4a and 3.4b, an initial ‘lag time’ is observed in the MB permeation data for all PVA–lignin composite hydrogels, where for a period of time, no MB is detected in the receiving reservoir. As this is observed with all lignin-containing composite hydrogels, we believe this initial lag in the permeability data is a direct result of electrostatic interactions between the diffusing MB molecules and the –OH groups of the lignins inside the membranes. In water, MB has a positive charge (i.e., cationic), which results in attractive electrostatic interactions with the phenolic and –OH groups in lignin.

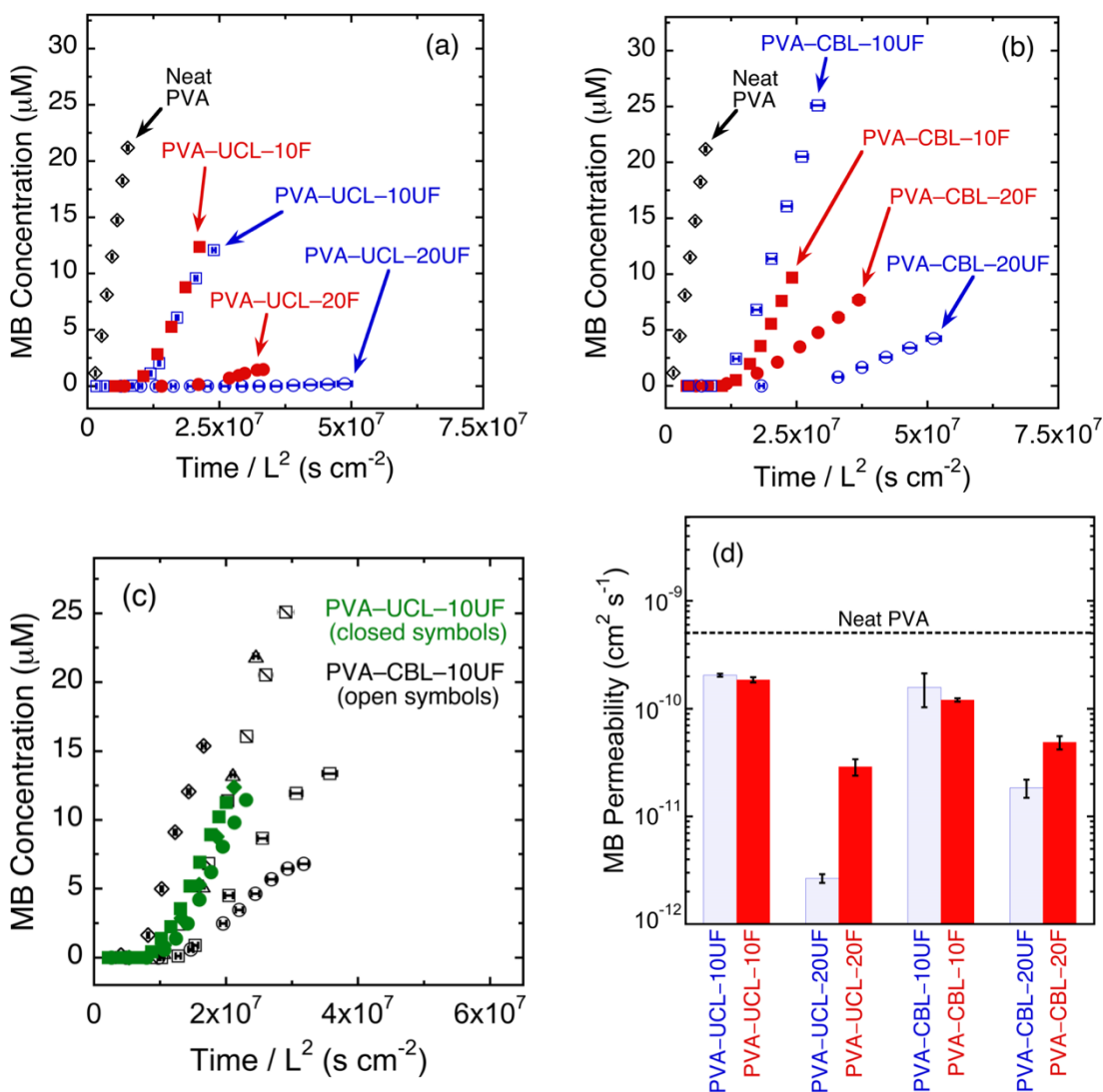


Figure 3.4. Concentration of methylene blue (MB) in the receiving cell as a function of time for neat PVA and PVA membranes containing various amounts of unfunctionalized and functionalized (a) ultraclean lignins (UCLs) and (b) crude bulk lignins (CBLs). Note, the data have been normalized by the square of the membrane thickness. (c) Concentration of MB in the receiving cell as a function of time for PVA membranes containing 10 wt % UCLs (closed green symbols) and CBLs (open black symbols), both unfunctionalized. Each data set is a unique MB permeation experiment on an individual hydrogel sample. Note, some of the data displayed in Figs. 3.4a & 3.4b was reshown in 3.4c, as part of a collection of multiple experiments. (d) Summary of the calculated MB permeabilities for neat PVA and PVA-lignin composite hydrogels. The dashed black line indicates the average MB permeability for neat (or pristine) PVA (i.e., PVA containing no lignin). Note, the error bars in the figure represent the standard deviation of (at least three) repeat experiments.

If we focus our attention on Figure 3.4a, this assertion appears to be further validated by the fact that the length of the initial lag is directly affected by both the amount of UCL in the composite membranes, as well as whether or not the UCL had undergone functionalization. With regards to the concentration of lignin, the time before initial MB breakthrough increased significantly as the UCL concentration in the hydrogel composites was increased from 10 wt % to 20 wt %. Further, it can be seen that this initial lag time is longer for composite membranes containing unfunctionalized UCLs. This is most easily seen when comparing PVA–UCL–20UF (open blue circles) to PVA–UCL–20F (closed red circles) in Figure 3.4a. The trends in these data follow what we would expect, based on the chemistry involved in the lignin functionalization.

As shown in Figure 3.2a (Reaction Schematic No. 2), acrylation of the lignins replaces the –OH groups in the lignins with C=C bonds, ultimately resulting in a lower concentration of –OH groups in the functionalized lignins (see Table A.1 in Appendix A for quantitative hydroxyl content). The lower hydroxyl content should lead to less electrostatic interactions between the diffusing MB and the functionalized lignins, resulting in longer initial lag times in the data for hydrogels containing unfunctionalized lignin versus their functionalized counterpart. This, for the most part, is what we observe in the data for both series of hydrogels containing UCLs and CBLs (open blue circles vs. closed red circles in Figures 3.4a and 3.4b, respectively). For hydrogels containing 10 wt % CBLs, the initial lag times in the data are approximately the same, regardless of lignin functionalization. Interestingly, when we compare the initial lag times for PVA–lignin composites containing unfunctionalized UCLs and CBLs at 20 wt %, we see that the length

of time before which MB is detected on the opposite side of membrane is significantly higher for membranes containing unfunctionalized UCLs. This result is worth noting, as it alludes to the possibility that for composite membranes containing unfunctionalized UCLs, a greater concentration of –OH groups are available (or are accessible) to electrostatically interact with the MB as it diffuses through the composite hydrogel.

While the proposed chemical structures of lignin show numerous –OH groups,²⁵⁷ access to these groups is hindered due to the complex (branched), collapsed structure of the CBLs. Our results appear to indicate that the UCLs have a less collapsed structure (or chemical architecture) inside of the composite hydrogel when compared to the CBLs. That is, the –OH groups in the UCLs are more easily accessible than those in the CBLs, which is more than likely due to the higher steric hindrance of the –OH groups in the higher MW, high dispersity CBLs. The higher concentration of accessible –OH groups on the UCL can be further suggested by the fact that the length of time before MB is measured on the other side of PVA–UCL–20F composite membranes is similar to that of PVA–CBL–20UF membranes (closed red circles vs. open blue circles in Figures 3.4a and 3.4b, respectively). That is, even after the UCLs have undergone functionalization, and quantitatively contain less hydroxyl groups than their unfunctionalized CBL counterparts, there still appears to be a higher degree of electrostatic interactions between the diffusing MB molecules and UCLs in the hydrogels, as compared to those containing CBLs, regardless of lignin functionalization.

To highlight the impact of \bar{D} on the variability of these time-dependent MB concentration data, Figure 3.4c shows the permeated MB concentration as a function of

(normalized) time for PVA–lignin composite hydrogels containing 10 wt % unfunctionalized UCLs (closed green symbols) and unfunctionalized CBLs (open black symbols). From Figure 3.4c, we observe a much higher scatter in the MB permeation data between experiments for composite hydrogels fabricated from unfunctionalized CBLs when compared to those fabricated from unfunctionalized UCLs. Although the average permeabilities of PVA–UCL–10UF ($2.05\text{E}-10 \pm 6.60\text{E}-12$) and PVA–CBL–10–UF ($1.58\text{E}-10 \pm 5.50\text{E}-11$) are not statistically significant from each other, it is evident that the standard deviation for PVA–UCL–10UF was one order of magnitude less than PVA–CBL–10UF with an 88% decrease. We believe this scatter in the permeation data alludes to the possibility that the higher \bar{D} in heterogeneous CBLs results in the fabrication of membranes with more heterogeneous network structures, leading to higher scatter (or variation) in the transport properties extracted from the permeation experiments performed on these membranes. Note, we would like to point out to the reader that acrylate-based networks are inherently heterogeneous,^{258–260} so the lower dispersity of the UCLs may not be the only factor to consider when examining the final heterogeneity of the network structure. However, as seen from Figure 3.4c, even when both samples are fabricated via the formation of acrylate-based networks, the spread in the experimental permeation data between individual experiments is greater for CBL-based networks, as compared to those fabricated with UCLs. While additional experiments are needed to fully validate these claims, this result underscores the potential importance of utilizing well-defined, fractionated lignins of prescribed MWs, as these materials may provide a more robust platform to help elucidate the structure-processing-property relationships in this emerging

class of ‘green’ hydrogels. A quantitative description regarding the impact of the UCL and CBL on the network structure of the composite hydrogels will be presented and discussed later in this section.

Figure 3.4d shows the MB permeability calculated (using eq 3.1 in the Experimental Section) for the PVA–lignin composite hydrogels containing both unfunctionalized and functionalized UCLs and CBLs. Note, as there was an initial lag time in the permeability data before any MB was detected in the receiving cell for PVA–lignin hydrogels, the permeability is extracted from the slope of the data post lag time. That is, the initial lag time was subtracted from the permeability data before the MB permeability was calculated. While this manipulation of the data does not alter the slope of the MB permeability data, the MB permeability calculated (and reported in Figure 3.4d) does not necessarily represent a ‘true’ permeability, as there is an initial period of time where the diffusing MB molecules electrostatically interact with the accessible hydroxyl groups within the composite hydrogel until ‘saturation’ occurs, after which, unassociated MB molecules are allowed to permeate due to the concentration gradient across the membrane. However, we believe the MB permeabilities calculated herein serve as an ‘effective’ MB permeability, and as such, provide insight into how the introduction of lignins, both UCLs and CBLs, alters the permselectivity of the resulting composite membranes.

As seen in Figure 3.4d, the concentration, type, and functionalization of the lignin affected the permeability of MB through the composite hydrogels. The MB permeability for the control membrane (that is, neat PVA) was approximately $5 \times 10^{-10} \text{ cm}^2 \text{ s}^{-1}$. Focusing on PVA–lignin composites containing UCLs, we observe that the introduction of 10 wt %

UCLs results in an approximately 60% reduction in the permeability of MB through the membrane, regardless if the UCLs were functionalized ($5 \times 10^{-10} \text{ cm}^2 \text{ s}^{-1}$ vs. $2 \times 10^{-10} \text{ cm}^2 \text{ s}^{-1}$). This observed decrease is due to the abundant phenolic and hydroxyl groups located within lignin, enhancing adsorption of MB and impeding its ability to permeate through. We observe a more significant decrease in the MB permeability when the concentration of UCLs is increased to 20 wt %. As seen in Figure 3.4d, the introduction of 20 wt % unfunctionalized UCLs resulted in almost a two orders of magnitude reduction in MB permeability. However, while still significant, only an order of magnitude reduction in MB permeability was observed for composite membranes fabricated with functionalized UCLs.

Focusing our attention on PVA–CBL composites hydrogels in Figure 3.4d, we see a similar qualitative behavior for the change in MB permeability with various concentrations of unfunctionalized and functionalized CBLs. With the introduction of 10 wt % CBLs (both unfunctionalized and functionalized), we see a similar reduction in MB permeability as was seen with membranes containing 10 wt % UCLs. That is, with the introduction of 10 wt % CBLs, the MB permeability dropped from a value of approximately $5 \times 10^{-10} \text{ cm}^2 \text{ s}^{-1}$ to approximately $2 \times 10^{-10} \text{ cm}^2 \text{ s}^{-1}$. However, unlike PVA–UCL–20UF membranes, only an order of magnitude reduction in MB permeability was observed with the introduction of 20 wt % unfunctionalized CBLs. Composite hydrogels containing 20 wt % functionalized UCLs and CBLs exhibited similar MB permeabilities ($\sim 3 \times 10^{-11} \text{ cm}^2 \text{ s}^{-1}$). With regards to MB permeability, PVA–UCL–20UF membranes exhibited both the longest initial time lag before MB was detectable in the receiving reservoir (see Figure 3.4a), as

well as the lowest ‘effective’ MB permeability (see Figure 3.4d) of all the membranes investigated.

3.3.3 *Young’s Modulus and Equilibrium Water Uptake*

Next, the mechanical (i.e., Young’s modulus) and hydration (i.e., equilibrium water uptake) properties of the composite hydrogels were investigated. The Young’s moduli and equilibrium water uptake of the hydrogels were measured, and the results of these measurements are summarized in Figures 3.5a and 3.5b, respectively. Note, here the phrase “hydrated Young’s modulus” refers to the Young’s modulus of the hydrogels after the membranes were equilibrated in liquid water for at least 48 hours prior to the measurement. As seen in Figure 3.5a, the Young’s modulus of hydrated neat PVA was approximately 8.5 MPa. Focusing our attention on PVA–UCL composite hydrogels, we observe that, at 10 wt % and 20 wt % lignin concentrations, and independent of lignin functionalization, the stiffnesses of these membranes are consistently lower than that of neat PVA, ranging in reductions of ~5% to ~25%, for PVA–UCL–10F and PVA–UCL–10UF membranes, respectively. An increase in Young’s modulus is finally observed when the UCL content was increased to 50 wt % (i.e., PVA–UCL–50UF), where a ~70% greater modulus than that of neat PVA was measured. In contrast, the stiffnesses of the PVA–CBL membranes, at all concentrations and independent of lignin functionalization, are consistently higher than that of neat PVA, ranging in increases of ~10% to ~40%, for PVA–CBL–20F and PVA–CBL–10F membranes, respectively. Following this same trend, PVA–CBL–50UF membranes exhibited a higher hydrated Young’s modulus, ~40% higher than that of neat PVA. For the most part, we believe that the higher stiffnesses exhibited by membranes

containing CBLs vs. those containing UCLs is primarily due to the higher apparent MW of the CBLs as compared to UCLs (1250 g mol⁻¹ vs. 4170 g mol⁻¹ for UCLs and CBLs, respectively). However, as mentioned above, we measured the highest Young's modulus for PVA-UCL-50UF membranes, so it appears that more than just the absolute MW of the

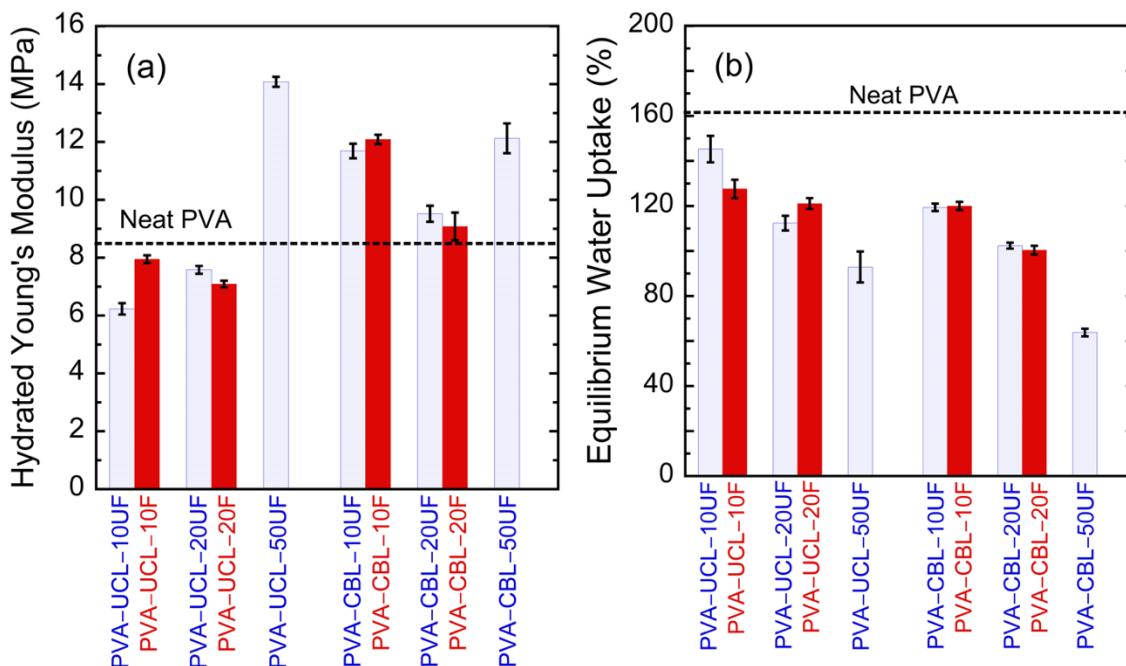


Figure 3.5. (a) Hydrated Young's modulus (that is, Young's modulus of the hydrogel equilibrated in liquid water) and (b) equilibrium liquid water uptake of neat PVA and PVA-lignin composite membranes containing various concentrations of unfunctionalized (light blue bars) and functionalized (solid red bars) UCLs and CBLs. The dashed black lines in (a) and (b) represent the average hydrated Young's modulus and equilibrium water uptake of neat (or pristine) PVA (i.e., PVA containing no lignin), respectively. Prior to both measurements, all hydrogels were hydrated in liquid water for at least 48 hours. Note, the error bars in the figure represent the standard deviation of (at least three) repeat experiments.

lignins is playing a role in the observed moduli for hydrogels containing 50 wt % lignins, potentially related to the lower dispersity of the UCLs. Finally, we see that the stiffness of PVA-CBL membranes initially decreases when the lignin content is increased from 10 wt

% to 20 wt %, but then increases again when the lignin content is further increased to 50 wt %. In conjunction with the permeability results shown in Figure 3.4b, these results highlight how both the mechanical and transport properties of these composite membranes can be tuned, yielding both soft and stiff membranes with significantly reduced permeation of MB.

The reduction in Young's modulus with the addition of UCLs is even more surprising when we look at the equilibrium liquid water uptake values for these membranes. As seen in Figure 4.5b, the water uptake percentages for PVA–lignin membranes containing UCLs range from ~95% to ~145% for PVA–UCL–50UF and PVA–UCL–10UF membranes, respectively. Note, water uptake for neat PVA is ~160%. For the most part, the introduction of UCLs results in a decrease in the equilibrium water uptake in the composite membrane. Even with this reduction in equilibrium water uptake, composite membranes containing 10 wt % and 20 wt % UCLs are softer than neat PVA. In line with the highest hydrated Young's modulus measured for PVA–UCL–50UF, these membranes exhibited the highest reduction in equilibrium water uptake of all composites containing UCLs. Similarly, the introduction of CBLs to the PVA membrane results in a decrease in the equilibrium liquid water uptake of the resulting composite membranes. Specifically, the water uptakes ranged from ~65% to 120% for the PVA–CBL–50UF and PVA–CBL–10F membranes, respectively. As the hydrated stiffness of these membranes, in some cases, increased by ~50%, it is not surprising that the equilibrium water uptake in these membranes is less than that of neat PVA. However, we must note that even when the equilibrium water uptake values between UCL and CBL membranes were similar, these

membranes exhibited drastically different Young's moduli. For example, comparing PVA–UCL–10F to PVA–CBL–10F, we observe that the water uptake values for these membranes are ~120%, though there is almost a 50% increase in Young's modulus when the UCLs are replaced by the CBLs. This result underscores that the introduction of UCLs and CBLs into the hydrogel is resulting in drastically different effects on the formation of the corresponding network structure.

3.3.4 Network Structure of the Composite Hydrogels

To gain insight into how the introduction of lignin changes the network structure of the composite hydrogels, the molecular weight between crosslinks, M_c , was calculated for each membrane. The results of this analysis are shown in Figure 3.6. Note, the dashed black line in Figure 3.6 represents the average M_c of neat PVA (i.e., PVA containing no lignin), which was calculated to be $\approx 800 \text{ g mol}^{-1}$. As seen in Figure 3.6, the M_c of the composite hydrogels varies drastically with increasing lignin concentration, and for hydrogels containing UCLs, is seen to depend on whether the composite hydrogels contained functionalized UCLs. In general, the M_c is seen to decrease as the lignin content is increased from 10 wt % to 50 wt %. Most notably, PVA–UCL–20UF, PVA–UCL–50UF, both PVA–CBL–20UF and PVA–CBL–20F, and PVA–CBL–50UF membranes all exhibit similar values of M_c ($\approx 400 \text{ g mol}^{-1}$), which is $\approx 50\%$ lower than that of neat PVA. Interestingly, for composites containing CBLs, the calculated M_c does not change appreciably once the lignin content reaches 20 wt %, regardless of whether the lignin has undergone functionalization. We also observe that the functionalization of the UCL has a significant effect on the M_c , where this value is seen to decrease with increasing unfunctionalized UCL content. For composite hydrogels

containing functionalized UCLs, the M_c for PVA-UCL-10F and PVA-UCL-20F are similar, where the average M_c is seen to increase from $\approx 600 \text{ g mol}^{-1}$ to $\approx 650 \text{ g mol}^{-1}$ when the concentration of functionalized UCL is doubled. In contrast, the average M_c is seen to

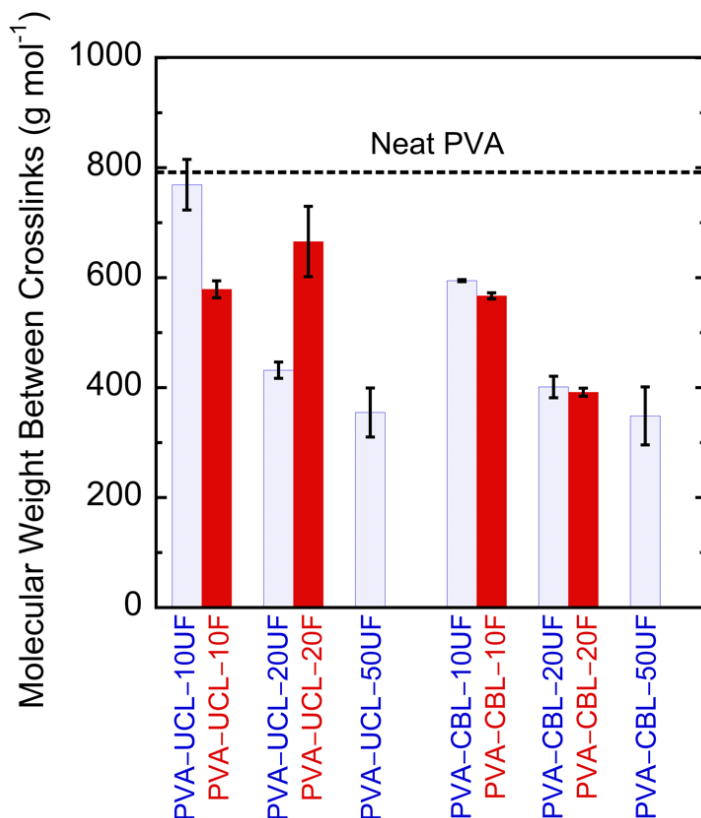


Figure 3.6. The molecular weight between crosslinks, M_c , of pristine PVA and PVA-lignin composite membranes containing various concentrations of unfunctionalized (light blue bars) and functionalized (solid red bars) UCLs and CBLs. The dashed black line represents the average M_c of neat (or pristine) PVA (i.e., PVA containing no lignin). Note, the error bars in the figure represent the standard deviation of (at least three) repeat experiments.

decrease from $\approx 770 \text{ g mol}^{-1}$ to $\approx 400 \text{ g mol}^{-1}$ when the concentration of unfunctionalized UCL is doubled, though as mentioned previously, the calculated M_c does not change appreciably when the concentration of unfunctionalized UCL is increased from 20 wt % to 50 wt %.

In general, the observed changes in the M_c between the various composite hydrogels correlate with the observed reductions in MB permeabilities shown in Figure 3.4d. First, with the exception of PVA–UCL–10UF, the calculated M_c for the composite hydrogels are lower than that of neat PVA, where, as seen in Figure 3.4d, all composite hydrogels containing lignins exhibited lower MB permeabilities. Second, with the exception of PVA–UCL–20F, lower values of M_c were calculated for hydrogels containing 20 wt % UCLs and 20 wt % CBLs than those calculated for their 10 wt % counterparts, where lower MB permeabilities were observed for composite membranes containing 20 wt % UCLs and CBLs. However, the trends in the MB permeability data cannot be completely correlated to changes in the M_c between samples, as little change in the average M_c is observed when the lignin content was increased to 50 wt %, even though no MB was seen to permeate across hydrogels containing 50 wt % lignins. This result supports the notion that transport of MB molecules is governed by a combination of electrostatic interactions between the charged MB molecules and the lignin inside the composite hydrogels. However, in general, composite hydrogels containing 50 wt % lignin exhibited the highest Young’s modulus and lowest equilibrium water uptake, which correlates well with the low values of M_c calculated for these membranes. Note, while these initial calculations of M_c obtained through swelling measurements provides a ‘rough’ picture of how the network structure changes with lignin content, obtaining independent calculations of the effective mesh size via mechanical indentation and neutron scattering is ongoing and the focus of our ongoing future work.

3.4 Conclusions

In conclusion, we have synthesized free-standing PVA–lignin composite hydrogels containing various concentrations of unfunctionalized and functionalized UCLs and CBLs, where ‘proof-of-concept’ membranes containing as high as 50 wt % unfunctionalized lignins were fabricated. Successful functionalization of the lignins with vinyl-containing acrylate groups was confirmed by a combination of ^1H and ^{31}P NMR spectroscopy, where a higher reactivity of the $-\text{OH}$ groups in the fractionated UCLs was quantitatively observed. All composite hydrogels were shown to exhibit superior MB separation performance when compared to neat PVA. Additionally, an initial breakthrough time in the permeation data was observed for all composite hydrogels, which was attributed to the electrostatic interactions of the diffusing MB with the lignin inside the composite hydrogels. The length of this breakthrough time was seen to be a function of both the functionalization and type of lignin from which the composite membranes were fabricated. Longer initial breakthrough times were observed for membranes containing 20 wt % lignin, where the longest breakthrough time was observed for PVA–UCL–20UF membranes ($\sim 4 \times 10^7 \text{ s cm}^{-2}$). In contrast, the shortest breakthrough time was observed for composite membranes containing 10 wt % lignin ($\sim 1 \times 10^7 \text{ s cm}^{-2}$), both for membranes containing UCLs and CBLs and irrespective of functionalization. Notably, for permeation experiments for composite hydrogels containing 50 wt % unfunctionalized lignins, no MB was ever detected in the receiving reservoir, indicating that all of the MB in the donating reservoir was adsorbed by the composite hydrogel.

While all composite membranes exhibited significantly reduced MB permeability when compared with neat PVA, an over two order of magnitude reduction in MB permeability was observed for PVA–UCL–20UF membranes ($\sim 5 \times 10^{-10} \text{ cm}^2 \text{ s}^{-1}$ vs. $\sim 2 \times 10^{-12} \text{ cm}^2 \text{ s}^{-1}$). The Young's moduli of the composite hydrogels fabricated with UCLs were consistently lower than that of the neat PVA. However, when the lignin concentration was increased to 50 wt % (PVA–UCL–50UF), a 70% increase in Young's modulus was observed. In contrast, the Young's moduli for membranes containing CBLs were consistently higher than that of the neat PVA hydrogels (over 50% in some cases). With the exception of the PVA–UCL–10UF membranes, the equilibrium liquid water uptake of the composite membranes was consistently lower than that of neat PVA. Notably, the equilibrium water uptake of the neat PVA ($\sim 160\%$) was most significantly suppressed for PVA–CBL–50UF membranes ($\sim 64\%$). Finally, the concentration and functionalization of the lignins was seen to have a direct impact on the network structure of the soft composites, where in general, the molecular weight between crosslinks is seen to decrease with increasing lignin concentration. Results from this work highlight how lignin MW, dispersity, and functionality can be used to fabricate composite hydrogels that span a broad landscape of mechanical and transport properties. Furthermore, results from this work underscore the importance of utilizing well-defined (i.e., low \bar{D}) lignins in the fabrication of these hydrogels, as they allow for a direct, systematic approach to elucidating the structure-processing-property relationships in this emerging class of 'green' composite materials.

CHAPTER FOUR

ENHANCED MECHANICAL PROPERTIES OF COMPOSITE HYDROGELS CONTAINING FRACTIONATED AND PURIFIED LIGNIN

Gregorich, N.; Kanhere, S.; Stutts, J.; Bethel, K.; Tindall, G.; Lynn, B.; Ogale, A. O.; Thies, M. C.; Davis, E. M. Enhanced Mechanical Properties of Composite Hydrogels Containing Fractionated and Purified Lignin. *ACS Appl. Polym. Mater.* **2022**, *X*, XXXX-XXXX.

4.1 Introduction

Due to their high hydrophilicity and tunable mechanical properties, which are directly influenced through manipulation of the network structure (i.e., mesh size), hydrogels have shown promise in a broad range of fields, particularly separations,^{13,261} drug delivery,²⁰ and tissue engineering.²⁷ Various approaches have been applied to alter the network structure, including manipulation of the reaction pathway,⁴⁰ crosslinker/initiator concentration,¹⁹ molecular weight (MW) of the host polymer,⁴⁷ and synthesis temperature.²¹ For example, PVA, a hydrogel utilized in biomedical and water purification applications, can be synthesized via thermal crosslinking,⁵⁶ chemical crosslinking,^{58,64} or a combination of both.^{60,67} Another common, less chemically invasive fabrication method of manipulating the network structure of PVA hydrogels is referred to as the “freeze-thaw method,” which induces physical crosslinks between PVA chains through sequential cycles between temperatures of <273K and >293K.⁶⁸ For chemically-crosslinked PVA films, covalent crosslinks between chains are achieved through the use of crosslinking agents such as glutaraldehyde (GA)^{47,58,61} or various acids (e.g., citric acid).⁴⁵ When GA is used to fabricate chemically-crosslinked PVA membranes, hydroxyl (–OH) groups along the PVA chains are consumed during the crosslinking process (i.e., condensation reaction). Further,

the consumption of –OH groups during fabrication can be leveraged as a means of altering the hydrophilicity of the resulting crosslinked membrane.⁶⁴

However, the synthesis of traditional hydrogels implements host polymers (e.g, PVA) that require the use of petroleum-based precursors (e.g., ethylene). As such, increased interest in fabricating soft composites from environmentally friendly, renewable biopolymers has grown. Many hydrogel studies have investigated how the incorporation of renewable biopolymers such as chitosan,³⁸ cellulose,⁸⁵ and lignin^{33,87,89,155,176} impact the mechanical and transport properties of the resulting “green” soft composites. As lignin, a by-product of biomass processing, is the world’s second most abundant natural polymer (behind only cellulose),^{87,173,211} this biopolymer presents an opportunity to substantially reduce the use of petroleum-based products in the fabrication of next-generation polymers.²¹³ In addition to its high abundance, lignin also exhibits numerous inherent properties, including high ultra-violet (UV) light absorption,¹⁰³ high thermal stability,¹⁰⁵ and antioxidant¹⁰⁶ and antimicrobial properties.¹⁰⁹ Further, lignin contains an abundance of hydroxyl groups that creates avenues for various chemical functionalizations¹¹⁰ and direct crosslinking, although access to these groups is not straightforward as a result of a highly complex and obfuscated structure.^{105,111}

Incorporating lignin into composite materials has been demonstrated as a viable means of altering the mechanical properties of resulting composite materials.^{89,105,155,159,160,218,262} Specifically, improvements to the Young’s^{159,160} and storage moduli,^{89,155,160} as well as the ultimate tensile strength¹⁵⁵ and toughness¹⁶¹ have been observed with the introduction of lignin, even at small lignin contents. For example, recent work by Oveissi et al.¹⁵⁹

demonstrated a 75% increase in Young's modulus (from 1.29 MPa to 2.26 MPa) with the addition of only 2.5 wt % lignin to their polyether-based polyurethane hydrogels. Additionally, work by Rajan et al.⁸⁹ showed that incorporating lignin into their crosslinking process led to a three orders of magnitude increase in the storage modulus of their 2-hydroxyethyl methacrylate (HEMA) hydrogels. While the introduction of lignin has led to improved mechanical properties in many different hydrogel materials, to date, the lion's share of studies involving the synthesis of lignin-based hydrogels involve fabrication methods that utilize lignin with high dispersity (\bar{D}).^{89,176} For example, recent work by Saito et al.²⁶³ employed a process where hardwood lignin was first fractionated with methanol and then crosslinked with formaldehyde, increasing the number-average MW of lignin from 1,840 g mol⁻¹ to 31,000 g mol⁻¹. Although the fractionation-crosslinking process effectively demonstrated a 228% increase in storage modulus in lignin-polybutadiene copolymers, this process only marginally reduced the \bar{D} of the hardwood lignin (in this case, from 122 to 20).

Current recovery methods indiscriminately precipitate lignin out of solution, leading to a final product with broad MW distributions (i.e., high \bar{D})¹⁰⁵ and high metals content (~1–2 wt %, primarily composed of sodium and potassium salts). These impurities can pose a risk for health or product contamination as these salts can leach out of the lignin-containing composite into an expensive product stream or the human body.¹¹⁸ Consequently, the development of lignin-based hydrogels for various applications is hindered by our limited understanding surrounding the role of lignin MW and purity in the formation of the network structure of the resulting hydrogel composite. Fortunately, recent work by Thies

and co-workers^{118,173,174} on the fractionation and purification of lignin presents a viable avenue for obtaining lignin of well-defined MWs and low Đ. The lignin purification procedure, referred to as the Aqueous Lignin Purification with Hot Agents (ALPHA) process,¹⁷⁵ continuously purifies, fractionates, and solvates lignin into various cuts of controlled MWs, narrow dispersity (i.e., Đ ≈ 2) and low metals contents (i.e., as low as 50 ppm).¹¹⁸ While several studies have fabricated composite membranes using fractionated lignin,^{264–266} the ALPHA process is unique among lignin fractionation processes due to its relatively low solvent usage and formation of two liquid phases. The absence of solids allows for the process to easily be made continuous and subsequently scaled.¹⁷³ Furthermore, the ALPHA process is more environmentally friendly as it uses only renewable solvents (i.e., water and acetic acid). Finally, previous techno-economic analysis (TEA) efforts on similar ALPHA-based separation and application schemes have resulted in an overall cost for producing the lignin fractions as low as \$0.45 per kg of lignin.²⁶⁷

Recent work by our group highlighted how the various lignin fractions, and thus various lignin MWs, can be leveraged to systematically tune the properties of physically crosslinked lignin–PVA soft composites synthesized via the freeze-thaw method,²⁶⁸ which have potential applications as materials for wound dressings due to the inherent antimicrobial/antioxidant properties of the lignin.^{106,109} In another investigation, fractionated lignin from the ALPHA process was also used to synthesize thermally and chemically crosslinked lignin–PVA soft composites for use in membrane-based water purification applications.²⁶⁹ For example, in that particular study, the incorporation of fractionated lignin resulted in soft composites that, most notably exhibited: (i) increased

Young's moduli and (ii) an over two orders of magnitude reduction in the permeability of a model organic dye, methylene blue. This work also underscored the importance of incorporating lignin of narrow MW dispersity to achieve more consistent network structures, which was evidenced by the lower variability between repeat measurements of soft composites fabricated with fractionated lignin (when compared to those fabricated using raw, unfractionated lignin).

Additionally, for the aforementioned lignin-based soft composites synthesized via the freeze-thaw method, hydrogels fabricated with unfractionated lignin had ill-formed, disrupted network structures. This led to membranes with unpredictable water uptake properties (i.e., hydrophilicity), illustrating the importance of fine control of lignin-precursors in soft composite fabrication. Further, it has recently been demonstrated that the incorporation of lignin fractionated via the ALPHA process resulted in a significant increase to the mechanical properties of dry-spun lignin-based carbon fibers.²⁷⁰ Specifically, increasing the precursor lignin molecular weight helped facilitate stable dry-spinning, which in turn helped to produce thinner precursor fibers that resulted in carbon fibers with over 30% increase in both tensile strength and modulus. Additionally, it has been shown that the storage modulus of lignin-based thermoset polymers can be increased by increasing the lignin molecular weight.²⁷¹ Such material systems containing well-defined lignin allow us to elucidate fundamental relationships between lignin molecular weight, resulting hydrogel network structure, and the resulting mechanical properties.

In this work, two series of PVA–lignin composite hydrogels containing both unfractionated and fractionated lignin, at concentrations ranging from 0 wt % to 40 wt %,

were synthesized. These soft composites were fabricated using both BioChoice™ lignin (BCL – apparent weight-average molecular weight $M_{W,app} \approx 16,100 \text{ g mol}^{-1}$, $\bar{D} \approx 3.9 \pm 0.2$) along with low and high MW fractions of lignin (Low MW – apparent weight-average molecular weight $M_{W,app} \approx 3,900 \text{ g mol}^{-1}$, $\bar{D} \approx 3.2 \pm 0.3$; and High MW – apparent weight-average molecular weight $M_{W,app} \approx 25,400 \text{ g mol}^{-1}$, $\bar{D} \approx 3.1 \pm 0.2$), which were isolated from the aforementioned BCL via the ALPHA process. PVA–lignin hydrogel composites were crosslinked via a condensation reaction involving GA under acidic ($\text{pH} \approx 3$) conditions. After fabrication, various mechanical properties of the soft composites were characterized. Specifically, the compressive Young’s moduli (E) for all hydrated composites were characterized using mechanical indentation. Further, to better understand stress-strain properties of these materials, ultimate tensile strength testing was performed on the hydrated soft composites. Finally, dynamic mechanical analysis was performed to acquire a storage modulus (E') for each soft composite, which was then used to determine the molecular weight between crosslinks (M_C). Results from this work underscore the importance of utilizing well-defined lignin in hydrogel composites to better understand the fundamental structure-process-property relationships in this emerging class of “green” materials.

4.2 Experimental Section

4.2.1 Materials

Dimethyl sulfoxide (DMSO) (ACS reagent, $\geq 99.9\%$), glutaraldehyde (GA) (50 wt % in H_2O), sulfuric acid (ACS reagent, 95.0-98.0%), Chloroform-D1 (deuteration degree

min. 99.8% for NMR spectroscopy (stabilized with silver) MagniSolv™), 2-Chloro-4,4,5,5-tetramethyl-1,3,2-dioxaphospholane (TMDP) (95%), Chromium(III) acetylacetonate (99.99% trace metals basis) were purchased from Sigma Aldrich. Pyridine (99+%, extra pure), N-hydroxy-5-norbornene-2,3-dicarboximide (99.0+%, TCI America™) was purchased from Fisher Scientific. N,N-dimethylformamide (DMF) (VWR, ≥99.9%, HiPerSolv CHROMANORM® for HPLC) was purchased from VWR. Poly(vinyl alcohol) ($M_w = 25,000 \text{ g mol}^{-1}$, 98% hydrolyzed) (PVA) was purchased from Polysciences, Inc. Kraft lignin (BCL – apparent weight-average molecular weight $M_{w,app} \approx 16,100 \text{ g mol}^{-1}$, $\text{Đ} \approx 3.9 \pm 0.2$), was obtained from BioChoice™. From this Kraft lignin, ultra-pure lignin fractions (Low MW – apparent weight-average molecular weight $M_{w,app} \approx 3,900 \text{ g mol}^{-1}$, $\text{Đ} \approx 3.2 \pm 0.3$; and High MW – apparent weight-average molecular weight $M_{w,app} \approx 25,400 \text{ g mol}^{-1}$, $\text{Đ} \approx 3.1 \pm 0.2$), were produced continuously via the Aqueous Lignin Purification with Hot Agents (ALPHA) process,¹¹⁸ developed by the Thies Group at Clemson University. Note, these differences in Đ are statistically significant with a two-tailed p-value of 0.0167 in a 95% confidence interval. Briefly, the High MW lignin was isolated from the BCL using a 75 wt % acetic acid–water solution at 95 °C, with a solvent-to-feed ratio of 6:1 (by mass). Note, the High MW lignin of interest was isolated from the lignin-rich phase. The Low MW lignin was isolated from the BCL using a 40 wt % acetic acid–water solution at 70 °C, with a solvent-to-feed ratio of 6:1 (by mass). Note, the Low MW lignin of interest was isolated from the solvent-rich phase. The Low MW lignin was then precipitated from the solvent-rich phase as a solid by adding deionized (DI) water in a 1:1 (v/v) ratio. Reverse osmosis (RO) water (resistivity $\approx 18 \text{ M}\Omega\cdot\text{cm}$) was used for all

experiments. Of mention, the hydroxyl content of the lignin MW fractions has no impact on the ALPHA process. As seen in Table B.1 in Appendix B, the hydroxyl contents of Low and High MW are very similar in value.

4.2.2 Characterization of Molecular Weight of Lignin

The molecular weights of the Low MW, High MW and BCL lignin were determined using gel permeation chromatography (GPC) and multiangle light scattering (MALS). Fluorescence from lignin is mitigated in light scattering measurements using a 785 nm incident laser along with bandwidth filters installed between the sample and the detectors. Dried lignin samples were analyzed via GPC with multiangle light scattering (MALS) (DAWN—Wyatt Technologies) being used for absolute weight average molecular weight (Mw) and refractive index (RI, Optilab-WREX-08) being used for concentration. Separation was performed using Styragel (Waters, HT5 WATO-44214) and Polargel-L (Agilent, PL1117- 6830) columns in series, using HPLC-grade DMF containing 0.05 mol L⁻¹ LiBr as the mobile phase at a flowrate of 0.6 mL min⁻¹. Samples were then prepared by dissolving lignin in the mobile phase at a concentration of 1.5 mg mL⁻¹. After complete dissolution, the samples were passed through a 0.20 µm PTFE syringe filter prior to analysis. The concentration of lignin, measured via ultraviolet-visible spectroscopy, remained constant before and after filtration. Thus, only a negligible amount of lignin was removed during filtration.

4.2.3 Nuclear Magnetic Resonance Spectroscopy

Characterization of the hydroxyl content for all lignin was performed using ^{31}P nuclear magnetic resonance (NMR) analysis on a Bruker NEO 500 MHz spectrometer equipped with a Bruker SmartProbeTM. This method was developed from previous work done by Pu et al.²⁵³ and Wang et al.²⁷² The solutions for dissolving lignin were prepared from the following: (1) 1:1.6 v/v of deuterated chloroform: pyridine, (2) 22 mg mL⁻¹ of N-hydroxy-5-norbornene-2,3-dicarboximide (internal standard), and (3) 6 mg mL⁻¹ of chromium (III) acetylacetonate. First, 30 mg of vacuum dried lignin was placed into a 4 mL amber vial with a polytetrafluoroethylene (PTFE) lined cap. Next, 400 μL of (1) were added to the amber vial along with 200 μL of dimethylformamide (DMF), 100 μL of (2) and 100 μL of (3). The amber vials were capped and subject to vortexing for ~ 2 min and then sonicated until no solids were present (as long as overnight). Addition of the phosphorylation agent took place in a nitrogen atmosphere where 100 μL of 2-chloro-4,4,5,5-tetramethyl-1,3,2-dioxaphospholane (TMDP) was added to the vial. The vial was then capped and shaken by hand for one min before transferring the solution to a 5 mm NMR tube (Wilmad Thin Walled High Throughput, 7 in). Upon phosphorylation, measurements were performed within 10 min using an inverse-gated decoupled pulse program with parameters set for a 25 s delay, 1.2 s acquisition time, and a total of 64 scans. All spectra were phased and a linear baseline correction was applied using Bruker TopSpin. Of interest to this investigation were NMR peaks corresponding to the internal standard ($\delta = 152\text{--}151.6$ ppm), along with aliphatic ($\delta = 150.0\text{--}145.0$ ppm), syringyl ($\delta = 144.4\text{--}142.4$ ppm), guaiacyl ($\delta = 142.4\text{--}141.5, 140\text{--}138.8$ ppm), p-hydroxyphenyl ($\delta = 138.5\text{--}137.0$ ppm),

and carboxylic acid ($\delta = 135.6\text{--}134.0$ ppm) hydroxyl ($-\text{OH}$) groups.^{273,274} Note, the characteristic peak at a chemical shift of 132.2 ppm represents the reaction of TMDP-water and served as the reference peak.

4.2.4 Lignin Hydrogel Synthesis

A solution of PVA and DMSO was produced by dissolving PVA in DMSO at 12% w/w for 6 h at 60 °C. The lignin (both BioChoice™ and ultra-pure, fractionated lignin) were dried in a room temperature oven under dynamic vacuum for 24 h. Note, to prevent thermal crosslinking of the lignin prior to their use in the fabrication procedure, the lignin was not dried at elevated temperatures (i.e., were not dried above 60 °C). After drying, a prescribed amount of lignin was added to DMSO and mixed until the lignin was fully dissolved, creating a dark black solution. The lignin–DMSO solution was then added to the PVA–DMSO solution, creating PVA–lignin–DMSO solutions at various lignin loadings (25 wt %, and 40 wt % relative to the mass of PVA) and was stirred for 5 min to ensure homogeneous mixing of the two solutions. 1 mol L⁻¹ H₂SO₄ was then added to the PVA-lignin-DMSO solution until the pH \approx 3. To measure the pH of the solution, a Mettler Toledo SevenCompact™ pH/Ion s220 meter with a Mettler Toledo InLab Science pH Electrode was used. After 5 min of stirring, the solution was brought into a nitrogen atmosphere (Cleatech Isolation Glove Box 2100-2-B) where GA was added to the solution in varying concentrations (1.5 wt % and 3 wt %). After 5 min of stirring, the solution was removed from the nitrogen atmosphere and cast onto a polytetrafluoroethylene (PTFE) dish and placed into an oven under partial static vacuum at 60 °C for 36 h or until all DMSO was removed, creating a robust, free-standing film. To remove any residual DMSO, the

hydrogels were subjected to multiple rinse-soak cycles with RO water whereby water is removed and replaced daily (for multiple days) after initial completion of fabrication. Once fabricated, all composite hydrogels were stored in RO water at room temperature ($\approx 20\text{ }^{\circ}\text{C}$) until they were used in experiments.

4.2.5 Characterization of Ultimate Tensile Strength (UTS)

The ultimate tensile strength (UTS) of the films was measured via tensile testing using an ATS Universal 900 machine, with a crosshead speed of 2.5 mm min^{-1} . Hydrated hydrogel composite films were cut into dog-bone shaped specimens with dimensions of 25 mm length and 10 mm width and mounted between paper tabs to protect films from damage due to pneumatic grips.

4.2.6 Dynamic Mechanical Analysis (DMA) Experiments

Dynamic mechanical analysis was performed by cutting the hydrated composite films into dimensions that were 10 mm long and 6.3 mm wide. The films were then mounted in tensile fixture of the RSA-3 dynamic mechanical analyzer (TA instrument; New Castle, DE). Dynamic frequency sweep measurements were conducted at room temperature from 0.1 rad s^{-1} to 100 rad s^{-1} . Note, a damp KimWipe was loosely wrapped around the hydrated membrane to ensure they remained hydrated during the entire duration of the test. A force-gap test was conducted on each sample to determine the strain and force used for auto-tension during dynamic frequency sweep.

4.2.7 Characterization of Molecular Weight Between Crosslinks

Using data from the DMA tests, the molecular weight between crosslinks (M_c) of the hydrated membranes was calculated using the following equation¹⁸³

$$M_c = \frac{\rho RT}{G'} \quad (4.1)$$

where ρ is the density of the hydrogel measured via mass in its dry state, and volume in hydrated state. R is the universal gas constant, T is temperature of the DMA measurements (room temperature, ≈ 25 °C), and G' is the shear modulus of the hydrogels. The shear modulus of each hydrogel was calculated from the following equation^{179,180,184}

$$G' = \frac{E'}{2(1 + \nu)} \quad (4.2)$$

where E' is the storage modulus and ν is the Poisson's ratio, which was assumed to be 0.5 for all hydrogels.¹⁸⁵ Note, the density of the hydrated hydrogel was obtained in the following manner: (1) making use of a die punch, each hydrogel was cut into a disc with a diameter of 0.5625 in and placed in RO water; (2) after being immersed in RO water for at least 24 h, the membranes were removed, quickly patted with a KimWipe to remove any liquid water on the membrane surface. Next, the mass (using an analytical balance; Mettler Toledo ME204E) and thickness (using a digital micrometer; Mahr Digital Indicator, 1086 R) of the hydrogel were obtained. The mass of water in the hydrogel was then subtracted

from this hydrated mass to acquire the mass of the hydrogel in dry state. With this information, the density of the hydrogel was determined.

4.2.8 Mechanical Indentation Experiments

Hydrated compressive Young's modulus measurements, based on the JKR (Johnson-Kendall-Roberts) theory of adhesion,²⁴⁶ were conducted using a custom-built mechanical indentation apparatus. The setup consisted of a high-resolution linear actuator (M-230.25, Physike Intrumente) and mercury servo controller (C-863.11, Physike Intrumente) connected to a S-beam load cell (Futek LSB200, FUTEK Advanced Sensor Technology, Inc) with a rigid glass indenter of radius of curvature $R = 3.308$ mm. The linear actuator was mounted to a high-performance linear stage with 46 mm of travel range (M433, Newport). A custom program designed in LabVIEW was used to acquire load and indenter height data as a function of time from the S-beam load cell and the linear actuator, respectively, during all indentation experiments. For these experiments, the indenter was lowered at a speed of $2 \mu\text{m s}^{-1}$ until the indenter contacted the swollen hydrogel. Upon contact, the indenter velocity increased to $4 \mu\text{m s}^{-1}$ until a prescribed load of 29.4 mN was reached, after which the indenter was retracted from the sample. Using Hertz's solution for spherical indentation, a solution to Hooke's law was used to acquire Young's modulus.¹⁹¹ Note, prior to beginning all indentation experiments, the membranes were equilibrated in liquid water for at least 48 h.

4.2.9 Equilibrium Liquid Water Uptake

The equilibrium liquid water uptake of the membranes was determined for each hydrogel by first immersing the hydrogel in RO water for at least 48 h. After 48 h, the hydrogels were removed from the RO water, quickly patted with a KimWipe to remove any liquid water on the membrane surface, and then weighed using an analytical balance (Mettler Toledo ME204E) to obtain the hydrated mass of the hydrogel. To measure the dry weight, the hydrogels were dried at 80 °C for 24 h under dynamic vacuum. After 24 h, the membranes were removed from the oven and quickly weighed using an analytical balance. The equilibrium liquid water uptake for each membrane was calculated using the following equation:

$$\text{Water Uptake} = \left(\frac{W_{\text{wet}} - W_{\text{dry}}}{W_{\text{dry}}} \right) \times 100\% \quad (4.3)$$

where W_{wet} and W_{dry} are the hydrated and dry mass of the hydrogel, respectively.

4.2.10 Scanning electron microscopy (SEM) imaging

The network structure of the swollen hydrogels was characterized using two variable-pressure scanning electron microscope systems (Hitachi SU-5000 and Hitachi SU-6600) and a high-pressure system (Hitachi Regulus 8230). Prior to preparing the samples for imaging, the membranes were hydrated in DI water for at least 48 h. Next, the swollen hydrogels were frozen into a block of ice and lyophilized. The hydrogels were freeze-dried for 24 h at -105 °C (using a Labconco FreeZone freeze dryer). Prior to inserting samples

into the SEM, the samples were attached to an aluminum specimen holder by conductive adhesive tape and sputter-coated with a thin layer of platinum (approximately 30 Å) using an Anatech LTD Hummer 6.2 sputtering system. SEM was performed under high pressure with an accelerating velocity of 10 kV, variable spot size, and variable working distance depending on the sample.

4.3 Results and Discussion

4.3.1 Soft Composite Nomenclature and Fabrication

The nomenclature for each of the composite hydrogels is summarized below in Table 4.1. This nomenclature will be used to differentiate samples in both the text and figures moving forward.

Table 4.1. Nomenclature for neat PVA and PVA–lignin composite hydrogels.

Lignin Fraction	Lignin Content	Glutaraldehyde Content	Nomenclature
Neat PVA (no lignin)	0 wt %	1.5 wt %	Neat–1.5
	0 wt %	3.0 wt %	Neat–3.0
Low MW	25 wt %	1.5 wt %	Low–25–1.5
	25 wt %	3.0 wt %	Low–25–3.0
	40 wt %	1.5 wt %	Low–40–1.5
	40 wt %	3.0 wt %	Low–40–3.0
BioChoice™.* (BCL)	25 wt %	1.5 wt %	BCL–25–1.5
	25 wt %	3.0 wt %	BCL–25–3.0
	40 wt %	1.5 wt %	BCL–40–1.5
	40 wt %	3.0 wt %	BCL–40–3.0
High MW	25 wt %	1.5 wt %	High–25–1.5
	25 wt %	3.0 wt %	High–25–3.0
	40 wt %	1.5 wt %	High–40–1.5
	40 wt %	3.0 wt %	High–40–3.0

*BioChoice™ lignin is the trademarked name of the feed Kraft lignin obtained from Domtar, which was then subjected to fractionation and purifying by the ALPHA process to produce the Low MW and High MW lignin fractions

For example, High-40-1.5 will be used to represent PVA-lignin hydrogels that were fabricated using 40 wt % High MW lignin and a GA content of 1.5 wt %. Note, the lignin concentration is given based on the total mass of polymer, i.e., $m_{\text{lignin}} / (m_{\text{PVA}} + m_{\text{lignin}})$. Figure 4.1a shows the proposed reaction schemes for the synthesis of neat PVA and PVA-lignin soft composites chemically crosslinked via a condensation reaction with GA as the crosslinker. Specifically, in the schematic, red -OH groups are used to represent hydroxyl groups along PVA chains, while green -OH groups are used to represent hydroxyl groups along lignin chains. The blue chains represent the glutaraldehyde that has reacted with -OH groups along both PVA and lignin chains (via a condensation reaction) to chemically crosslink PVA and lignin chains together into the resulting hydrogel network structure. Note, the total -OH content of each of the lignin fractions was measured. A summary of these results can be found in Table B.1 in Appendix B. To verify chemical crosslinking of the lignin using GA as a crosslinker, a solubility test in dimethyl sulfoxide was performed on ‘membranes’ formed from pure lignin, lignin and GA (no acid), and lignin and GA (with acid, pH \approx 3). Highlighting successful chemical crosslinking, the ‘membrane’ fabricated from lignin and GA at a pH \approx 3 did not fully dissolve in the DMSO (Vial C), while samples fabricated from pure lignin (Vial A) and lignin and GA with no acid (Vial B) completely dissolved in DMSO (see Figure B.1). More details regarding this part of our investigation, along with photos of the final samples in solution, can be found in Appendix B.

As shown in Figure 4.1b, we successfully synthesized robust, free-standing hydrogels following the reaction schematic shown in Figure 4.1a. Most notable is the change in color observed with the introduction of lignin, where the soft composites became darker and less

translucent as the lignin loading was increased from 0 wt % to 25 and 40 wt %. Also note, Low-25-1.5 and Low-25-3.0 were quite soft and as such, do not appear as robust as the

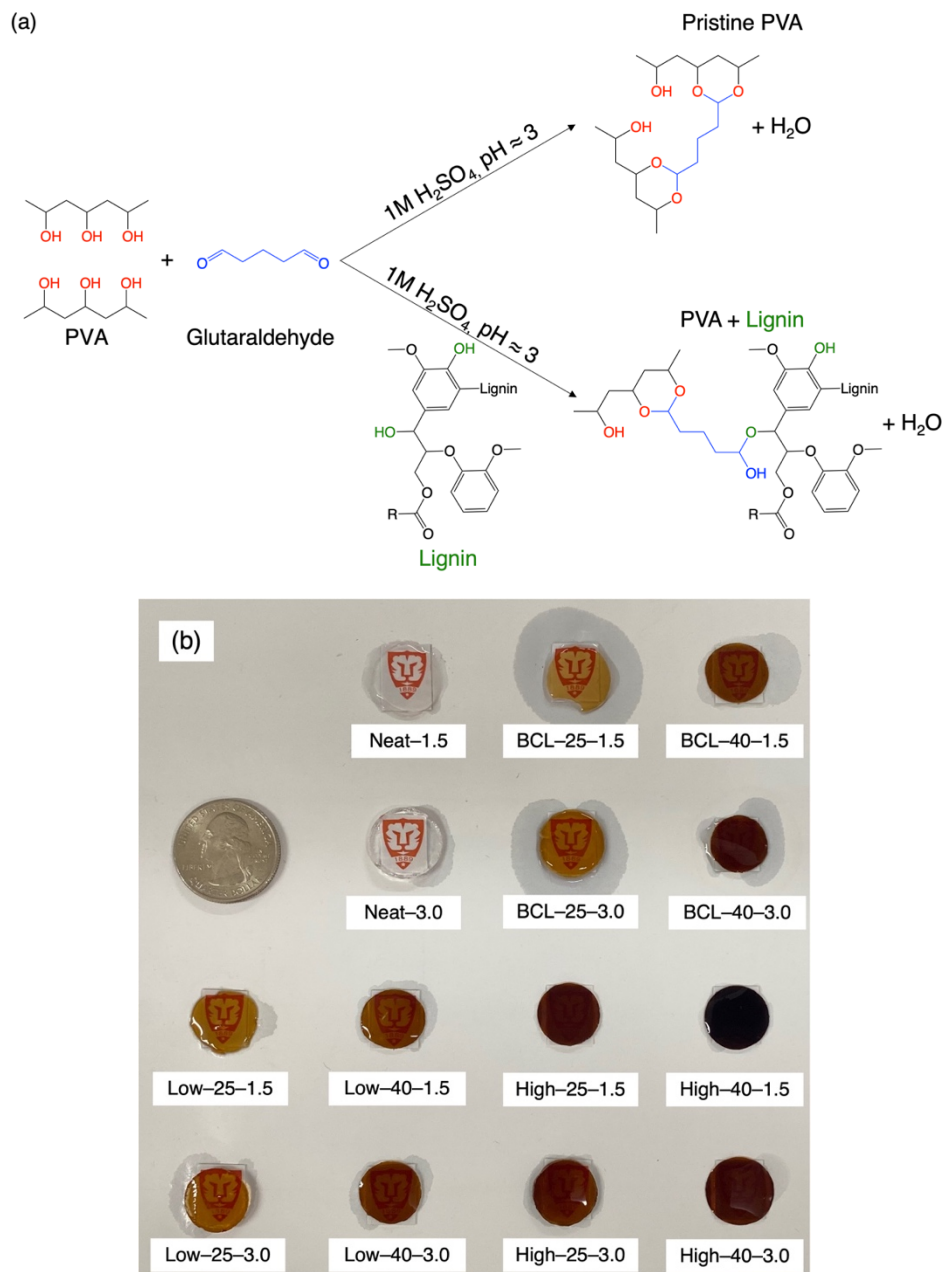


Figure 4.1. (a) Reaction schematic and proposed network structure for chemically crosslinked neat PVA and PVA–lignin composite hydrogels via condensation reaction. (b) Picture of free-standing, robust membranes of varying lignin concentration, lignin MW, and crosslinker content.

other soft composites in Figure 4.1b. This will be revisited in the next section of the chapter.

4.3.2 Ultimate tensile strength (UTS), dynamic mechanical analysis (DMA), and Young's modulus

To elucidate the impact of lignin MW and content on the stress-strain properties of the soft composites, the ultimate tensile strength (UTS) of each hydrated hydrogel was characterized. Results from the UTS experiments are summarized in Figure 4.2. Note that the UTS is the maximum stress a material can withstand while being stretched (at a constant rate) before failure. As seen in Figure 4.2, the weakest sample measured was Neat-3.0, which had a UTS of 0.07 ± 0.02 MPa. These results are generally consistent with prior studies where a PVA-starch system crosslinked with glutaraldehyde exhibited a tensile strength of approximately 0.2 MPa.⁴² When concentrating on soft composites containing 25 wt % lignin, we observe that the introduction of lignin resulted in an increase in tensile strength for the soft composites containing High MW lignin. Most notably, High-25-1.5 exhibited a UTS of 1.08 ± 0.24 MPa, which was approximately equal to a 1400% increase when compared to the weakest sample, Neat-3.0. Interestingly, hydrogels containing BCL and Low MW lignin fractions at 25 wt % exhibited UTS values similar in value to the neat PVA hydrogels. For soft composites containing Low MW, we posit that an increase in UTS is not observed due to a combination of the low MW of this lignin fraction and the low lignin content (25 wt %) for these hydrogels.

When lignin loading is increased to 40 wt %, we observe an increase in UTS for all soft composites, regardless of lignin MW. For example, the UTS of BCL-40-3.0 was measured as 1.03 ± 0.25 MPa, a $\approx 1340\%$ increase when compared to Neat-3.0. A similar increase in UTS was also observed for Low-40-1.5 and Low-40-3.0, which exhibited UTS values

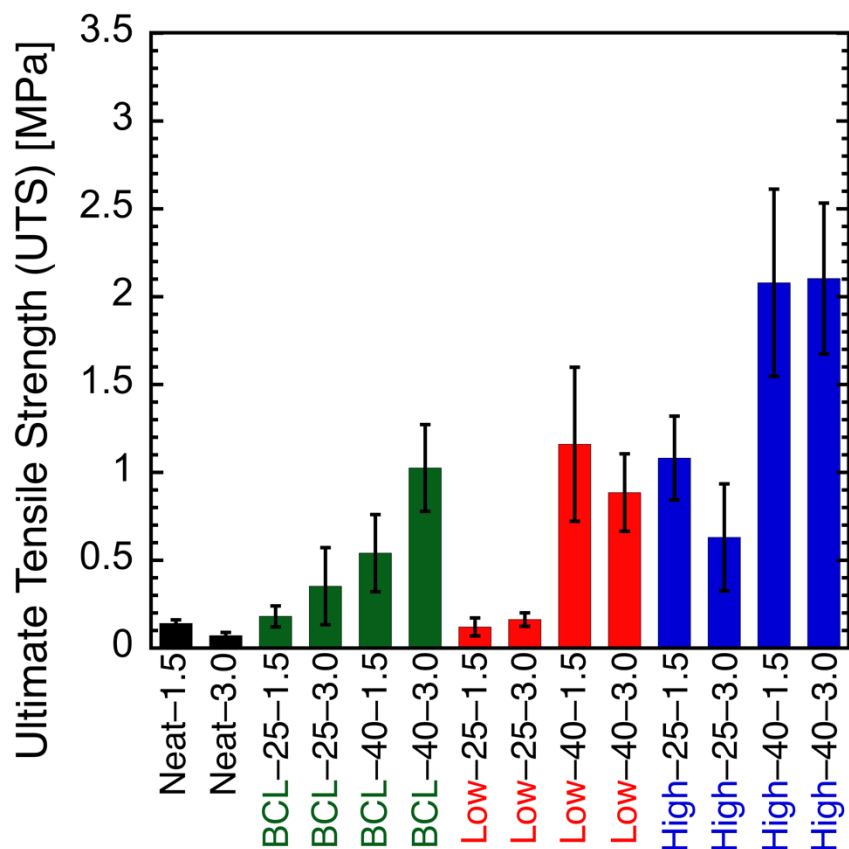


Figure 4.2. Ultimate tensile strength values for neat PVA (solid black bars) and PVA-lignin composites containing BCL (solid green bars), Low MW (solid red bars), and High MW (solid blue bars). Note, the error bars in the figure represent the standard deviation of the average, which was calculated from repeat measurements on at least three separate membranes.

of 1.16 ± 0.44 MPa and 0.89 ± 0.22 MPa, respectively. The largest increase in UTS was observed for soft composites containing 40 wt % High MW lignin. Specifically, the UTS of High-40-1.5 was measured as 2.08 ± 0.53 MPa, a $\approx 2800\%$ increase when compared

to Neat-3.0, though no appreciable difference was observed between the UTS values of High-40-1.5 and High-40-3.0. Along with the results of the solubility tests shown in Appendix B, the observed increase in UTS with lignin loading supports the assertion that lignin is actively participating in the crosslinking process (i.e., condensation reaction forming chemical crosslinks). If the lignin were not participating in the chemical crosslinking that forms the network structure of the soft composites, we expect the lignin chains would slide past each other when the hydrogels were being pulled, potentially resulting in a lower value of UTS, which we do not see in any of our lignin-containing composites.

Manipulation of lignin MW had a noticeable impact on the UTS values of the hydrogel composites, though this impact was most pronounced in soft composites with a lignin content of 25 wt %. For example, comparing Low-25-1.5 and High-25-1.5, we observe an 800% increase in the UTS. Further, comparing Low-40-3.0 and High-40-3.0, we see an $\approx 140\%$ increase in UTS. We attribute this increase to the longer lignin chains in the High MW lignin fraction, as increases in polymer MW have historically been shown to result in improved strength (i.e., improved UTS).^{275,276} Interestingly, the same trend of increasing strength with increasing lignin MW does not hold when these samples are compared to their BCL-containing counterparts. For example, there was no measurable difference in UTS values among soft composites containing 25 wt % Low (Low-25-1.5, 0.12 ± 0.05 MPa) and BCL (BCL-25-1.5, 0.18 ± 0.06 MPa) MW lignin. However, this same behavior does not apply to 40 wt % Low- and BCL-containing samples. In fact, a decrease in UTS (from 1.16 ± 0.44 MPa to 0.54 ± 0.22 MPa) was observed when the

lignin MW was increased (Low-40-1.5 vs. BCL-40-1.5). While the reason behind this peculiar behavior is not fully understood, we posit that this may be related to the wide range of MWs present in the BCL fraction, making the impact of this lignin fraction on the final properties of these soft composites less predictable. Further, given that the ALPHA process simultaneously fractionates and purifies the BCL, this difference may also be a result of the higher impurities (i.e., higher metals content) present in this lignin prior to fractionation. When considering the difference in ash content before and after fractionation (0.89% for BCL, 0.02% for High), these values are very low, and as such, the reason for these differences in UTS are most likely a result of differences in MW and \bar{D} . Lastly, the largest increase in UTS was seen when the lignin and GA content were 40 wt % and 3.0 wt %, respectively, where an almost two orders of magnitude increase in strength from 0.07 ± 0.02 MPa (Neat-3.0) to 2.10 ± 0.43 MPa (High-40-3.0) was observed.

Next, dynamic mechanical analysis was performed to characterize the storage moduli of the composite hydrogels. This technique is commonly employed to characterize changes in the network structure (e.g., crosslinking density) of crosslinked materials.^{89,155,176} For this analysis, all experiments were performed in tensile mode. The storage modulus values of the hydrogel composites, at a frequency of 10 rad s^{-1} , are shown in Figure 4.3. The full frequency sweeps from 0.1 rad s^{-1} to 100 rad s^{-1} can be found in Figures B.2-5 in Appendix B. Note, there are no values reported in Figure 4.3 for the following samples (indicated by a star): (1) Neat-1.5; (2) Low-25-1.5; and (3) Low-25-3.0 – these samples were too soft to mount in the apparatus. As such, the storage modulus of these hydrogels is expected to be <0.09 MPa, which is the lowest value of storage modulus successfully measured. The

introduction of lignin generally resulted in an increase in storage modulus, apart from soft composites containing BCL at a GA content of 1.5 wt %, as these hydrogels exhibited similar storage moduli to that of Neat-3.0. The impact of lignin MW, as well as lignin and

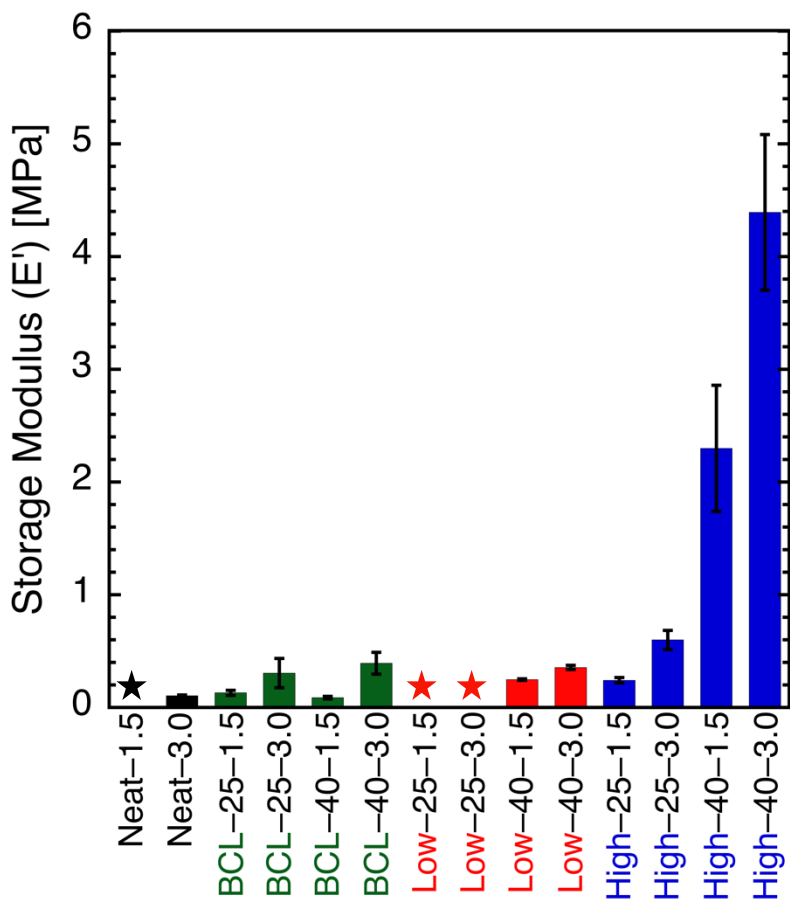


Figure 4.3. Storage modulus values for neat PVA (solid black bars) and PVA–lignin composites containing BCL (solid green bars), Low MW (solid red bars), and High MW (solid blue bars). All experiments were measured in tensile mode. Note, the error bars in the figure represent the standard deviation of the average, which was calculated from repeat measurements on at least three separate membranes. Also note, stars denote samples whose storage moduli could not be measured as these samples were too soft to be mounted in the apparatus.

crosslinker concentration on the storage modulus of the soft composites can be seen from the data presented in Figure 4.3. For instance, soft composites containing 25 wt % High

MW lignin and 3.0 wt % GA (High-25-3.0) exhibited storage moduli that were higher than any of the other Low MW- and BCL-containing soft composites, even when compared to composites containing 40 wt % Low MW and BCL. This difference is further magnified when the High MW content is increased to 40 wt %. When considering soft composites fabricated with 1.5 wt % GA, we observe an $\approx 860\%$ increase in storage modulus (from 0.24 ± 0.02 MPa to 2.30 ± 0.56 MPa) when the High MW content increases from 25 wt % to 40 wt %. We observe a similar increase in storage modulus (from 0.60 ± 0.08 MPa to 4.39 ± 0.69 MPa; $\approx 630\%$ increase) when comparing High-25-3.0 and High-40-3.0. These results are consistent with those previously reported by Rajan et al.,⁸⁹ where an increase in E' with increasing lignin concentration was observed.

Next, when comparing soft composites containing 40 wt % Low MW to their High MW counterparts, we observe noticeable increases in the storage moduli with increasing molecular weight. Specifically, when comparing Low-40-1.5 to High-40-1.5, we see $\approx 830\%$ increase in storage modulus from 0.25 ± 0.01 MPa to 2.30 ± 0.56 MPa. Additionally, we see over an order of magnitude increase in storage modulus when comparing Low-40-3.0 to High-40-3.0 (from 0.36 ± 0.02 MPa to 4.39 ± 0.69 MPa). We again attribute these increases in storage moduli to the longer lignin chains present in the High MW-containing soft composites, as such increases in storage modulus with increases in polymer molecular weight have been previously reported.^{277,278} Finally, we also observe a direct impact on the storage modulus as a result of changes in the concentration of crosslinker. With respect to High MW-containing hydrogels, we observe an increase in storage modulus of $\approx 90\%$ when the concentration of GA is doubled to 3.0 wt % ($2.30 \pm$

0.56 MPa vs. 4.39 ± 0.69 MPa), demonstrating a tightening of the network structure. Additionally, previous work has shown that increasing the crosslinker concentration in PVA-based hydrogels leads to increases in storage modulus,^{279,280} further supporting the results we observe with increasing GA content.

To further elucidate the impact of lignin MW and content, as well as GA content on the network structure of the composite hydrogels, the storage moduli obtained from DMA were used to calculate the molecular weight between crosslinks (M_C) of the hydrogels (using eqn 4.1). The M_C values for all the hydrogel composites are shown in Figure 4.4. Note, there are no values reported in Figure 4.4 for the following samples (indicated by a star): (1) Neat-1.5; (2) Low-25-1.5; and (3) Low-25-3.0 – no storage modulus was obtained from DMA for these hydrogels. Note, to help the reader more directly visualize correlations between changes in M_C and changes in measured mechanical properties of the soft composites, plots of the various measured mechanical properties vs. M_C have been provided in Appendix B (see Figures B.6–B.9). As seen in Figure 4.4, apart from BCL-40-1.5 and High-25-1.5, all soft composites have smaller M_C values than the neat PVA hydrogels, which is indicative of a tighter network structure for these hydrogels. We also observed a noticeable decrease in M_C for all soft composites when the GA content was increased from 1.5 wt % to 3.0 wt %. For example, when comparing BCL-25-1.5 to BCL-25-3.0, we observed a $\approx 20\%$ decrease (from 4.84 ± 0.47 kg mol⁻¹ to 3.88 ± 0.32 kg mol⁻¹) in the molecular weight between crosslinks. This reduction in M_C with increasing GA content is even more pronounced when the BCL content is increased to 40 wt % where we

see a $\approx 65\%$ decrease when comparing BCL-40-1.5 to BCL-40-3.0. The largest reduction in M_C with GA increase was observed in High-containing samples where a $\approx 70\%$ decrease

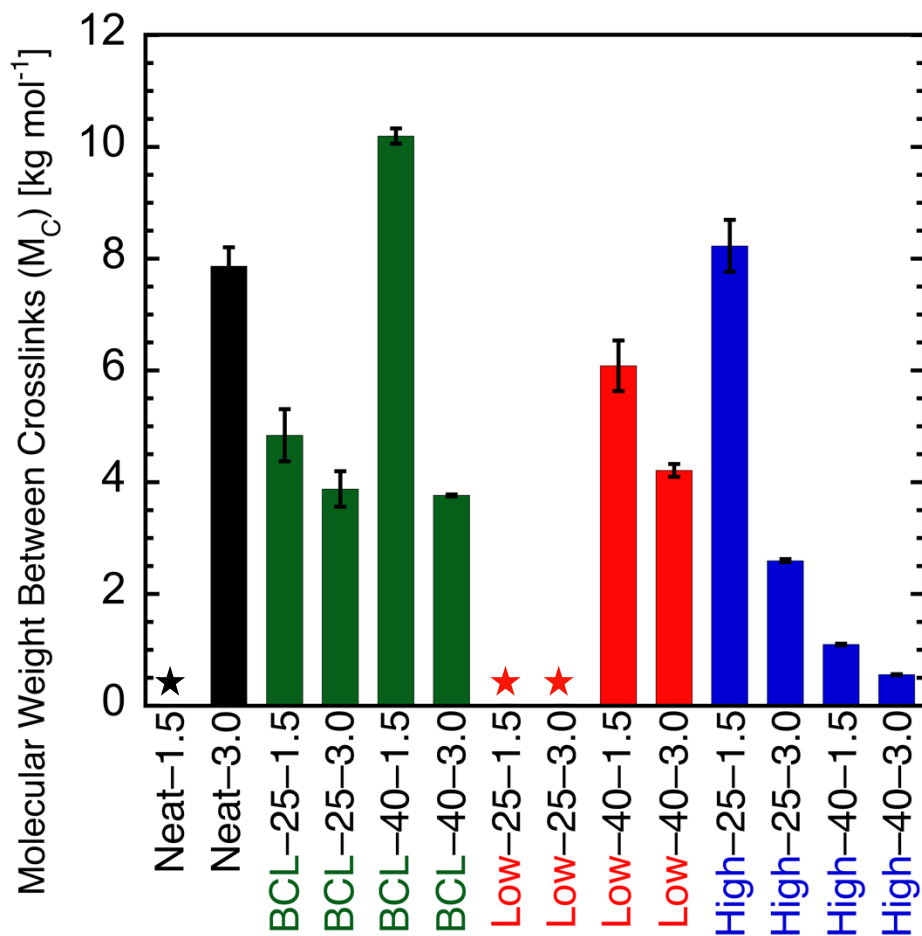


Figure 4.4. The molecular weight between crosslinks values for neat PVA (solid black bars) and PVA-lignin composites containing BCL (solid green bars), Low MW (solid red bars), and High MW (solid blue bars). Note, the error bars in the figure represent the standard deviation of (at least three) repeat experiments. Also note, stars denote samples whose storage moduli could not be measured, and consequently M_C , as these samples were too soft to be mounted in the apparatus.

was observed when comparing High-25-1.5 to High-25-3.0 (from 8.23 ± 0.47 kg mol⁻¹ to 2.60 ± 0.03 kg mol⁻¹). This is not necessarily surprising given the higher concentration of branched lignin chains²⁸¹ in these samples. A similar decrease, though not quite as large,

is observed for soft composites containing Low MW lignin. Again, this general decrease in M_C with increasing crosslinker content demonstrates a tightening of the network structure, which is reflected in the UTS values measured for these soft composites.

Focusing our attention on soft composites containing 40 wt % Low MW and High MW lignin, we observe a significant decrease in M_C when simply increasing the lignin MW fraction from Low to High, underscoring the impact of the ALPHA process. For example, when comparing Low-40-1.5 ($6.08 \pm 0.45 \text{ kg mol}^{-1}$) with High-40-1.5 ($1.10 \pm 0.01 \text{ kg mol}^{-1}$), there is an $\approx 80\%$ decrease in M_C . The same behavior is seen for Low-40-3.0 ($4.21 \pm 0.11 \text{ kg mol}^{-1}$) and High-40-3.0 ($0.56 \pm 0.01 \text{ kg mol}^{-1}$), our lowest reported sample, where there is $\approx 90\%$ decrease in M_C . This decrease in M_C between soft composites containing Low MW and High MW lignin may be a result of increased crosslinking of the -OH groups of the High MW lignin and PVA, a higher degree of physical entanglements due to the more branched structure of the High MW lignin, or more than likely, some combination of both.

If we focus our attention on soft composites containing High MW lignin, we observe the impact of lignin loading in reducing the M_C of the resulting network structure. For example, when the lignin loading was increased from 25 wt % to 40 wt %, there was $\approx 90\%$ decrease in M_C when comparing High-25-1.5 ($8.23 \pm 0.47 \text{ kg mol}^{-1}$) with High-40-1.5 ($1.10 \pm 0.01 \text{ kg mol}^{-1}$). This same behavior was seen in High MW samples containing 3.0 wt % GA. When considering BCL-containing samples, we do not see this same reduction in M_C . Instead, the M_C increased when lignin loading was increased from 25 wt % to 40 wt % at 1.5 wt % GA concentration. Correlating trends with these BCL-containing samples

(BCL–25–1.5, BCL–40–1.5) becomes more uncertain when considering the water uptake values, shown later in this paper, for these two samples represent a decrease in water uptake characteristic of a decrease in M_C and tighter network structure. Similar to what was stated above, we believe this may be related to the wide range of MWs present in the BCL fraction, making the impact of this lignin fraction on the final properties of these soft composites less predictable. Further, as the ALPHA process simultaneously fractionates and purifies the BCL, this unusual behavior could also be the result of higher impurities (i.e., higher metals content) present in this lignin prior to fractionation, limiting access to the –OH groups of the BCL needed for chemical crosslinking.

To further characterize the mechanical properties of the soft composites, the stiffness of the hydrated hydrogels was investigated via mechanical indentation. The compressive Young’s moduli for the hydrogel composites are shown in Figure 4.5. Note, here the phrase “hydrated Young’s modulus” refers to the Young’s modulus of the water-swollen hydrogels – i.e., after the hydrogels were equilibrated in liquid water for at least 48 hours prior to the measurement. For reference, the Young’s moduli of hydrated Neat–1.5 and Neat–3.0 are approximately 0.30 MPa and 0.10 MPa, respectively. As seen in Figure 4.5, the introduction of lignin resulted in a significant increase in the Young’s modulus, where, for example, High–40–3.0 exhibited over an order of magnitude increase in E (12.77 ± 0.97 MPa). This trend is expected as lignin is a stiff filler (glass transition temperature >100 °C) and thus its addition to the softer PVA (especially once the PVA has been plasticized upon hydration) should result in an increase of the Young’ modulus. Overall, for each lignin type, there are two trends observed in the data shown in Figure 4.5: (1) the stiffness

of the hydrogels increases as the lignin content is increased and (2) the stiffness of the hydrogels increases as the GA content is increased. The increase in E with increasing

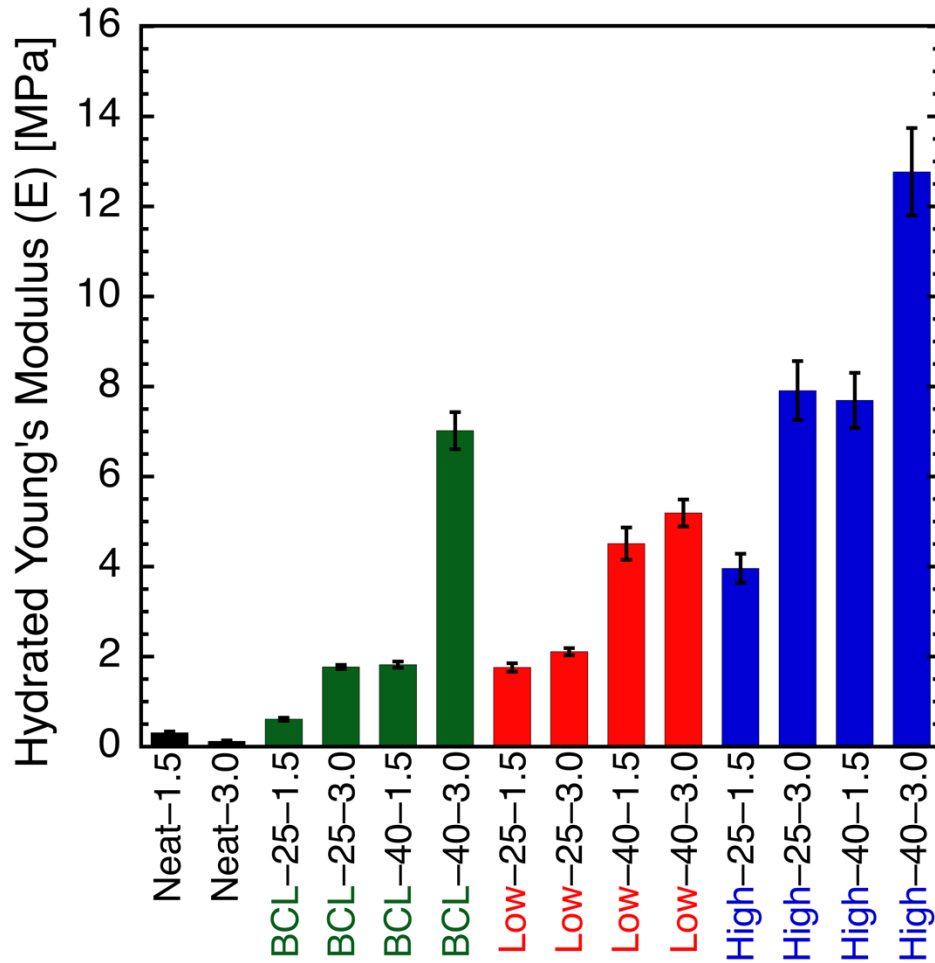


Figure 4.5. Hydrated Young's modulus results for neat PVA (solid black bars) and PVA-lignin composites containing BCL (solid green bars), Low MW (solid red bars), and High MW (solid blue bars). Note, the error bars in the figure represent the standard deviation of (at least three) repeat experiments.

lignin content can be attributed a higher concentration of stiff filler (lignin) and lower concentration of soft host polymer (PVA). When considering the increase in E with

increasing GA content, this is attributed to the tighter network structure (i.e., smaller mesh size) created by fabricating the hydrogels with a higher crosslinker content.^{282,283}

With respect to increasing GA content, for example, we observed a two-fold increase in modulus from 3.96 ± 0.32 MPa (High-25-1.5) to 7.91 ± 0.65 MPa (High-25-3.0) when the GA content was increased from 1.5 wt % to 3 wt %. However, as seen with the DMA, the systematic impact of lignin MW on the mechanical properties of the soft composites is only observed for hydrogels containing Low MW and High MW lignin. That is, at the same lignin and GA contents, the hydrated Young's modulus of High MW lignin-containing hydrogels was always significantly higher than those of their Low MW lignin counterparts. For example, comparing Low-25-3.0 to High-25-3.0, we observed an almost four-fold increase in E , from 2.11 ± 0.08 MPa to 7.91 ± 0.65 MPa. This increase in modulus between soft composites containing Low MW and High MW lignin is attributed to increased crosslinking of the -OH groups of the High MW lignin and PVA, a higher degree of physical entanglements due to the more branched structure of the High MW lignin, or more than likely, some combination of both.

In contrast, while the overall MW of the BCL was approximately four times higher than that of the Low MW lignin ($M_{w,app} \approx 16,100$ g mol⁻¹ vs. $M_{w,app} \approx 3,900$ g mol⁻¹), BCL-40-3.0 was the only soft composite to exhibit a higher value of E than its Low MW lignin counterpart. For all other compositions, hydrogels containing Low MW lignin exhibited higher hydrated Young's modulus. If we combine these results with those obtained from DMA, we see that hydrogel composites with the highest lignin content have both the highest elastic modulus and highest UTS. Specifically, High-40-3.0 demonstrated both the

highest UTS and Young's modulus, while pristine PVA showed the lowest modulus and the lowest UTS. These results underscore the benefits of the ALPHA process, whereby the molecular weight of the lignin, as well as the lignin purity, can be controlled and utilized to directly manipulate the mechanical properties of the soft composites.

4.3.3 *Equilibrium Water Uptake*

To elucidate the impact of lignin MW and content, as well as GA content on the hydration properties of the composite hydrogels, the equilibrium water uptake of each hydrogel was measured (using eqn 4.3). The equilibrium water uptake values of neat PVA and all PVA–lignin composites are summarized in Figure 4.6. The highest equilibrium water uptake values were observed for Neat–1.5 and Neat–3.0, where values of $2240 \pm 380\%$ and $2850 \pm 540\%$, respectively, were measured. The introduction of lignin, in general, resulted in a decrease in equilibrium water uptake of the composite hydrogels, especially when the GA content was 3 wt %. For example, soft composites containing BCL (BCL–25–3.0, $750 \pm 63\%$), Low MW (Low–25–3.0, $1170 \pm 79\%$), and High (High–25–3.0, $470 \pm 110\%$) MW lignin demonstrated lower water uptake values than Neat–1.5 ($2240 \pm 380\%$). Hydrogels containing BCL and Low MW lignin at 25 wt % and 1.5% GA demonstrated similar water uptake values to Neat–1.5. This result agrees with UTS measurements on these membranes, where hydrated Neat–1.5 and Low–25–1.5 were too soft to mount in the apparatus, indicating a more open network structure (i.e., larger mesh sizes), and thus, higher water uptake for these composites. As seen in the other mechanical property measurements, altering the lignin content had a significant impact on the resulting equilibrium water uptake. For example, when the content of Low MW lignin was increased

from 25 wt % (Low-25-1.5, $2010 \pm 140\%$) to 40 wt % (Low-40-1.5, $440 \pm 1.8\%$), an almost five-fold decrease in equilibrium water uptake was observed.

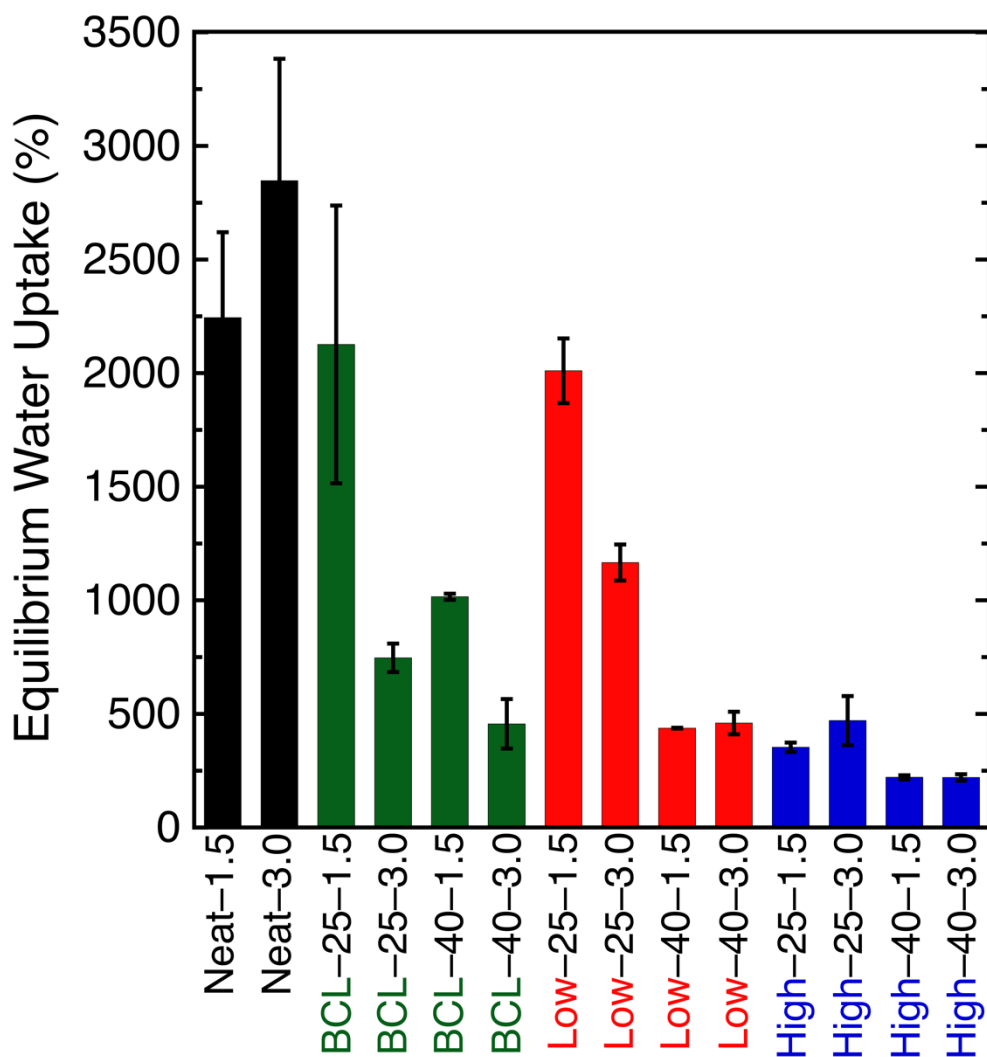


Figure 4.6. Equilibrium water uptake results for results for neat PVA (solid black bars) and PVA–lignin composites containing BCL (solid green bars), Low MW (solid red bars), and High MW (solid blue bars). Note, the error bars in the figure represent the standard deviation of (at least three) repeat experiments.

An analogous change in water uptake behavior with increasing lignin content is observed for soft composites containing BCL and High MW lignin, irrespective of

crosslinker concentration prior to fabrication. This observed decrease in water uptake is consistent with the increased Young's modulus. With a tighter mesh size (i.e., smaller M_C), one would expect lower water uptake to naturally follow. Most notably, High-40-1.5 and High-40-3.0 exhibited the largest reduction in water uptake as compared to Neat-1.5, where an order of magnitude reduction was observed. This significant decrease in equilibrium water uptake can be attributed to the high content of relatively hydrophobic lignin, as well as the low molecular weight between crosslinks calculated for these samples. This lower equilibrium water uptake also agrees with UTS and hydrated Young's modulus characterizations, where these two soft composites exhibited the highest UTS and elastic modulus. Another important observation from Figure 4.6 is the water uptake behavior of BCL-containing composites. Interestingly, BCL-25-3.0 exhibited lower equilibrium water uptake than BCL-40-1.5, which was not a behavior observed in Low and High MW lignin hydrogels. These results again underscore the unpredictability in final properties of soft composites synthesized with unfractionated BCL, further highlighting the benefit of using more well-defined lignin from the ALPHA process.

4.3.4 Scanning Electron Microscopy (SEM) Imaging

To provide more insight into the impact of lignin and GA content, as well as lignin MW, on the network structure, the water-swollen network structure of the soft composites was directly imaged using scanning electron microscopy (SEM). The images of neat PVA, as well as PVA-lignin composites containing BCL, Low MW lignin, and High MW lignin are shown in Figures 4.7, 4.8, and 4.9, respectively. Note, for ease of comparison, the SEM images for Neat-1.5 and Neat-3.0 have been reproduced in each figure. Note, due to the

nature of any microscopy-based technique, special care must be taken to ensure selected images are genuinely representative of the overall structure and not simply a localized outlier. To ensure a confident conclusion could be drawn, the single SEM image shown for each sample in Figures 4.7–4.9 was selected as it best represented the 20+ areas of each sample that were analyzed under the electron microscope. Interestingly, we see a drastic difference in network structure between neat PVA membranes at 1.5 wt % and 3.0 wt % GA. Specifically, the hydrated structure of Neat–1.5 is more well defined, with pores on the order of 1-2 μm , while the crosslinked network structure of Neat–3.0 is not evident. The relatively undefined network structure may help to explain why Neat–3.0 had the lowest UTS and hydrated Young’s modulus, along with one of the highest equilibrium water uptake values.

Next, when considering composites containing BCL in Figure 4.7, we observe that the introduction of lignin has a noticeable impact the hydrated network structure of the soft composites. Specifically, the introduction of 25 wt % BCL resulted in a tightening of the network structure, both for BCL–25–1.5 (Figure 4.7b) and BCL–25–3.0 (Figure 4.7e), where smaller pores can be seen in these SEM images. The tighter network structure of these composites correlates with the improved values of UTS, storage modulus, and hydrated Young’s modulus for these samples. However, when the BCL content is increased to 40 wt %, the network structure of the soft composites becomes less defined, with higher heterogeneity, exhibiting an overall ‘loosening’ of the network structure. This breakdown of the network structure seen in BCL–40–1.5 may explain why these hydrogels exhibited similar mechanical properties to soft composites containing only 25 wt % BCL. It appears

that while the network structure of these soft composites becomes disrupted when the BCL content is increased from 25 wt % to 40 wt %, the large MW distribution of the BCL

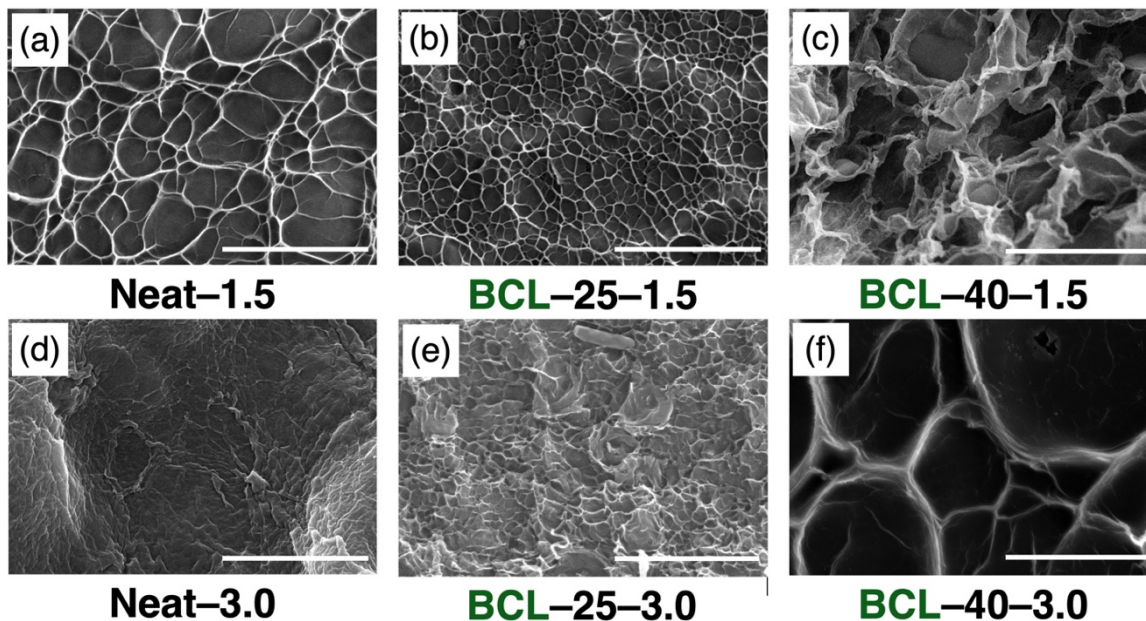


Figure 4.7. SEM images for (a,d) neat PVA and (b,c,e,f) PVA–lignin composites containing unfractionated BCL lignin. Specific labels, following the nomenclature listed in Table 4.1, are provided below each SEM image. Also note, the scale bar in all the images is 5 μm .

ultimately serves to reinforce the mechanical integrity of the BCL-containing hydrogels, where the UTS and Young’s modulus values increased from ~ 0.4 MPa to ~ 1.0 MPa and ~ 1.8 MPa to ~ 7 MPa (both at a GA content of 3.0 wt %), respectively.

Next, focusing our attention on soft composites containing Low MW lignin (Figure 4.8), we observe that these hydrogels generally have well-defined crosslinked network structures, apart from Low-25-1.5, which exhibited a diffuse, loosely crosslinked network. The network structure of the Low-25 hydrogels noticeably improves when the crosslinker content is increased to 3.0 wt %. The improved network structure was seen to result in improved hydrogel stiffness, as the Young’s modulus was seen to increase from ~ 1.8 MPa

to ~2.1 MPa. However, this did not translate to improved yield stress for these membranes, as these samples were too soft to mount (in tensile mode) for characterization of the storage

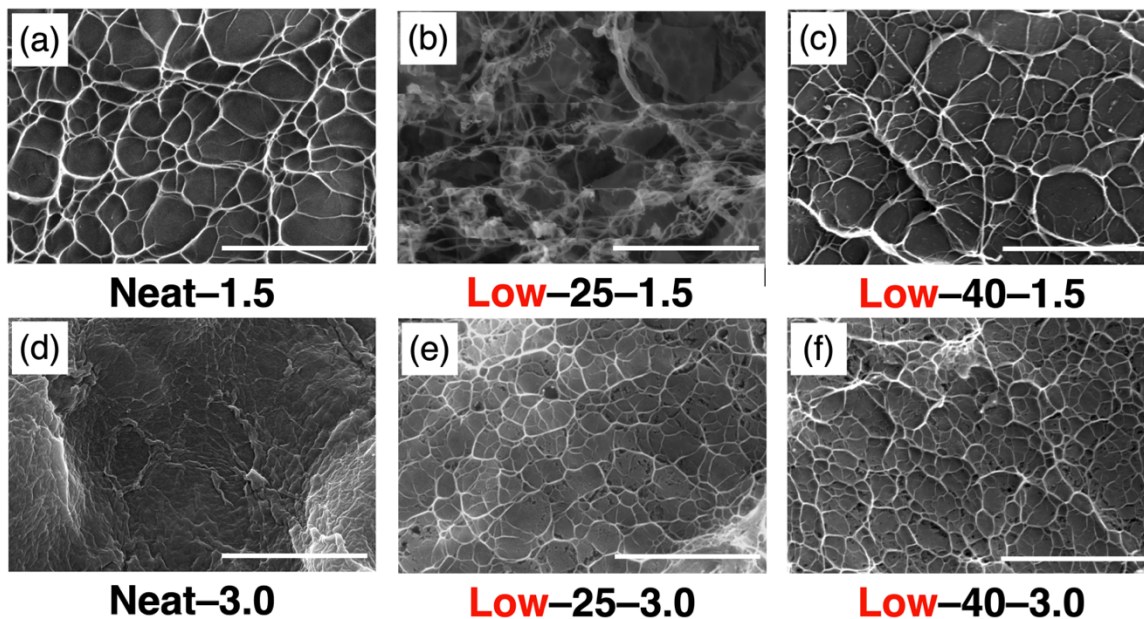


Figure 4.8. SEM images for (a,d) neat PVA and (b,c,e,f) PVA–lignin composites containing **Low** molecular weight lignin. Specific labels, following the nomenclature listed in Table 4.1, are provided below each SEM image. Note, the SEM images of neat PVA are the same as those shown in Figures 4.7a and 4.7d. Also note, the scale bar in all the images is 5 μm .

modulus and exhibited some of the lowest UTS values. This result may be due to overall low MW of the Low MW lignin fraction utilized. It is not until the content of Low MW lignin is increased to 40 wt % that we begin to see a correlation between the network structure and enhanced mechanical properties. For example, the values of UTS, storage modulus, and hydrated Young’s modulus of hydrogels containing 40 wt % Low MW lignin are similar to those measured for BCL- containing hydrogels at the same lignin content, even though those samples did not form well-defined networks. We attribute the improved network structure of soft composites in Figure 4.8 to improved homogeneity of the starting

Low MW lignin obtained from the ALPHA process. A slight tightening of the network structure can be observed for hydrogels containing 40 wt % Low MW lignin when the GA content was doubled from 1.5 wt % (Figure 4.8c) to 3.0 wt % (Figure 4.8f). This shrinking of the network structure is supported by the slight increase in storage modulus, and subsequent decrease in M_C , as seen in Figures 4.3 and 4.4, respectively.

Finally, when considering hydrogels containing High MW lignin, we observe a noticeable expansion of the network structure with the introduction of 25 wt % High MW lignin (Figure 4.9b). When the GA content is doubled to 3.0 wt % (Figure 4.9e), we observe a tightening of the network structure, indicating an increase in crosslink density for these hydrogels. The tightening of the network structure between High-25-1.5 and High-25-3.0 is indicated by increases in storage (~ 0.2 MPa vs. ~ 0.6 MPa) and Young's moduli (~ 4 MPa vs. ~ 8 MPa), as well as a decrease in M_C (~ 8.2 kg mol⁻¹ vs. ~ 2.6 kg mol⁻¹). Surprisingly, the equilibrium water uptake values for these two membranes were similar, where no measurable difference was observed (see solid blue bars in Figure 4.6). When the High MW lignin content is increased to 40 wt %, we observe that only membranes containing 3.0 wt % GA formed an ordered, relatively homogeneous crosslinked network structure with pores on the order of 1 μ m (Figure 4.9f), while those containing 1.5 wt % GA did not exhibit a well-defined crosslinked structure (Figure 4.9c) with pores larger than those seen in High-40-3.0. The improved network structure of High-40-3.0, when compared to High-40-1.5, is validated by increases in both the storage (~ 2.3 MPa vs. ~ 4.4 MPa) and Young's moduli (~ 8 MPa vs. ~ 13 MPa) of these soft composites. As the equilibrium water uptake values for these two membranes are the same, we believe these

improved mechanical properties can be directly attributed to the improved network structure of High-40-3.0. However, the translation of an improved network structure to

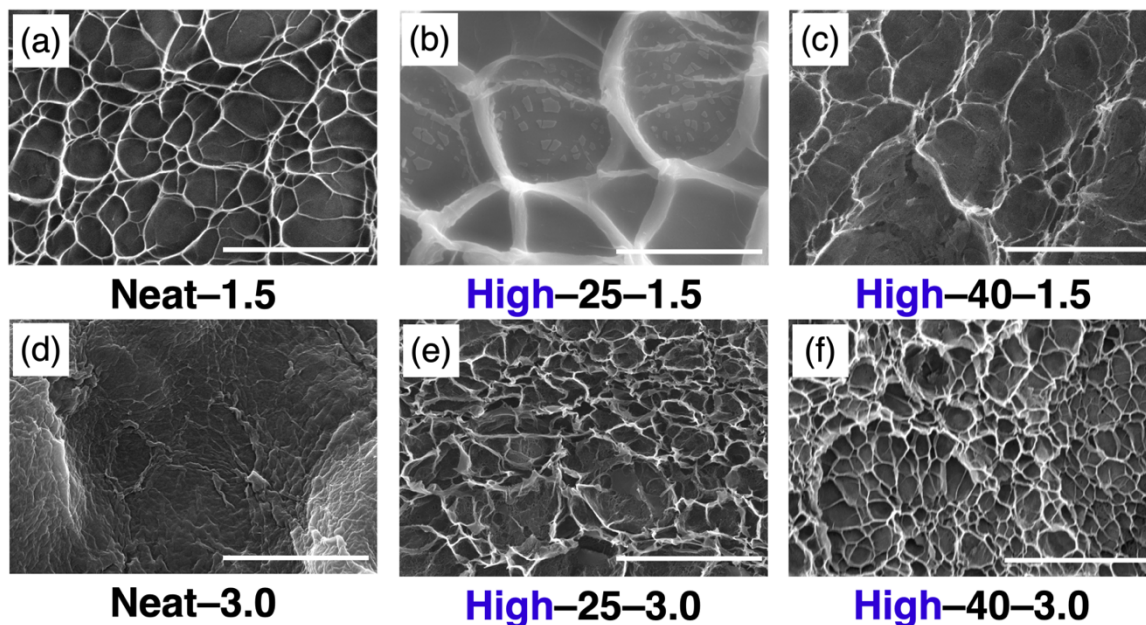


Figure 4.9. SEM images for (a,d) neat PVA and (b,c,e,f) PVA–lignin composites containing **High** molecular weight lignin. Specific labels, following the nomenclature listed in Table 4.1, are provided below each SEM image. Note, the SEM images of neat PVA are the same as those shown in Figures 4.7a and 4.7d. Also note, the scale bar in all the images is 5 μm.

improved mechanical properties was not seen for all cases as both samples exhibited similar values for UTS (see solid blue bars in Figure 4.2). Overall, when comparing the SEM images in Figures 4.7, 4.8, and 4.9, it is apparent that the ALPHA process has a profound impact on the network structure of these composite PVA–lignin hydrogels. In Figures 4.8 and 4.9, there were distinguishable trends with the introduction of lignin, as well as changes in both lignin and GA contents within each series containing Low and High lignin obtained from the ALPHA process. In contrast, hydrogels containing BCL (see

Figure 4.7) exhibited inconsistent trends and very heterogeneous network structures, which is potentially a result of the higher dispersity in MW for the feed (raw) lignin.

4.4 Conclusion

In conclusion, we have successfully synthesized robust, free-standing PVA–lignin composite hydrogels containing two concentrations of unfractionated (referred to as BCL) and fractionated (referred to as Low and High MW) lignin (25 wt % and 40 wt %). The fractionated lignin was obtained by subjecting the BCL to the ALPHA process, which simultaneously fractionated and purified the BCL feed. Additionally, the hydrogel composites were fabricated with varying concentrations of glutaraldehyde, a traditional crosslinker for PVA hydrogels, which forms covalent crosslinks by consuming –OH groups via a condensation reaction under acidic conditions. The mechanical properties of the hydrated composites were characterized via UTS, Young’s modulus, and dynamic mechanical analysis. Increases in UTS were seen with the introduction of lignin, along with increases in lignin concentration from 0 wt % to 25 and 40 wt %. Increases in UTS, storage modulus, and Young’s modulus were also observed when the lignin MW was increased from Low MW to High MW, demonstrating the impact lignin MW has on the network structure and mechanical properties of these composite membranes. When considering the tunable mechanical properties, these soft composites could prove suitable for biomedical applications, particularly where modulus matching is imperative for injectable in vivo hydrogels designed for tissue engineering applications. Results from the DMA analysis were utilized to calculate the M_C of the PVA–lignin composites, where noticeable decreases in M_C were seen when the GA concentration was doubled from 1.5 wt% to 3.0

wt %. This decrease in molecular weight between crosslinks was also seen as a general decrease in equilibrium water uptake with increasing GA content. SEM was employed to directly image the water-swollen network structure of the various soft composites. Notably, more control over forming a well-defined, homogeneous network structures was observed for Low MW- and High MW-containing samples, alluding to the importance of the ALPHA process in lowering the dispersity of (and purifying the) lignin prior to hydrogel synthesis.

CHAPTER FIVE

CONCLUSIONS AND FUTURE WORK

5.1 Conclusions

Hydrogel composites containing PVA and lignin were fabricated using two different fabrication methods. In one route, lignin was first functionalized with a vinyl-containing acrylate functional group that was verified by ^1H NMR and ^{31}P NMR. Upon functionalization, lignin chains were able to free radically crosslink with themselves, along with PVA chains that were thermally crosslinked, creating an interpenetrating network of PVA and lignin chains. These PVA-lignin hydrogel composites demonstrated an effective reduction of methylene blue permeability, where the highest performing sample showed an over two orders of magnitude reduction in MB permeability. Characteristic increases in Young's modulus were measured with the introduction of lignin, which was supported by reductions in the molecular weight between crosslinks.

Incorporating lignin of high dispersity into PVA hydrogels lead to a wide range in MB permeability measurements. Notably, the impact of the ALPHA-fractionation process had a profound impact on the resulting transport properties of the PVA-lignin hydrogel composites where an enhancement in the repeatability of MB permeability experimentation was discovered. This improved repeatability in permeability, as evidenced by a one order of magnitude decrease in standard deviation, underscores the importance of incorporating lignin of narrow, prescribed molecular weights with low ash content to homogenize the network structure of these hydrogel composites, unlocking fundamental structure-process-property relationships in this emerging class of soft materials.

In another fabrication pathway, PVA and lignin were crosslinked via condensation reaction whereby glutaraldehyde was utilized as the crosslinker under acidic conditions. A traditional crosslinking method for PVA hydrogels is via condensation with GA during which hydroxyl groups are consumed along PVA chains. Due to a high abundance of hydroxyl groups along its chemical structure, lignin was able to actively participate in this chemical crosslinking process whereby lignin chains were able to crosslink with both PVA and other lignin chains. This crosslinking mechanism was confirmed via solubility test during which pure lignin chains reacted under acidic conditions in the presence of GA were unable to redissolve back into solution. A full mechanical characterization was performed on this series of PVA-lignin hydrogel composites where characteristic increases in UTS, storage modulus, and Young's modulus were observed with increases in lignin content, lignin molecular weight, and crosslinker concentration. Additionally, these general increases in mechanical properties correlated with decreases in equilibrium water uptake and decreases in molecular weight between crosslinks. These decreases were supportive of a general shrinking of the network structure which was visually observed via SEM imaging. When considering the SEM images taken, high dispersity, BCL-containing samples demonstrated a loosely connected network structure with little to no ordering or pore structure. The importance of the ALPHA-fractionation process was seen in SEM imaging where Low- and High-containing samples displayed a more ordered, porous-like structure, alluding to the formation of a more homogeneous network structure when narrower, low dispersity lignin is utilized in PVA hydrogel composites.

In all, this Dissertation aimed to elucidate the role of lignin in this emerging class of green materials where most of the literature utilizes lignin of high dispersity, obfuscating the ability to uncover fundamental structure-process-property relationships. By utilizing lignin of narrow dispersity, these soft materials can be tuned and optimized for various separation applications and potentially tissue engineering avenues where modulus matching is of importance.

5.2 Future Work

5.2.1 General Future Work

All work in this Dissertation aims to uncover fundamental structure-process-property relationships in PVA-lignin hydrogel composites. While PVA is a very popular and useful polymer, it would be useful to see how other polymers behave with ALPHA-fractionated lignin. When considering the ALPHA process and its inability to predict dispersity upon processing, it would be beneficial to develop a method to fractionate two lignin samples that have the same MW, but different dispersity.

5.2.2 Elucidating the Impact of Lignin Dispersity on PVA-Lignin Hydrogel Composites Containing Lignin of Constant Molecular Weight

The ALPHA process allows for the fractionation of lignin into prescribed molecular weights above or below the molecular weight of the feed lignin. One of the underlying issues with the process is the inability to predetermine the dispersity of the lignin prior to fractionation. For instance, if a particular molecular weight was produced in two separate processes, there is no way to be sure their dispersity will be the same. It is also very challenging to obtain the same exact molecular weight between two fractionations. This

creates a lot of inconsistency in lignin obtained from the process, meaning all lignin used in a particular study must be acquired from one large fractionation.

An avenue of work that would be interesting to investigate in continuing this project would be to optimize the ALPHA process such that multiple batches of the exact same molecular weight were generated, all containing varying dispersity. One would then fabricate PVA-lignin hydrogels containing lignin of identical MW and ranges of \bar{D} . A full characterization of mechanical and transport properties would then be performed as seen in Chapters 3 and 4 to elucidate the impact of dispersity on these characteristic properties. This would resolve the issue that currently resides in all investigations of this Dissertation where both lignin MW and \bar{D} differentiate between lignin samples, making it challenging to delineate whether MW or \bar{D} is impacting changes in results for hydrogel composites.

In Chapter three of this Dissertation, it was highlighted how the dispersity of lignin had an impact on the scatter of permeability for methylene blue. The two samples contained CBL and UCL lignin of different molecular weight and dispersity. When considering two properties are changing between the CBL and UCL containing samples, it would be interesting to create samples containing lignin of the same molecular weight, and widely different dispersity. Performing these experiments would reveal the impact of dispersity on MB permeability and repeatability of measurements.

5.2.3 Elucidating PVA-Lignin Hydrogel Composites for the Removal of Hexavalent Chromium

Much research in the literature has investigated lignin-based materials for separations applications tailored towards the adsorption and removal of hexavalent chromium from water. Using a similar approach as seen in Chapter 4, it would be interesting to see the impact of lignin molecular weight, lignin concentration, and glutaraldehyde crosslinker concentration on the removal of hexavalent chromium from water via adsorption from a source of water, or static permeation as seen in Chapter 3 with methylene blue.

5.2.4 Characterizing Lignin Hydrogel Composites Crosslinked with Chitosan or Cellulose

Much research in the literature has investigated chitosan and cellulose hydrogels for various applications in the biomedical space. When considering the presence of hydroxyl groups in both chitosan and cellulose, along with the chemistry present in Chapter 4 that exploited hydroxyl groups along PVA and lignin chains, it would be interesting to see what kinds of materials could be formed crosslinking lignin with either chitosan or cellulose via condensation reaction and glutaraldehyde. These materials could serve suitable for tissue engineering or drug delivery, and would be a completely biopolymer based material that no longer contains a traditional, petroleum-based polymer.

5.2.5 Characterizing Methylene Blue Solubility into Lignin Hydrogel Composites

It was shown in Chapter 3 that methylene blue both adsorbs into and permeates through PVA-lignin hydrogel composites. To better understand the impact of adsorbed MB into the films during these experiments, it would be beneficial to measure the maximum solubility of MB into the hydrogel composites. This would provide context towards what percentages

of MB are remaining in the membrane or permeating through, uncovering a better understanding between partition coefficient, solubility, and diffusivity for this system. It would also provide insight as to the relationship between amount of lignin in the sample and concentration of MB adsorbed.

5.2.6 Characterizing the Mesh Size Lignin Hydrogel Composites Saturated with Methylene Blue

To better understand the network structure during MB permeation experiments, it would be advantageous to perform small angle neutron scattering (SANS) measurements on lignin-hydrogel composites before and after saturation with MB. As we know from Chapter 3, methylene blue both adsorbs into and permeates through PVA-lignin hydrogel composites to the receiving reservoir. During the MB adsorption process, the overall mesh size for the hydrogel composite is more than likely decreasing in size due to MB particles remaining in the membrane. Performing SANS measurements and acquiring a mesh size would provide context towards how much the mesh size changes before and during a MB permeation experiment for this system. As a result, correlations could be drawn between changes in mesh size with increases in lignin content leading to decreasing MB permeabilities.

APPENDICES

Appendix A

A.1 ^1H NMR Spectroscopy

As mentioned in the Experimental Section of Chapter 3, ^1H NMR was performed on the lignins pre- and post-functionalization to confirm the addition of the vinyl-containing acrylate groups. The results from this analysis are shown in Figure A.1.

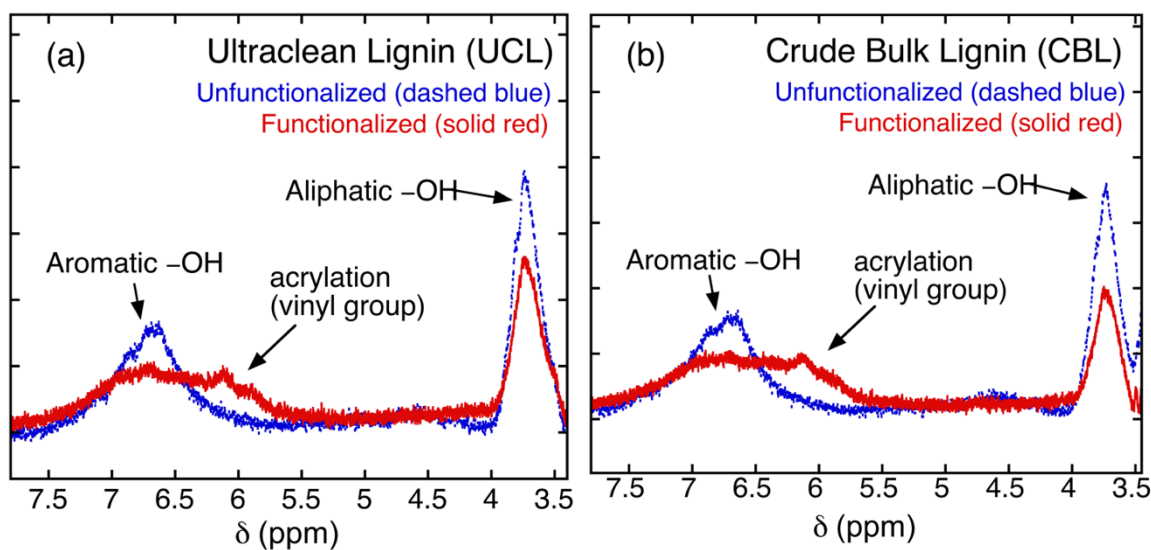


Figure A.1. ^1H NMR spectra of unfunctionalized (dotted blue line) and functionalized (solid red line) (a) ultraclean lignin (UCL) and (b) crude bulk lignin (CBL).

As seen in Fig. A.1, the NMR peaks associated with the aliphatic and aromatic $-\text{OH}$ groups decrease after acrylation. This decrease in spectral peaks associated with the $-\text{OH}$ groups is accompanied by the emergence of broad peak centered around 6.2 ppm, which is indicative of the hydrogens on the $\text{C}=\text{C}$ double (i.e., double bond a vinyl group).

A.2 Hydroxyl ($-\text{OH}$) Content of Crude Bulk and Ultraclean Lignins

The hydroxyl content of the unfunctionalized and functionalized crude bulk lignins (CBLs) and ultra-clean lignins (UCLs) was determined from the ^{31}P NMR spectrum for

each sample (shown in Figures 3.3a and 3.3c in Chapter three). A summary of these data is presented in Table A.1.

Table A.1. Aliphatic and aromatic hydroxyl (–OH) content for both unfunctionalized (UF) and functionalized (F) crude bulk lignins (CBLs) and ultraclean lignins (UCLs)

Type of lignin	Aliphatic –OH (mmol OH/g lignin)	Aromatic –OH		
		syringyl (S)	guaiacyl (G)	<i>p</i> -hydroxyl phenol (H)
		(mmol OH/g lignin)		
<i>CBLs</i>				
UF	1.88	0.64	2.25	0.38
F	0.23	0.59	1.14	0.40
<i>UCLs</i>				
UF	1.60	0.64	2.40	0.43
F	0.44	0.26	1.06	0.22

A.3 Infrared Characterization of UCLs and CBLs

To further confirm successful functionalization of the UCLs and CBLs, the lignins were analyzed using FTIR spectroscopy using a Thermo Scientific Nicolet iS50R FT-IR equipped with Specac Golden Gate attenuated total reflectance (ATR) attachment. All spectra were collected using a liquid nitrogen-cooled mercury-cadmium-telluride detector with 64 scans per spectrum at a resolution of 4 cm⁻¹. FTIR spectra of pre- and post-functionalized UCLs and CBLs are presented in Figures A.2a and A.2b, respectively.

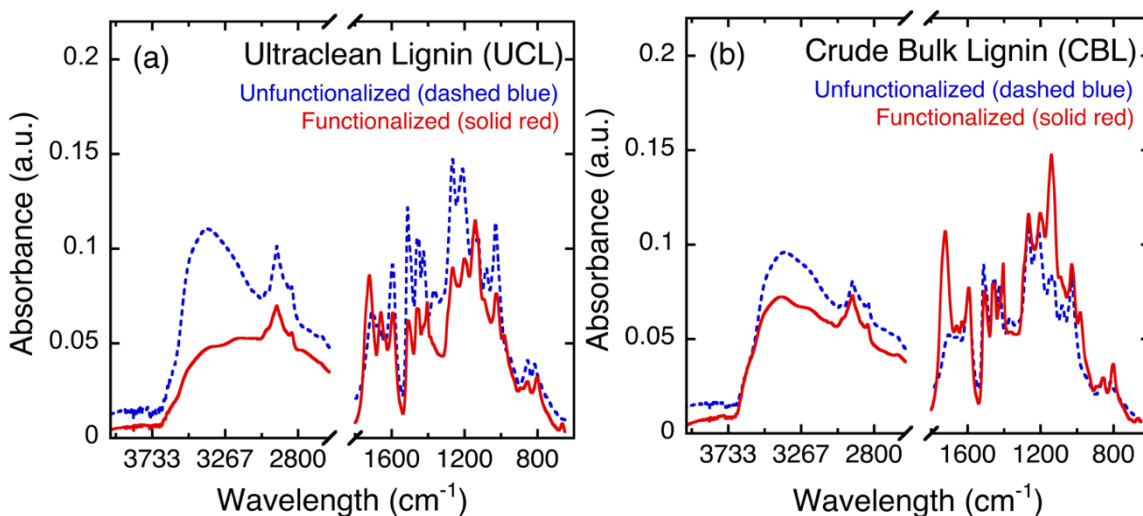





































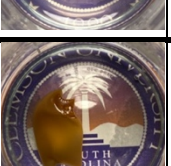
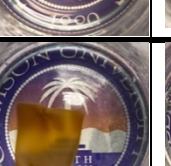



Figure A.2. FTIR spectra of unfunctionalized (dashed blue line) and functionalized (solid red line) for (a) ultraclean lignin and (b) crude bulk lignin.

A.4 Thermal Stability of Composite Hydrogels

To confirm the stability of the fabricated hydrogels at lower temperatures, the hydrogels were cut and soaked in DI water, at room temperature ($\sim 20\text{ }^{\circ}\text{C}$) for at >120 days. Following this initial soaking, the membranes were exposed to increasing temperatures to visually detect the thermal stability of the composite membranes when compared to the thermally-crosslinked PVA hydrogel. A summary of the images for each membrane, at each temperature, is provided in Table A.2.

Table A.2. The following table contains images of the two series PVA–lignin hydrogel composite membranes under hydration at temperatures ranging from room temperature (~25 °C) to 80 °C. Note, the first column shows the membranes that have been under hydration for >120 days.

	20 °C, >120 days	40 °C, 4 h	60 °C, 4 h	80 °C, 4 h	80 °C, 24 h
Neat PVA					
PVA–UCL–10UF					
PVA–UCL–20UF					
PVA–UCL–10F					
PVA–UCL–20F					
PVA–UCL–50UF					
PVA–CBL–10UF					
PVA–CBL–20UF					



As seen in Table A.2, all of the PVA–lignin composite hydrogels are stable in room temperature water for >120 days.

Appendix B

B.1 Solubility Investigation of Crosslinked and Uncrosslinked Lignin

To verify successful chemical crosslinking of lignin using glutaraldehyde (GA) as a crosslinker, the solubility of unmodified lignin, as well as lignin samples that were prepared with GA in both neutral and acidic conditions ($\text{pH} \approx 3$) in dimethyl sulfoxide (DMSO) was investigated. Note, we first tried to verify chemical crosslinking via NMR; however, lignin samples that were fabricated with GA in acidic conditions would not dissolve in the necessary NMR solvent. Furthermore, we do not have access to solid-state NMR at Clemson University. However, we believe the approach described below adequately (though indirectly) verifies chemical crosslinking of the lignin using GA as the crosslinker.

Briefly, High MW lignin was placed into a scintillation vial (Vial A) containing DMSO and stirred until all lignin completely dissolved into solution. In a separate vial (Vial B), High MW lignin and GA, at a concentration of 3 wt % (with respect to lignin), was stirred in DMSO (containing no acid) until all the lignin dissolved. A third vial (Vial C) containing High MW lignin and GA, at a concentration of 3 wt % (with respect to lignin), was stirred in DMSO (with sulfuric acid added dropwise until a $\text{pH} \approx 3$ was reached) until all lignin dissolved. Vial B and Vial C were then placed into an oven under partial static vacuum (~ 10 inHg) at 60°C for 36 h or until all DMSO was removed. This heat treatment procedure follows the same one used in fabricating the PVA–lignin composite membranes detailed in the Experimental Section. After drying, fresh DMSO was added to the samples in Vial B and Vial C and the solution was stirred for >1 h.

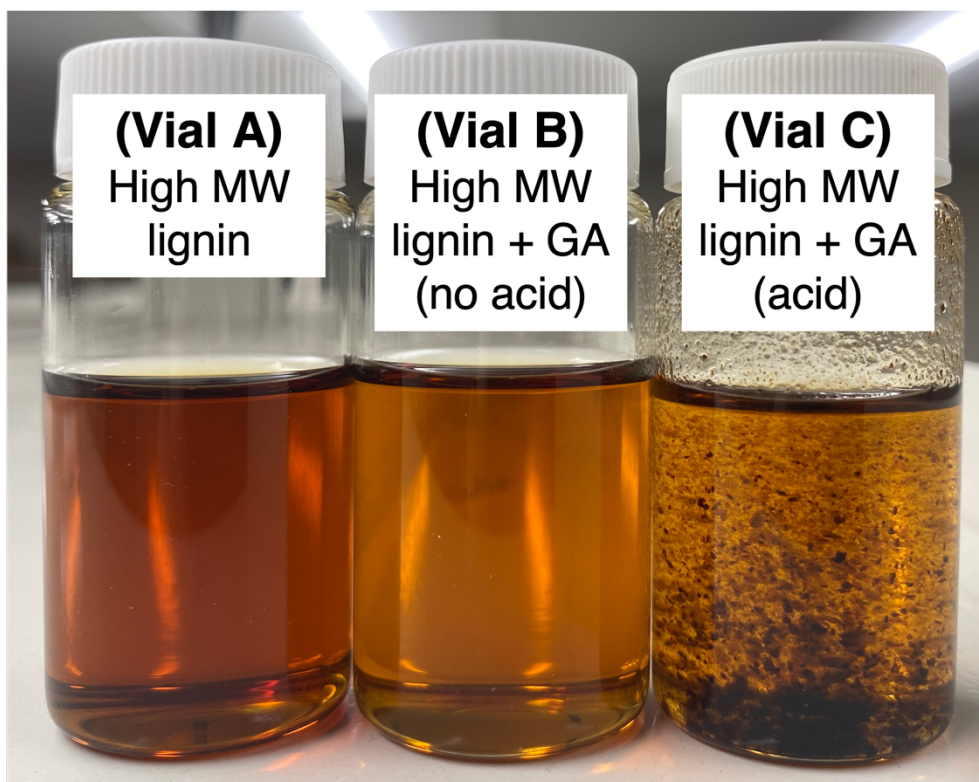


Figure B.1. Scintillation vials containing DMSO and (a) unmodified High MW lignin, (b) heat-treated High MW lignin + glutaraldehyde (fabricated with no sulfuric acid), and (c) heat-treated High MW lignin + glutaraldehyde (fabricated in a sulfuric acid solution with $\text{pH} \approx 3$).

The aforementioned three lignin samples, in their respective scintillation vials, are shown in Figure S1. Note, each vial contains 15 mL of DMSO, at a lignin concentration of 2.64 mg mL^{-1} . As seen in Figure B.1, the lignin contained in Vials A and B have completely dissolved, creating a transparent, brown solution. However, as seen in Vial C, the lignin crosslinked with GA under acidic conditions was unable to redissolve when fresh DMSO was added back. The inability of this lignin sample to completely dissolve verifies chemical crosslinking is occurring between the lignin and the GA chains in our fabrication process.

B.2 Hydroxyl (–OH) Content of BioChoice™ and ALPHA-Fractionated Lignin

The hydroxyl (–OH) contents of the feed BioChoice™ lignin (BCL), along with the ALPHA-fractionated Low MW and High MW lignin were determined via ³¹P nuclear magnetic resonance (NMR) spectrum for each sample. A summary of these data is presented in Table B.1.

Table B.1. Quantitative hydroxyl (–OH) content for BCL, Low MW lignin, and High MW lignin used in the synthesis of the PVA–lignin hydrogels. All values are reported in mmol OH/g lignin.

Lignin Fraction	Aliphatic	Syringyl (S)	Guaiacyl (G)	p-hydroxyphenyl (H)	Carboxylic Acid	Total
BCL	2.01	0.76	2.09	0.32	0.53	5.71
Low MW	1.80	0.78	2.29	0.33	0.65	5.85
High MW	1.99	0.80	1.96	0.32	0.52	5.59

B.3 Dynamic Mechanical Analysis (DMA) of Lignin Soft Composites

As mentioned in Experimental Section 4.2.7, DMA was performed on the PVA–lignin hydrogel composites in tensile mode over a frequency range of 0.1 to 100 rad s⁻¹. The full DMA frequency sweep results – i.e., the storage modulus – for all PVA–lignin hydrogel composites containing BCL lignin are shown in Figure B.2. As seen in Figure B.2, the storage modulus values for all BCL samples remain relatively constant over the entire range of frequencies explored. Notably, for both soft composites containing 25 wt % and 40 wt % lignin, there is a statistically significant increase in storage modulus when the

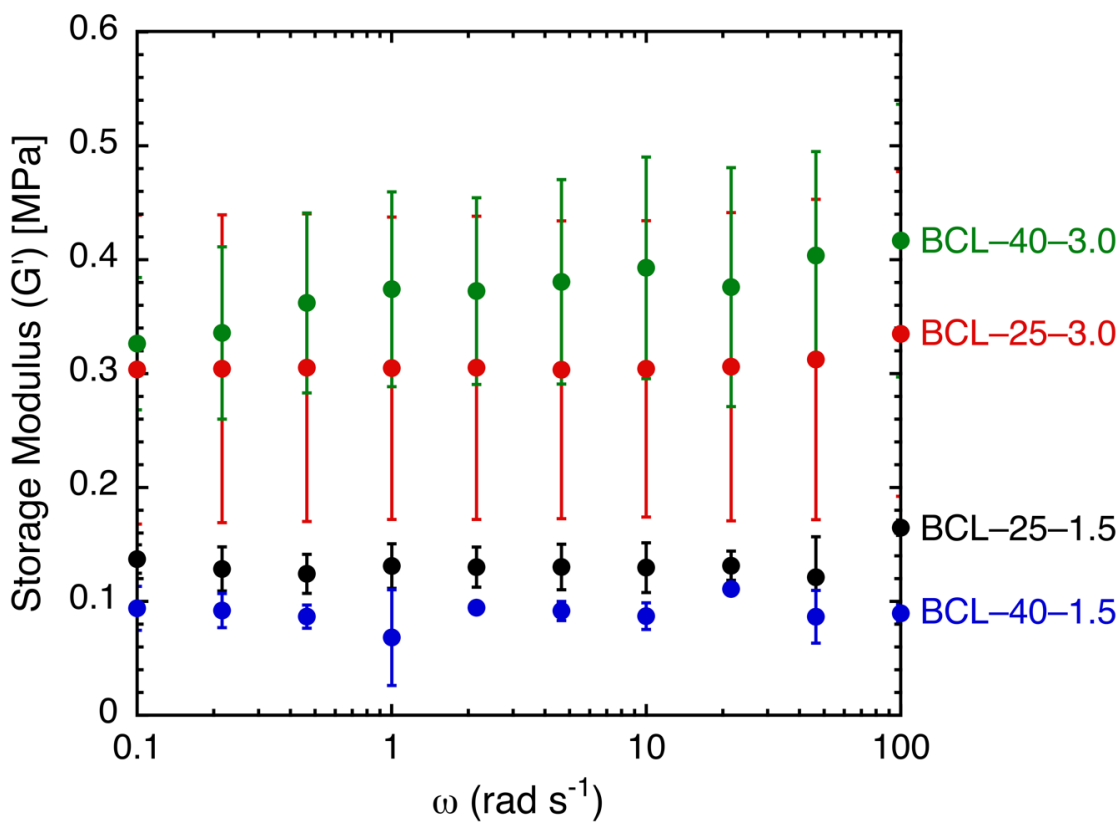


Figure B.2. Dynamic mechanical analysis spectra from 0.1 to 100 rad s⁻¹ for BCL molecular weight lignin-based PVA hydrogel composites. Note, the error bars in the figure represent the standard deviation of the average, which was calculated from repeat measurements on at least three separate membranes.

crosslinker concentration (glutaraldehyde (GA)) was increased from 1.5 wt % to 3.0 wt %, alluding to the tighter network structure formed in these membranes. For example, the storage modulus of BCL-40-3.0 (0.39 ± 0.01 MPa) is observed to be almost four-fold higher than that of BCL-40-1.5 (0.09 ± 0.01 MPa). A t test analysis reveals that these values are statistically significant for a 95% confidence interval with a p-value of 0.0252. Interestingly, within the uncertainty (error) of the data, almost no difference in the storage modulus is observed when the lignin content was increased to 40 wt %. The high variability/error in the data is an indirect indication of the increased heterogeneity of the

BCL lignin. We will revisit this shortly when presenting the data for soft composites containing fractionated, cleaned lignin.

The full DMA frequency sweep results – i.e., the storage modulus – for all PVA–lignin hydrogel composites containing the high molecular weight lignin are shown in Figure B.3. Analogous to the behavior observed for BCL-containing samples, the storage modulus values for all High-containing samples remain relatively constant over the entire range of frequencies explored. In contrast to the BCL storage modulus values shown in Figure B.2, there is noticeably less variability/error in the data for High-containing samples. We

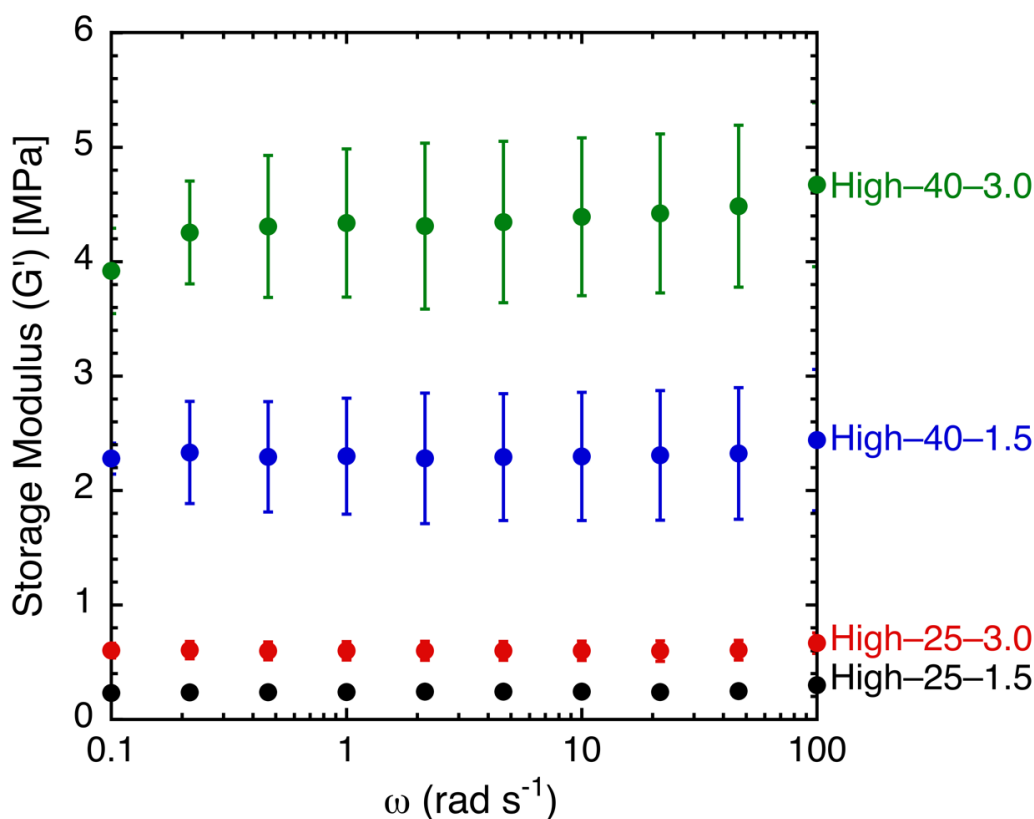


Figure B.3. Dynamic mechanical analysis spectra from 0.1 to 100 rad s⁻¹ for High molecular weight lignin-based PVA hydrogel composites. Note, the error bars in the figure represent the standard deviation of the average, which was calculated from repeat measurements on at least three separate membranes.

attribute this to the High lignin being fractionated from the Aqueous Lignin Purification with Hot Agents (ALPHA) process, creating membranes with more homogeneous network structures and higher repeatability from a membrane fabrication standpoint.

As was seen with the BCL-containing samples, there is a significant increase in storage modulus when the GA concentration was increased from 1.5 wt % to 3.0 wt %, alluding to the tighter network structure formed in these membranes. Specifically, the storage modulus of High-40-3.0 is observed to be almost double that of High-40-1.5. Interestingly, there are increases in storage modulus when the lignin concentration was increased from 25 wt % to 40 wt %, alluding to the tighter network structure formed in these membranes. For instance, the storage modulus of High-40-3.0 is observed to be almost four-fold that of High-25-3.0.

The full DMA frequency sweep results for PVA-lignin hydrogel composites containing 40 wt % low molecular weight lignin are shown in Figure B.4. Note, as mentioned in the main text of Chapter 4.3.2, Low-25-1.5 and Low-25-3.0 were too soft to mount into the apparatus, and hence, no data for these two membranes are shown in Figure S4. As seen with BCL- and High-containing soft composites, the storage moduli for hydrogels containing 40 wt % low molecular weight lignin remain relatively constant over the entire range of frequencies explored. Further, there was a statistically significant (p -value is 0.008 for a 95% confidence interval) increase in the storage modulus when the GA concentration was increased from 1.5 wt % (Low-40-1.5, 0.25 ± 0.01 MPa) to 3.0 wt % (Low-40-3.0, 0.36 ± 0.02 MPa), again, alluding to the tighter network structure formed in these membranes. In contrast to the data shown in Figure B.2, the data from soft composites

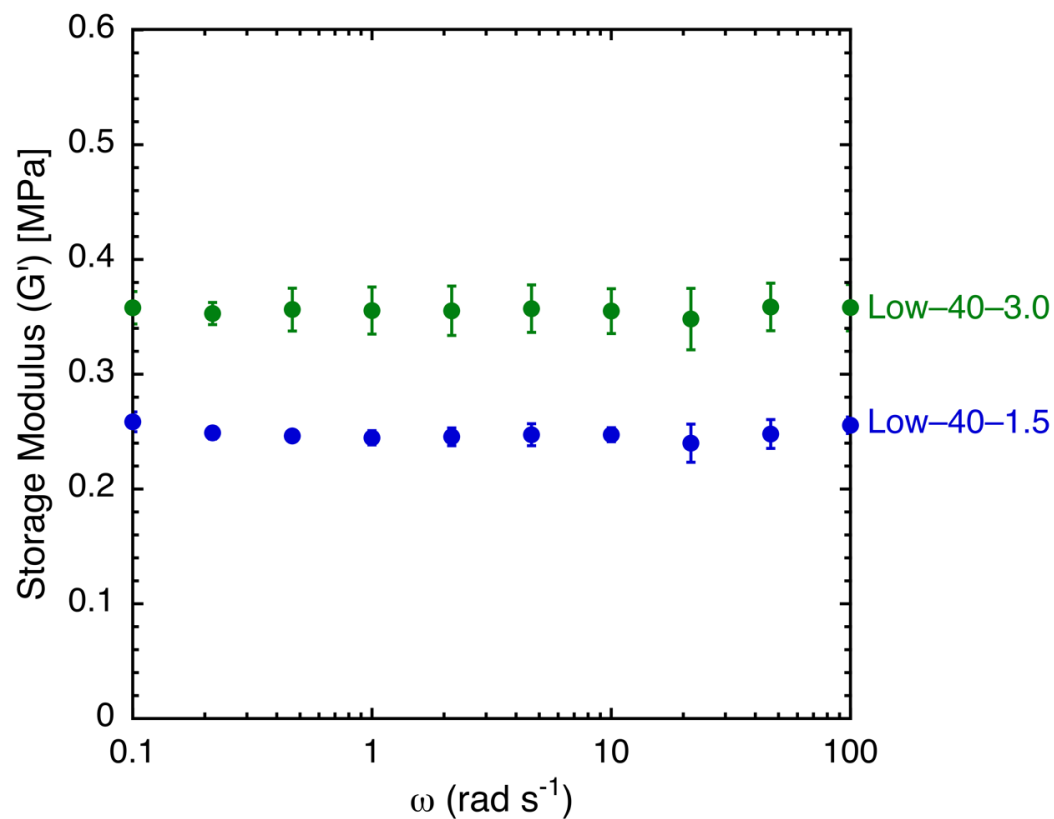


Figure B.4. Dynamic mechanical analysis spectra from 0.1 to 100 rad s⁻¹ for Low molecular weight lignin-based PVA hydrogel composites. Note, the error bars in the figure represent the standard deviation of the average, which was calculated from repeat measurements on at least three separate membranes.

containing the low molecular weight lignin showed significantly lower error/variability between individual samples. In combination with the high error/variability observed for the data in Figure B.2, these results underscore the significance of incorporating lignin of narrow dispersity into soft hydrogel composites. Lignin fractionated from the ALPHA process has demonstrated a significant impact on the repeatability of lignin-based soft composites and the lessening of their variability/error in storage modulus experimentation.

The full DMA frequency sweep results for neat PVA hydrogel composites containing 0 wt % lignin are shown in Figure B.5. Note, as mentioned in the main text of Chapter

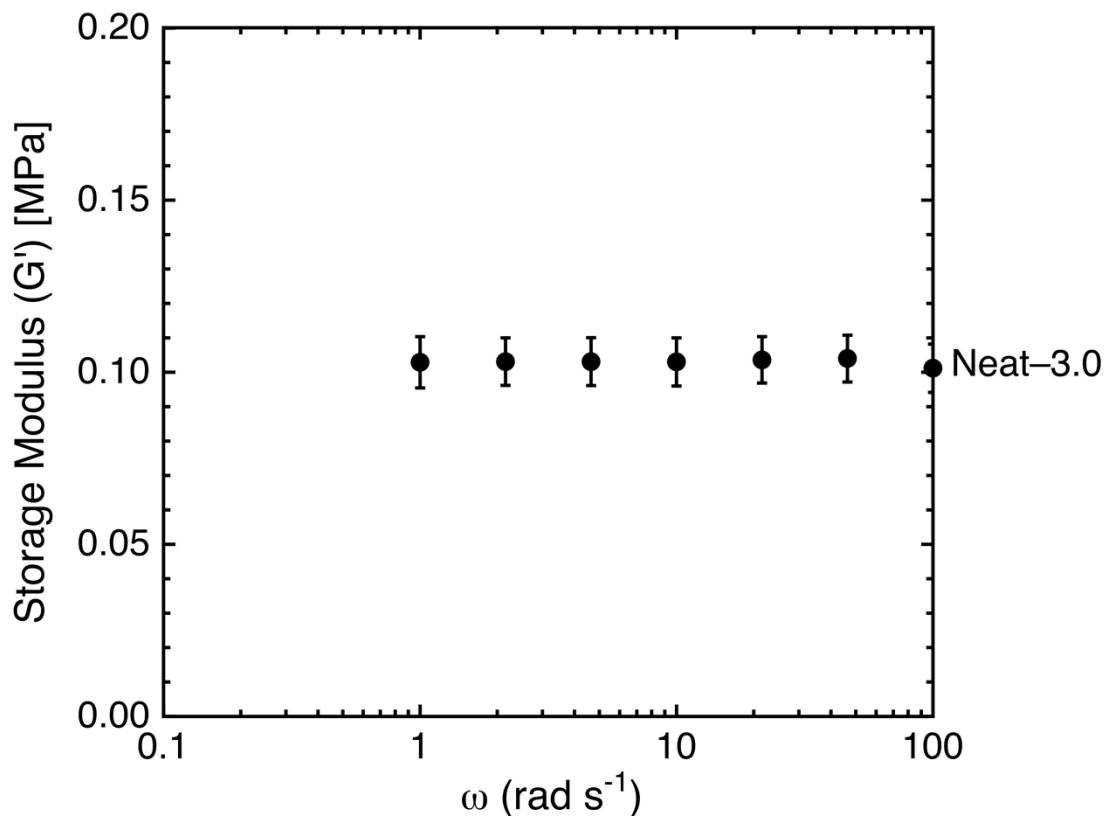


Figure B.5. Dynamic mechanical analysis spectra from 0.1 to 100 rad s^{-1} for neat PVA hydrogel composites. Note, the error bars in the figure represent the standard deviation of the average, which was calculated from repeat measurements on at least three separate membranes.

4.3.2, Neat-1.5 were too soft to mount into the apparatus, and hence, no data for this membrane is shown in Figure B.5.

B.4 Molecular Weight Between Crosslinks versus Other Properties

To better illustrate the correlation between changes in mechanical properties with changes in molecular weight between crosslinks (M_C) of the various soft composites, the

ultimate tensile strength (UTS), storage modulus, hydrated Young's modulus, and equilibrium water uptake have been plotted vs. M_C in Figures B.6, B.7, B.8, and B.9,

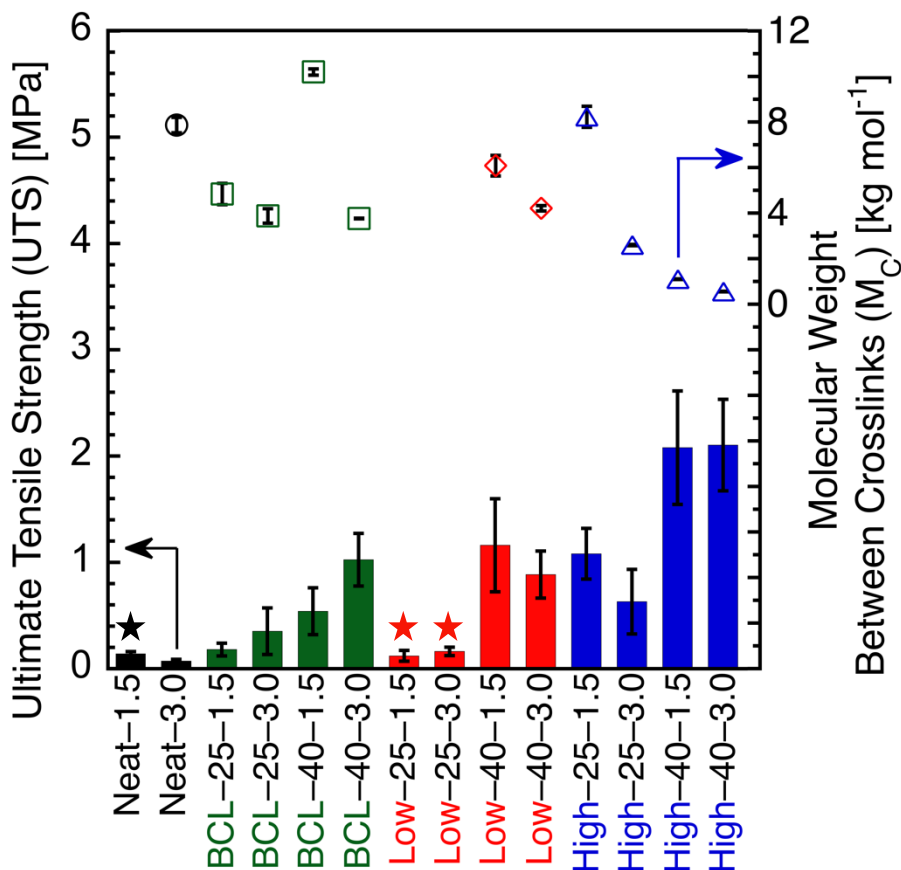


Figure B.6. Ultimate tensile strength values for neat PVA (solid black bars) and PVA–lignin composites containing BCL (solid green bars), Low MW (solid red bars), and High MW (solid blue bars). The molecular weight between crosslinks values for neat PVA (open black circles) and PVA–lignin composites containing BCL (open green squares), Low MW (open red diamonds), and High MW (open blue triangles). Note, the error bars in the figure represent the standard deviation of the average, which was calculated from repeat measurements on at least three separate membranes. Also note, stars denote samples whose storage moduli could not be measured as these samples were too soft to be mounted in the apparatus.

respectively. Specifically, data for the M_C was plotted on the right y-axis of the bar charts shown in the main body of Chapter 4.3.2.

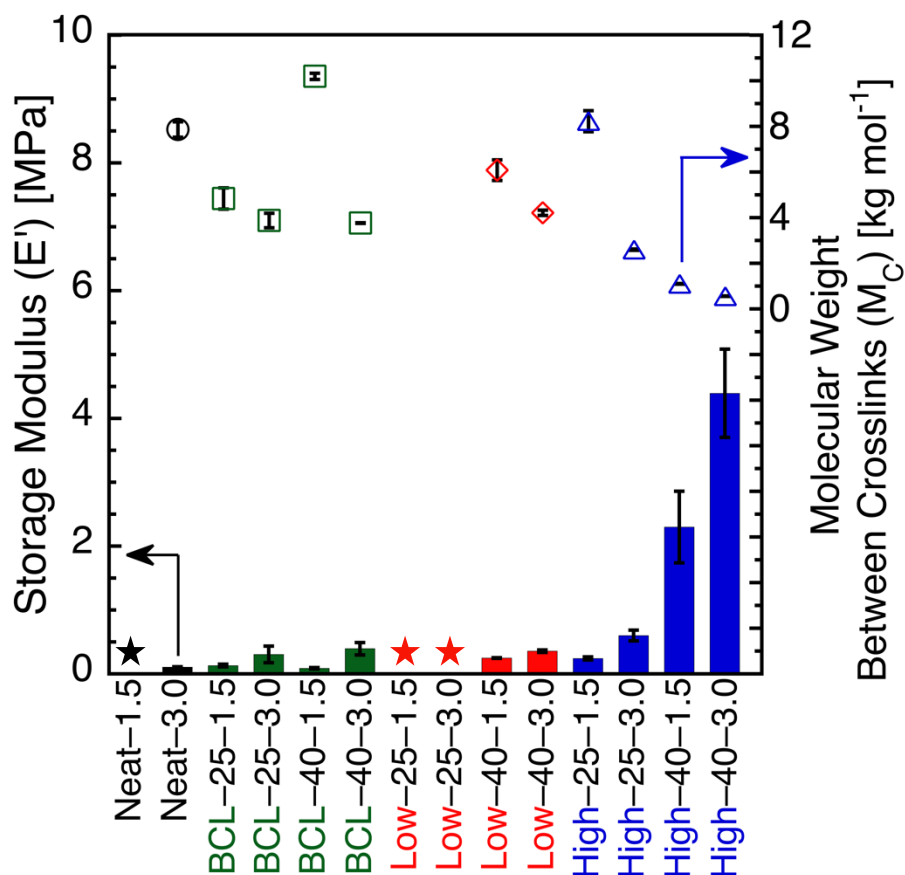


Figure B.7. Storage modulus values for neat PVA (solid black bars) and PVA–lignin composites containing BCL (solid green bars), Low MW (solid red bars), and High MW (solid blue bars). The molecular weight between crosslinks values for neat PVA (open black circles) and PVA–lignin composites containing BCL (open green squares), Low MW (open red diamonds), and High MW (open blue triangles). Note, the error bars in the figure represent the standard deviation of the average, which was calculated from repeat measurements on at least three separate membranes. Also note, stars denote samples whose storage moduli could not be measured as these samples were too soft to be mounted in the apparatus.

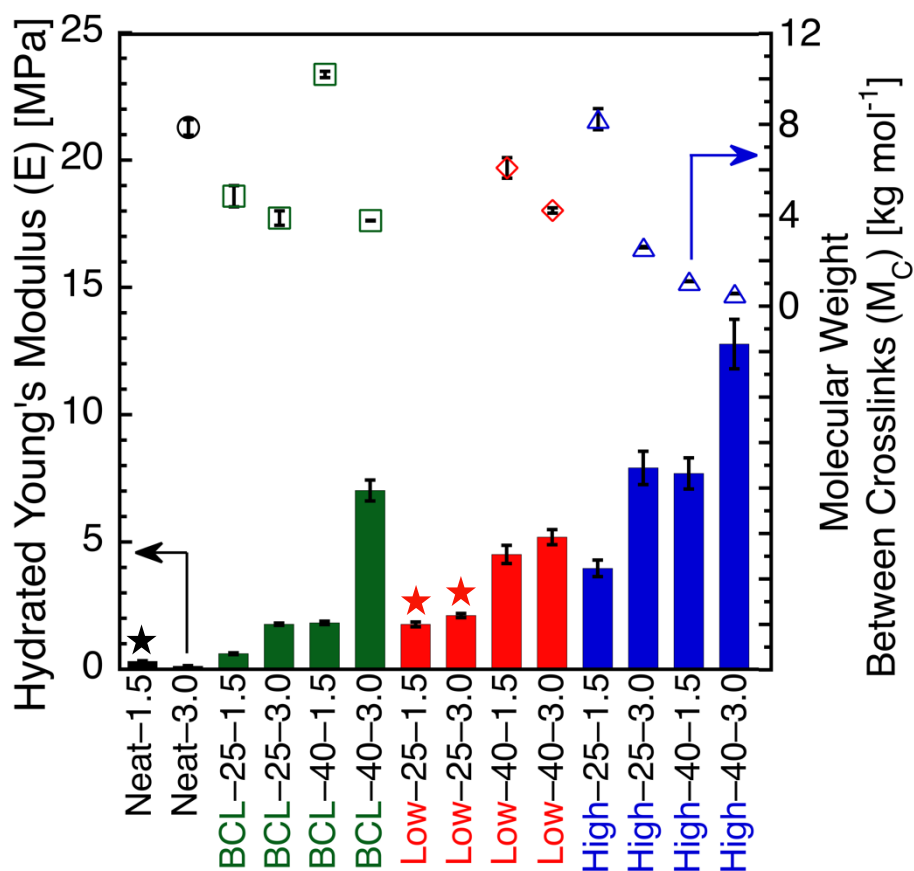


Figure B.8. Hydrated Young's modulus values for neat PVA (solid black bars) and PVA–lignin composites containing BCL (solid green bars), Low MW (solid red bars), and High MW (solid blue bars). The molecular weight between crosslinks values for neat PVA (open black circles) and PVA–lignin composites containing BCL (open green squares), Low MW (open red diamonds), and High MW (open blue triangles). Note, the error bars in the figure represent the standard deviation of the average, which was calculated from repeat measurements on at least three separate membranes. Also note, stars denote samples whose storage moduli could not be measured as these samples were too soft to be mounted in the apparatus.

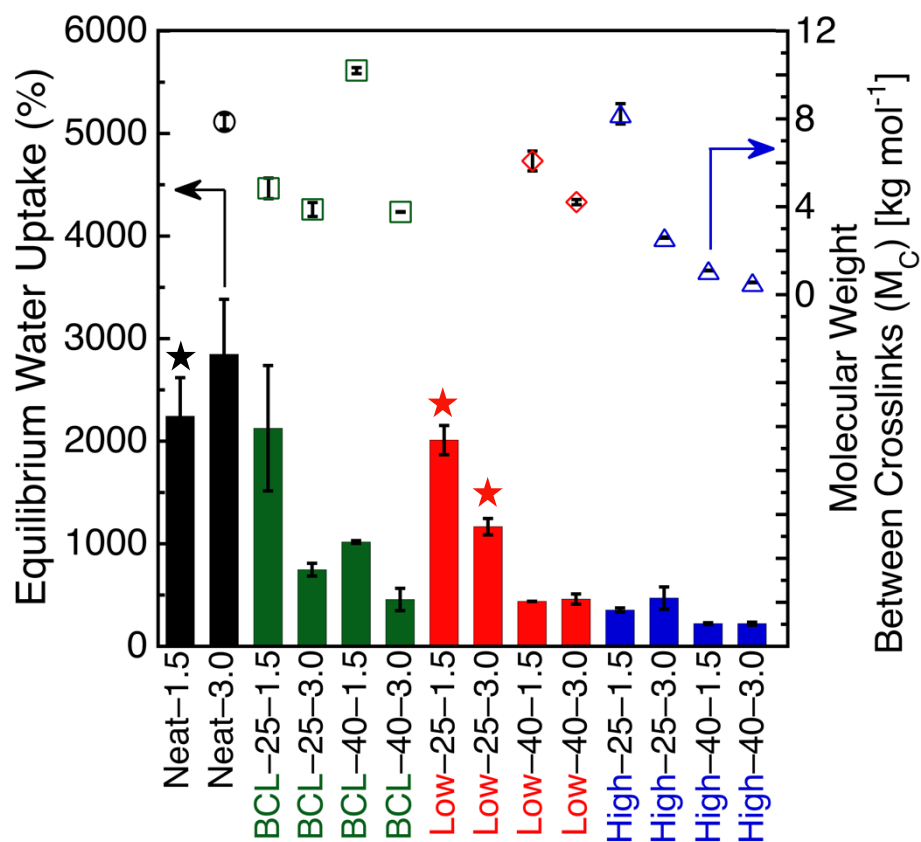


Figure B.9. Equilibrium water uptake values for neat PVA (solid black bars) and PVA–lignin composites containing BCL (solid green bars), Low MW (solid red bars), and High MW (solid blue bars). The molecular weight between crosslinks values for neat PVA (open black circles) and PVA–lignin composites containing BCL (open green squares), Low MW (open red diamonds), and High MW (open blue triangles). Note, the error bars in the figure represent the standard deviation of the average, which was calculated from repeat measurements on at least three separate membranes. Also note, stars denote samples whose storage moduli could not be measured as these samples were too soft to be mounted in the apparatus.

Appendix C

C.1 All Properties of Lignin Hydrogels Containing SLRP and BCL Lignin

The following tables present valuable information and characteristic property values for hydrogels containing ALPHA-fractionated lignin from the SLRP process. Nomenclature is as follows: PVA–lignin MW–lignin loading content (%) and UF/F for whether it was functionalized or not prior to fabrication.

Table C.1. Number average molecular weight and dispersity for CBL lignin acquired from the SLRP process and fractionated, UCL lignin.

Lignin	Number Average Molecular Weight (g mol ⁻¹)	Dispersity (Đ)
CBL (SLRP)	4170	3.9
UCL	1250	2.2

Table C.2. MB permeability, hydrated Young's modulus, and equilibrium water uptake for hydrogels containing UCL and CBL lignin.

Sample	MB Permeability (cm ² s ⁻¹)	Hydrated Young's Modulus (MPa)	Equilibrium Water Uptake (%)
PVA–Neat	5.05E-10 ± 3.3E-11	8.46 ± 0.21	145 ± 11
PVA–UCL–10UF	2.05E-10 ± 6.6E-12	6.23 ± 0.20	145 ± 6
PVA–UCL–10F	1.86E-10 ± 1.0E-11	7.95 ± 0.13	128 ± 4
PVA–UCL–20UF	2.66E-12 ± 2.4E-13	7.58 ± 0.14	112 ± 3
PVA–UCL–20F	2.89E-11 ± 5.0E-12	7.09 ± 0.12	121 ± 2
PVA–UCL–50UF	N/A	14.08 ± 0.17	93 ± 7
PVA–CBL–10UF	1.58E-10 ± 5.5E-11	11.69 ± 0.25	119 ± 2
PVA–CBL–10F	1.21E-10 ± 4.2E-12	12.09 ± 0.16	120 ± 2
PVA–CBL–20UF	1.84E-11 ± 3.5E-12	9.52 ± 0.28	102 ± 1
PVA–CBL–20F	4.87E-11 ± 6.9E-12	9.08 ± 0.48	100 ± 2
PVA–CBL–50UF	N/A	12.13 ± 0.52	64 ± 2

Table C.3. Molecular weight between crosslinks values for hydrogels containing UCL and CBL lignin.

Sample	Molecular Weight Between Crosslinks (g mol ⁻¹)
PVA–Neat	710 ± 3
PVA–UCL–10UF	770 ± 46
PVA–UCL–10F	579 ± 15
PVA–UCL–20UF	432 ± 15
PVA–UCL–20F	666 ± 64
PVA–UCL–50UF	355 ± 45
PVA–CBL–10UF	595 ± 2
PVA–CBL–10F	567 ± 6
PVA–CBL–20UF	401 ± 20
PVA–CBL–20F	392 ± 7
PVA–CBL–50UF	349 ± 53

The following tables present valuable information and characteristic property values for hydrogels containing ALPHA-fractionated lignin from BioChoice™(BCL). Nomenclature is as follows: lignin MW–lignin loading content (%)–crosslinker concentration (%).

Table C.4. Weight average molecular weight and dispersity for BCL, Low, and High MW lignin.

Lignin	Weight Average Molecular Weight (g mol ⁻¹)	Dispersity (Đ)
BCL	16100	3.9
Low	3900	3.2
High	25400	3.1

Table C.5. Ultimate tensile strength, storage modulus, molecular weight between crosslinks, and hydrated Young's modulus values for samples containing BCL, Low, and High lignin.

Sample	Ultimate Tensile Strength (MPa)	Storage Modulus (MPa)	Molecular Weight Between Crosslinks (kg mol ⁻¹)	Hydrated Young's Modulus (MPa)
Neat-1.5	0.14 ± 0.02	N/A	N/A	0.31 ± 0.03
Neat-3.0	0.07 ± 0.02	0.10 ± 0.01	7.86 ± 0.34	0.12 ± 0.02
Low-25-1.5	0.12 ± 0.05	N/A	N/A	1.76 ± 0.10
Low-25-3.0	0.16 ± 0.04	N/A	N/A	2.11 ± 0.08
Low-40-1.5	1.16 ± 0.44	0.25 ± 0.01	6.08 ± 0.45	4.51 ± 0.36
Low-40-3.0	0.89 ± 0.22	0.36 ± 0.02	4.21 ± 0.11	5.19 ± 0.30
BCL-25-1.5	0.18 ± 0.06	0.13 ± 0.02	4.84 ± 0.47	0.61 ± 0.04
BCL-25-3.0	0.35 ± 0.22	0.30 ± 0.13	3.88 ± 0.32	1.77 ± 0.04
BCL-40-1.5	0.54 ± 0.22	0.09 ± 0.01	10.19 ± 0.14	1.82 ± 0.07
BCL-40-3.0	1.03 ± 0.25	0.39 ± 0.10	3.76 ± 0.01	7.02 ± 0.41
High-25-1.5	1.08 ± 0.24	0.24 ± 0.02	8.23 ± 0.47	3.96 ± 0.32
High-25-3.0	0.63 ± 0.3	0.60 ± 0.08	2.60 ± 0.03	7.91 ± 0.65
High-40-1.5	2.08 ± 0.53	2.30 ± 0.56	1.10 ± 0.01	7.69 ± 0.61
High-40-3.0	2.10 ± 0.43	4.39 ± 0.69	0.56 ± 0.01	12.77 ± 0.97

Table C.6. Equilibrium water uptake values for samples containing BCL, Low, and High MW lignin.

Sample	Equilibrium Water Uptake (%)
Neat-1.5	2240 \pm 380
Neat-3.0	2850 \pm 550
Low-25-1.5	2010 \pm 140
Low-25-3.0	1170 \pm 80
Low-40-1.5	440 \pm 2
Low-40-3.0	460 \pm 50
BCL-25-1.5	2130 \pm 610
BCL-25-3.0	750 \pm 60
BCL-40-1.5	1020 \pm 10
BCL-40-3.0	460 \pm 110
High-25-1.5	350 \pm 20
High-25-3.0	470 \pm 110
High-40-1.5	220 \pm 10
High-40-3.0	220 \pm 14

Appendix D

D.1 Inductive Coupled Plasma Analysis, and Ash Content for SLRP and BCL Lignin

The following tables present inductive coupled plasma (ICP) analysis for SLRP and BCL lignin, along with their post fractionation values.

Table D.1. ICP values for SLRP and BCL lignin.

Lignin	Potassium (ppm)	Sodium (ppm)	Total metals (ppm)
SLRP	314	1401	8680
ALPHA processed SLRP	33	70	849
BioChoice	569	7157	2281
ALPHA processed BioChoice	81	649	192

Table D.2. Ash content values for BCL, Low and High MW lignin.

Lignin	Ash content at 750 °C
BCL	0.89%
Low	0.02%
High	0.07%

REFERENCES

- (1) Hegab, R. A.; Pardue, S.; Shen, X.; Kevil, C.; Peppas, N. A.; Caldorera-Moore, M. E. Effect of Network Mesh Size and Swelling to the Drug Delivery from PH Responsive Hydrogels. *J Appl Polym Sci* **2020**, *137* (25), 48767. <https://doi.org/10.1002/app.48767>.
- (2) Turner, J. G.; White, L. R.; Estrela, P.; Leese, H. S. Hydrogel-Forming Microneedles: Current Advancements and Future Trends. *Macromol. Biosci.* **2021**, *21* (2), 2000307. <https://doi.org/10.1002/mabi.202000307>.
- (3) Teodorescu, M.; Bercea, M.; Morariu, S. Biomaterials of Poly(Vinyl Alcohol) and Natural Polymers. *Polymer Reviews* **2018**, *58* (2), 247–287. <https://doi.org/10.1080/15583724.2017.1403928>.
- (4) Zare, M.; Bigham, A.; Zare, M.; Luo, H.; Rezvani Ghomi, E.; Ramakrishna, S. PHEMA: An Overview for Biomedical Applications. *IJMS* **2021**, *22* (12), 6376. <https://doi.org/10.3390/ijms22126376>.
- (5) Tang, L.; Wang, L.; Yang, X.; Feng, Y.; Li, Y.; Feng, W. Poly(N-Isopropylacrylamide)-Based Smart Hydrogels: Design, Properties and Applications. *Progress in Materials Science* **2021**, *115*, 100702. <https://doi.org/10.1016/j.pmatsci.2020.100702>.
- (6) Franco, P.; De Marco, I. The Use of Poly(N-Vinyl Pyrrolidone) in the Delivery of Drugs: A Review. *Polymers* **2020**, *12* (5), 1114. <https://doi.org/10.3390/polym12051114>.
- (7) Lu, X.; Perera, T. H.; Aria, A. B.; Smith Callahan, L. A. Polyethylene Glycol in Spinal Cord Injury Repair: A Critical Review. *JEP* **2018**, *Volume 10*, 37–49. <https://doi.org/10.2147/JEP.S148944>.
- (8) Peppas, N. A.; Keys, K. B.; Torres-Lugo, M.; Lowman, A. M. Poly(Ethylene Glycol)-Containing Hydrogels in Drug Delivery. *Journal of Controlled Release* **1999**, *62* (1–2), 81–87. [https://doi.org/10.1016/S0168-3659\(99\)00027-9](https://doi.org/10.1016/S0168-3659(99)00027-9).
- (9) Lin, C.-C. Recent Advances in Crosslinking Chemistry of Biomimetic Poly(Ethylene Glycol) Hydrogels. *RSC Adv.* **2015**, *5* (50), 39844–39853. <https://doi.org/10.1039/C5RA05734E>.
- (10) Moore, E. M.; West, J. L. Bioactive Poly(Ethylene Glycol) Acrylate Hydrogels for Regenerative Engineering. *Regen. Eng. Transl. Med.* **2019**, *5* (2), 167–179. <https://doi.org/10.1007/s40883-018-0074-y>.
- (11) Tang, S. C. N.; Yan, D. Y. S.; Lo, I. M. C. Sustainable Wastewater Treatment Using Microsized Magnetic Hydrogel with Magnetic Separation Technology. *Ind. Eng. Chem. Res.* **2014**, *53* (40), 15718–15724. <https://doi.org/10.1021/ie502512h>.
- (12) Hu, X.-S.; Liang, R.; Sun, G. Super-Adsorbent Hydrogel for Removal of Methylene Blue Dye from Aqueous Solution. *J. Mater. Chem. A* **2018**, *6* (36), 17612–17624. <https://doi.org/10.1039/C8TA04722G>.
- (13) Hu, T.; Liu, Q.; Gao, T.; Dong, K.; Wei, G.; Yao, J. Facile Preparation of Tannic Acid–Poly(Vinyl Alcohol)/Sodium Alginate Hydrogel Beads for Methylene Blue Removal from Simulated Solution. *ACS Omega* **2018**, *3* (7), 7523–7531. <https://doi.org/10.1021/acsomega.8b00577>.

- (14) Zhu, Y.; Zheng, Y.; Wang, F.; Wang, A. Monolithic Supermacroporous Hydrogel Prepared from High Internal Phase Emulsions (HIPEs) for Fast Removal of Cu²⁺ and Pb²⁺. *Chemical Engineering Journal* **2016**, *284*, 422–430. <https://doi.org/10.1016/j.cej.2015.08.157>.
- (15) Li, C.; Yan, Y.; Zhang, Q.; Zhang, Z.; Huang, L.; Zhang, J.; Xiong, Y.; Tan, S. Adsorption of Cd²⁺ and Ni²⁺ from Aqueous Single-Metal Solutions on Graphene Oxide-Chitosan-Poly(Vinyl Alcohol) Hydrogels. *Langmuir* **2019**, *35* (13), 4481–4490. <https://doi.org/10.1021/acs.langmuir.8b04189>.
- (16) Njuguna, D. G.; Schönherr, H. Xanthan Gum Hydrogels as High-Capacity Adsorbents for Dye Removal. *ACS Appl. Polym. Mater.* **2021**, *3* (6), 3142–3152. <https://doi.org/10.1021/acsapm.1c00343>.
- (17) Rohrbach, K.; Li, Y.; Zhu, H.; Liu, Z.; Dai, J.; Andreasen, J.; Hu, L. A Cellulose Based Hydrophilic, Oleophobic Hydrated Filter for Water/Oil Separation. *Chem. Commun.* **2014**, *50* (87), 13296–13299. <https://doi.org/10.1039/C4CC04817B>.
- (18) Gao, Y.; Guo, R.; Feng, Y.; Zhang, L.; Wang, C.; Song, J.; Jiao, T.; Zhou, J.; Peng, Q. Self-Assembled Hydrogels Based on Poly-Cyclodextrin and Poly-Azobenzene Compounds and Applications for Highly Efficient Removal of Bisphenol A and Methylene Blue. *ACS Omega* **2018**, *3* (9), 11663–11672. <https://doi.org/10.1021/acsomega.8b01810>.
- (19) Pandit, A. H.; Nisar, S.; Imtiyaz, K.; Nadeem, M.; Mazumdar, N.; Rizvi, M. M. A.; Ahmad, S. Injectable, Self-Healing, and Biocompatible *N*, *O*-Carboxymethyl Chitosan/Multialdehyde Guar Gum Hydrogels for Sustained Anticancer Drug Delivery. *Biomacromolecules* **2021**, *22* (9), 3731–3745. <https://doi.org/10.1021/acs.biomac.1c00537>.
- (20) Rial-Hermida, M. I.; Rey-Rico, A.; Blanco-Fernandez, B.; Carballo-Pedraes, N.; Byrne, E. M.; Mano, J. F. Recent Progress on Polysaccharide-Based Hydrogels for Controlled Delivery of Therapeutic Biomolecules. *ACS Biomater. Sci. Eng.* **2021**, *acsbiomaterials.0c01784*. <https://doi.org/10.1021/acsbiomaterials.0c01784>.
- (21) Ribeiro, M.; Boudoukhani, M.; Belmonte-Reche, E.; Genicio, N.; Sillankorva, S.; Gallo, J.; Rodríguez-Abreu, C.; Moulai-Mostefa, N.; Bañobre-López, M. Xanthan-Fe₃O₄ Nanoparticle Composite Hydrogels for Non-Invasive Magnetic Resonance Imaging and Magnetically Assisted Drug Delivery. *ACS Appl. Nano Mater.* **2021**, *4* (8), 7712–7729. <https://doi.org/10.1021/acsanm.1c00932>.
- (22) Cheng, X.; Jin, Y.; Sun, T.; Qi, R.; Fan, B.; Li, H. Oxidation- and Thermo-Responsive Poly(N-Isopropylacrylamide-Co-2-Hydroxyethyl Acrylate) Hydrogels Cross-Linked via Diselenides for Controlled Drug Delivery. *RSC Advances* **2015**, *5* (6), 4162–4170. <https://doi.org/10.1039/C4RA13500H>.
- (23) Narayanaswamy, R.; Torchilin, V. P. Hydrogels and Their Applications in Targeted Drug Delivery. *Molecules* **2019**, *24* (3), 603. <https://doi.org/10.3390/molecules24030603>.
- (24) Sun, Z.; Song, C.; Wang, C.; Hu, Y.; Wu, J. Hydrogel-Based Controlled Drug Delivery for Cancer Treatment: A Review. *Mol. Pharmaceutics* **2020**, *acs.molpharmaceut.9b01020*. <https://doi.org/10.1021/acs.molpharmaceut.9b01020>.

- (25) Hong, S.; Sycks, D.; Chan, H. F.; Lin, S.; Lopez, G. P.; Guilak, F.; Leong, K. W.; Zhao, X. 3D Printing of Highly Stretchable and Tough Hydrogels into Complex, Cellularized Structures. *Adv. Mater.* **2015**, *27* (27), 4035–4040. <https://doi.org/10.1002/adma.201501099>.
- (26) Balavigneswaran, C. K.; Muthuvijayan, V. Nanohybrid-Reinforced Gelatin-Ureidopyrimidinone-Based Self-Healing Injectable Hydrogels for Tissue Engineering Applications. *ACS Appl. Bio Mater.* **2021**, *4* (6), 5362–5377. <https://doi.org/10.1021/acsabm.1c00458>.
- (27) Gu, X.; Xu, Y.; Li, S.; Wang, Z.; Meng, Q.; Yu, J. Preparation of a Photocured Biocompatible Hydrogel for Urethral Tissue Engineering. *ACS Appl. Polym. Mater.* **2021**, *3* (7), 3519–3527. <https://doi.org/10.1021/acsapm.1c00427>.
- (28) Jordan, A. M.; Kim, S.-E.; Van de Voorde, K.; Pokorski, J. K.; Korley, L. T. J. In Situ Fabrication of Fiber Reinforced Three-Dimensional Hydrogel Tissue Engineering Scaffolds. *ACS Biomater. Sci. Eng.* **2017**, *3* (8), 1869–1879. <https://doi.org/10.1021/acsbiomaterials.7b00229>.
- (29) Osi, A. R.; Zhang, H.; Chen, J.; Zhou, Y.; Wang, R.; Fu, J.; Müller-Buschbaum, P.; Zhong, Q. Three-Dimensional-Printable Thermo/Photo-Cross-Linked Methacrylated Chitosan–Gelatin Hydrogel Composites for Tissue Engineering. *ACS Appl. Mater. Interfaces* **2021**, *13* (19), 22902–22913. <https://doi.org/10.1021/acsami.1c01321>.
- (30) Liang, Y.; He, J.; Guo, B. Functional Hydrogels as Wound Dressing to Enhance Wound Healing. *ACS Nano* **2021**, *15* (8), 12687–12722. <https://doi.org/10.1021/acsnano.1c04206>.
- (31) Xu, Z.; Han, S.; Gu, Z.; Wu, J. Advances and Impact of Antioxidant Hydrogel in Chronic Wound Healing. *Adv. Healthcare Mater.* **2020**, *9* (5), 1901502. <https://doi.org/10.1002/adhm.201901502>.
- (32) Fan, Z.; Liu, B.; Wang, J.; Zhang, S.; Lin, Q.; Gong, P.; Ma, L.; Yang, S. A Novel Wound Dressing Based on Ag/Graphene Polymer Hydrogel: Effectively Kill Bacteria and Accelerate Wound Healing. *Adv. Funct. Mater.* **2014**, *24* (25), 3933–3943. <https://doi.org/10.1002/adfm.201304202>.
- (33) Larrañeta, E.; Imízcoz, M.; Toh, J. X.; Irwin, N. J.; Ripolin, A.; Perminova, A.; Domínguez-Robles, J.; Rodríguez, A.; Donnelly, R. F. Synthesis and Characterization of Lignin Hydrogels for Potential Applications as Drug Eluting Antimicrobial Coatings for Medical Materials. *ACS Sustainable Chem. Eng.* **2018**, *6* (7), 9037–9046. <https://doi.org/10.1021/acssuschemeng.8b01371>.
- (34) Gao, Y.; Guo, R.; Feng, Y.; Zhang, L.; Wang, C.; Song, J.; Jiao, T.; Zhou, J.; Peng, Q. Self-Assembled Hydrogels Based on Poly-Cyclodextrin and Poly-Azobenzene Compounds and Applications for Highly Efficient Removal of Bisphenol A and Methylene Blue. *ACS Omega* **2018**, *3* (9), 11663–11672. <https://doi.org/10.1021/acsomega.8b01810>.
- (35) Gull, N.; Khan, S. M.; Butt, O. M.; Islam, A.; Shah, A.; Jabeen, S.; Khan, S. U.; Khan, A.; Khan, R. U.; Butt, M. T. Z. Inflammation Targeted Chitosan-Based Hydrogel for Controlled Release of Diclofenac Sodium. *International Journal of*

- Biological Macromolecules* **2020**, *162*, 175–187.
<https://doi.org/10.1016/j.ijbiomac.2020.06.133>.
- (36) Varnier, K.; Vieira, T.; Wolf, M.; Belfiore, L. A.; Tambourgi, E. B.; Paulino, A. T. Polysaccharide-Based Hydrogels for the Immobilization and Controlled Release of Bovine Serum Albumin. *International Journal of Biological Macromolecules* **2018**, *120*, 522–528. <https://doi.org/10.1016/j.ijbiomac.2018.08.133>.
- (37) Naddaf, A. A.; Tsibranska, I.; Bart, H.-J. Kinetics of BSA Release from Poly(N-Isopropylacrylamide) Hydrogels. *Chemical Engineering and Processing: Process Intensification* **2010**, *49* (6), 581–588. <https://doi.org/10.1016/j.cep.2010.05.008>.
- (38) Mondal, S.; Li, C.; Wang, K. Bovine Serum Albumin Adsorption on Glutaraldehyde Cross-Linked Chitosan Hydrogels. *Journal of Chemical & Engineering Data* **2015**, *60* (8), 2356–2362.
<https://doi.org/10.1021/acs.jced.5b00264>.
- (39) Tong, X.; Lee, S.; Bararpour, L.; Yang, F. Long-Term Controlled Protein Release from Poly(Ethylene Glycol) Hydrogels by Modulating Mesh Size and Degradation: Long-Term Controlled Protein Release from Poly(Ethylene Glycol) Hydrogels.... *Macromolecular Bioscience* **2015**, *15* (12), 1679–1686.
<https://doi.org/10.1002/mabi.201500245>.
- (40) Lee, S.; Tong, X.; Yang, F. The Effects of Varying Poly(Ethylene Glycol) Hydrogel Crosslinking Density and the Crosslinking Mechanism on Protein Accumulation in Three-Dimensional Hydrogels. *Acta Biomaterialia* **2014**, *10* (10), 4167–4174. <https://doi.org/10.1016/j.actbio.2014.05.023>.
- (41) Annabi, N.; Tamayol, A.; Uquillas, J. A.; Akbari, M.; Bertassoni, L. E.; Cha, C.; Camci-Unal, G.; Dokmeci, M. R.; Peppas, N. A.; Khademhosseini, A. 25th Anniversary Article: Rational Design and Applications of Hydrogels in Regenerative Medicine. *Advanced Materials* **2014**, *26* (1), 85–124.
<https://doi.org/10.1002/adma.201303233>.
- (42) Gadhawe, R. V.; Mahanwar, P. A.; Gadekar, P. T. Effect of Glutaraldehyde on Thermal and Mechanical Properties of Starch and Polyvinyl Alcohol Blends. *Designed Monomers and Polymers* **2019**, *22* (1), 164–170.
<https://doi.org/10.1080/15685551.2019.1678222>.
- (43) Jain, E.; Kumar, A. Designing Supermacroporous Cryogels Based on Polyacrylonitrile and a Polyacrylamide–Chitosan Semi-Interpenetrating Network. *Journal of Biomaterials Science, Polymer Edition* **2009**, *20* (7–8), 877–902.
<https://doi.org/10.1163/156856209X444321>.
- (44) Morandim-Giannetti, A. de A.; Rubio, S. R.; Nogueira, R. F.; Ortega, F. dos S.; Magalhães Junior, O.; Schor, P.; Bersanetti, P. A. Characterization of PVA/Glutaraldehyde Hydrogels Obtained Using Central Composite Rotatable Design (CCRD): CHARACTERIZATION OF PVA/GLUTARALDEHYDE HYDROGELS. *Journal of Biomedical Materials Research Part B: Applied Biomaterials* **2017**. <https://doi.org/10.1002/jbm.b.33958>.
- (45) Wang, S.; Ren, J.; Li, W.; Sun, R.; Liu, S. Properties of Polyvinyl Alcohol/Xylan Composite Films with Citric Acid. *Carbohydrate Polymers* **2014**, *103*, 94–99.
<https://doi.org/10.1016/j.carbpol.2013.12.030>.

- (46) Rudra, R.; Kumar, V.; Kundu, P. P. Acid Catalysed Cross-Linking of Poly Vinyl Alcohol (PVA) by Glutaraldehyde: Effect of Crosslink Density on the Characteristics of PVA Membranes Used in Single Chambered Microbial Fuel Cells. *RSC Adv.* **2015**, *5* (101), 83436–83447. <https://doi.org/10.1039/C5RA16068E>.
- (47) Alfayyadh, A. A. M.; Lotfy, S.; Basfar, A. A.; Khalil, M. I. Influences of Poly (Vinyl Alcohol) Molecular Weight and Carbon Nanotubes on Radiation Crosslinking Shape Memory Polymers. *Progress in Natural Science: Materials International* **2017**, *27* (3), 316–325. <https://doi.org/10.1016/j.pnsc.2017.04.015>.
- (48) Dragan, E. S. Design and Applications of Interpenetrating Polymer Network Hydrogels. A Review. *Chemical Engineering Journal* **2014**, *243*, 572–590. <https://doi.org/10.1016/j.cej.2014.01.065>.
- (49) Zerpa, A.; Pakzad, L.; Fatehi, P. Hardwood Kraft Lignin-Based Hydrogels: Production and Performance. *ACS Omega* **2018**, *3* (7), 8233–8242. <https://doi.org/10.1021/acsomega.8b01176>.
- (50) Lee, Y.-P.; Liu, H.-Y.; Lin, P.-C.; Lee, Y.-H.; Yu, L.-R.; Hsieh, C.-C.; Shih, P.-J.; Shih, W.-P.; Wang, I.-J.; Yen, J.-Y.; Dai, C.-A. Facile Fabrication of Superporous and Biocompatible Hydrogel Scaffolds for Artificial Corneal Periphery. *Colloids and Surfaces B: Biointerfaces* **2019**, *175*, 26–35. <https://doi.org/10.1016/j.colsurfb.2018.11.013>.
- (51) Zhan, Y.; Fu, W.; Xing, Y.; Ma, X.; Chen, C. Advances in Versatile Anti-Swelling Polymer Hydrogels. *Materials Science and Engineering: C* **2021**, *127*, 112208. <https://doi.org/10.1016/j.msec.2021.112208>.
- (52) Ju, H.; McCloskey, B. D.; Sagle, A. C.; Kusuma, V. A.; Freeman, B. D. Preparation and Characterization of Crosslinked Poly(Ethylene Glycol) Diacrylate Hydrogels as Fouling-Resistant Membrane Coating Materials. *Journal of Membrane Science* **2009**, *330* (1–2), 180–188. <https://doi.org/10.1016/j.memsci.2008.12.054>.
- (53) Liu, Y.; Wang, P.; Wang, J.; Xu, B.; Xu, J.; Yuan, J.; Yu, Y.; Wang, Q. Transparent and Tough Poly(2-Hydroxyethyl Methacrylate) Hydrogels Prepared in Water/IL Mixtures. *New J. Chem.* **2020**, *44* (10), 4092–4098. <https://doi.org/10.1039/D0NJ00214C>.
- (54) Wang, Y.; Chen, Q.; Chen, M.; Guan, Y.; Zhang, Y. PHEMA Hydrogel Films Crosslinked with Dynamic Disulfide Bonds: Synthesis, Swelling-Induced Mechanical Instability and Self-Healing. *Polym. Chem.* **2019**, *10* (35), 4844–4851. <https://doi.org/10.1039/C9PY00670B>.
- (55) Hobzova, R.; Hrib, J.; Sirc, J.; Karpushkin, E.; Michalek, J.; Janouskova, O.; Gatenholm, P. Embedding of Bacterial Cellulose Nanofibers within PHEMA Hydrogel Matrices: Tunable Stiffness Composites with Potential for Biomedical Applications. *Journal of Nanomaterials* **2018**, *2018*, 1–11. <https://doi.org/10.1155/2018/5217095>.
- (56) Xia, L. L.; Li, C. L.; Wang, Y. In-Situ Crosslinked PVA/Organosilica Hybrid Membranes for Pervaporation Separations. *Journal of Membrane Science* **2016**, *498*, 263–275. <https://doi.org/10.1016/j.memsci.2015.10.025>.

- (57) Liu, Y.; Geever, L. M.; Kennedy, J. E.; Higginbotham, C. L.; Cahill, P. A.; McGuinness, G. B. Thermal Behavior and Mechanical Properties of Physically Crosslinked PVA/Gelatin Hydrogels. *Journal of the Mechanical Behavior of Biomedical Materials* **2010**, *3* (2), 203–209. <https://doi.org/10.1016/j.jmbbm.2009.07.001>.
- (58) Mansur, H. S.; Sadahira, C. M.; Souza, A. N.; Mansur, A. A. P. FTIR Spectroscopy Characterization of Poly (Vinyl Alcohol) Hydrogel with Different Hydrolysis Degree and Chemically Crosslinked with Glutaraldehyde. *Materials Science and Engineering: C* **2008**, *28* (4), 539–548. <https://doi.org/10.1016/j.msec.2007.10.088>.
- (59) Mansur, H. S.; Oréfice, R. L.; Mansur, A. A. P. Characterization of Poly(Vinyl Alcohol)/Poly(Ethylene Glycol) Hydrogels and PVA-Derived Hybrids by Small-Angle X-Ray Scattering and FTIR Spectroscopy. *Polymer* **2004**, *45* (21), 7193–7202. <https://doi.org/10.1016/j.polymer.2004.08.036>.
- (60) Hasimi, A.; Stavropoulou, A.; Papadokostaki, K. G.; Sanopoulou, M. Transport of Water in Polyvinyl Alcohol Films: Effect of Thermal Treatment and Chemical Crosslinking. *European Polymer Journal* **2008**, *44* (12), 4098–4107. <https://doi.org/10.1016/j.eurpolymj.2008.09.011>.
- (61) Wang, Y.; Hsieh, Y.-L. Crosslinking of Polyvinyl Alcohol (PVA) Fibrous Membranes with Glutaraldehyde and PEG Diacylchloride. *J. Appl. Polym. Sci.* **2010**, *116*, 3249–3255. <https://doi.org/10.1002/app.31750>.
- (62) Park, J.-S.; Park, J.-W.; Ruckenstein, E. Thermal and Dynamic Mechanical Analysis of PVA/MC Blend Hydrogels. *Polymer* **2001**, *42* (9), 4271–4280. [https://doi.org/10.1016/S0032-3861\(00\)00768-0](https://doi.org/10.1016/S0032-3861(00)00768-0).
- (63) Figueiredo, K. C. S.; Alves, T. L. M.; Borges, C. P. Poly(Vinyl Alcohol) Films Crosslinked by Glutaraldehyde under Mild Conditions. *J. Appl. Polym. Sci.* **2009**, *111* (6), 3074–3080. <https://doi.org/10.1002/app.29263>.
- (64) Yeom, C.-K.; Lee, K.-H. Pervaporation Separation of Water-Acetic Acid Mixtures through Poly (Vinyl Alcohol) Membranes Crosslinked with Glutaraldehyde. *Journal of Membrane Science* **1996**, *109* (2), 257–265.
- (65) Stone, S. A.; Gosavi, P.; Athauda, T. J.; Ozer, R. R. In Situ Citric Acid Crosslinking of Alginate/Polyvinyl Alcohol Electrospun Nanofibers. *Materials Letters* **2013**, *112*, 32–35. <https://doi.org/10.1016/j.matlet.2013.08.100>.
- (66) Shi, R.; Bi, J.; Zhang, Z.; Zhu, A.; Chen, D.; Zhou, X.; Zhang, L.; Tian, W. The Effect of Citric Acid on the Structural Properties and Cytotoxicity of the Polyvinyl Alcohol/Starch Films When Molding at High Temperature. *Carbohydrate Polymers* **2008**, *74* (4), 763–770. <https://doi.org/10.1016/j.carbpol.2008.04.045>.
- (67) Rynkowska; Fatyeyeva; Marais; Kujawa; Kujawski. Chemically and Thermally Crosslinked PVA-Based Membranes: Effect on Swelling and Transport Behavior. *Polymers* **2019**, *11* (11), 1799. <https://doi.org/10.3390/polym11111799>.
- (68) Hassan, C. M.; Peppas, N. A. Structure and Morphology of Freeze/Thawed PVA Hydrogels. *Macromolecules* **2000**, *33* (7), 2472–2479. <https://doi.org/10.1021/ma9907587>.

- (69) Guo, Y.; Bae, J.; Fang, Z.; Li, P.; Zhao, F.; Yu, G. Hydrogels and Hydrogel-Derived Materials for Energy and Water Sustainability. *Chem. Rev.* **2020**, *120* (15), 7642–7707. <https://doi.org/10.1021/acs.chemrev.0c00345>.
- (70) Hickey, A. S.; Peppas, N. A. Mesh Size and Diffusive Characteristics of Semicrystalline Poly (Vinyl Alcohol) Membranes Prepared by Freezing/Thawing Techniques. *Journal of membrane science* **1995**, *107* (3), 229–237.
- (71) Hou, Y.; Chen, C.; Liu, K.; Tu, Y.; Zhang, L.; Li, Y. Preparation of PVA Hydrogel with High-Transparence and Investigations of Its Transparent Mechanism. *RSC Advances* **2015**, *5* (31), 24023–24030. <https://doi.org/10.1039/C5RA01280E>.
- (72) Saffer, E. M.; Lackey, M. A.; Griffin, D. M.; Kishore, S.; Tew, G. N.; Bhatia, S. R. SANS Study of Highly Resilient Poly(Ethylene Glycol) Hydrogels. *Soft Matter* **2014**, *10* (12), 1905. <https://doi.org/10.1039/c3sm52395k>.
- (73) Zander, Z. K.; Hua, G.; Wiener, C. G.; Vogt, B. D.; Becker, M. L. Control of Mesh Size and Modulus by Kinetically Dependent Cross-Linking in Hydrogels. *Adv. Mater.* **2015**, *27* (40), 6283–6288. <https://doi.org/10.1002/adma.201501822>.
- (74) Mihajlovic, M.; Staropoli, M.; Appavou, M.-S.; Wyss, H. M.; Pyckhout-Hintzen, W.; Sijbesma, R. P. Tough Supramolecular Hydrogel Based on Strong Hydrophobic Interactions in a Multiblock Segmented Copolymer. *Macromolecules* **2017**, *50* (8), 3333–3346. <https://doi.org/10.1021/acs.macromol.7b00319>.
- (75) Lawrence, M. B.; Desa, J. A. E.; Aswal, V. K. Reentrant Behaviour in Polyvinyl Alcohol–Borax Hydrogels. *Mater. Res. Express* **2018**, *5* (1), 015315. <https://doi.org/10.1088/2053-1591/aaa6e6>.
- (76) Papagiannopoulos, A.; Vlassi, E.; Pispas, S.; Tsitsilianis, C.; Radulescu, A. Polyethylene Oxide Hydrogels Crosslinked by Peroxide for the Controlled Release of Proteins. *Macromol* **2020**, *1* (1), 37–48. <https://doi.org/10.3390/macromol1010004>.
- (77) Priyadarshi, R.; Roy, S.; Purohit, S. D.; Ghosh, T. Biopolymers for Food Packaging and Biomedical Applications: Options or Obligations? *Coatings* **2022**, *12* (9), 1261. <https://doi.org/10.3390/coatings12091261>.
- (78) United States Environmental Protection Agency. Advancing Sustainable Materials Management: 2018 Fact Sheet. **2018**, 25.
- (79) Jambeck, J. R.; Geyer, R.; Wilcox, C.; Siegler, T. R.; Perryman, M.; Andrady, A.; Narayan, R.; Law, K. L. Plastic Waste Inputs from Land into the Ocean. *Science* **2015**, *347* (6223), 768–771. <https://doi.org/10.1126/science.1260352>.
- (80) Gnanasekaran, D. Green Biopolymers and Its Nanocomposites in Various Applications: State of the Art. In *Green Biopolymers and their Nanocomposites*; Gnanasekaran, D., Ed.; Materials Horizons: From Nature to Nanomaterials; Springer Singapore: Singapore, 2019; pp 1–27. https://doi.org/10.1007/978-981-13-8063-1_1.
- (81) Miller, S. A. Sustainable Polymers: Replacing Polymers Derived from Fossil Fuels. *Polym. Chem.* **2014**, *5* (9), 3117. <https://doi.org/10.1039/c4py90017k>.
- (82) Dergunov, S. A.; Mun, G. A. γ -Irradiated Chitosan-Polyvinyl Pyrrolidone Hydrogels as PH-Sensitive Protein Delivery System. *Radiation Physics and*

- Chemistry* **2009**, 78 (1), 65–68.
<https://doi.org/10.1016/j.radphyschem.2008.07.003>.
- (83) Vaghani, S. S.; Patel, M. M. PH-Sensitive Hydrogels Based on Semi-Interpenetrating Network (Semi-IPN) of Chitosan and Polyvinyl Pyrrolidone for Clarithromycin Release. *Drug Development and Industrial Pharmacy* **2011**, 37 (10), 1160–1169. <https://doi.org/10.3109/03639045.2011.563422>.
- (84) Sannino, A.; Demitri, C.; Madaghiele, M. Biodegradable Cellulose-Based Hydrogels: Design and Applications. *Materials* **2009**, 2 (2), 353–373.
<https://doi.org/10.3390/ma2020353>.
- (85) Peng, N.; Wang, Y.; Ye, Q.; Liang, L.; An, Y.; Li, Q.; Chang, C. Biocompatible Cellulose-Based Superabsorbent Hydrogels with Antimicrobial Activity. *Carbohydrate Polymers* **2016**, 137, 59–64.
<https://doi.org/10.1016/j.carbpol.2015.10.057>.
- (86) Domínguez-Robles, J.; Peresin, M. S.; Tamminen, T.; Rodríguez, A.; Larrañeta, E.; Jääskeläinen, A.-S. Lignin-Based Hydrogels with “Super-Swelling” Capacities for Dye Removal. *International Journal of Biological Macromolecules* **2018**, 115, 1249–1259. <https://doi.org/10.1016/j.ijbiomac.2018.04.044>.
- (87) Thakur, V. K.; Thakur, M. K. Recent Advances in Green Hydrogels from Lignin: A Review. *International Journal of Biological Macromolecules* **2015**, 72, 834–847. <https://doi.org/10.1016/j.ijbiomac.2014.09.044>.
- (88) Thakur, S.; Govender, P. P.; Mamo, M. A.; Tamulevicius, S.; Mishra, Y. K.; Thakur, V. K. Progress in Lignin Hydrogels and Nanocomposites for Water Purification: Future Perspectives. *Vacuum* **2017**, 146, 342–355.
<https://doi.org/10.1016/j.vacuum.2017.08.011>.
- (89) Rajan, K.; Mann, J. K.; English, E.; Harper, D. P.; Carrier, D. J.; Rials, T. G.; Labbé, N.; Chmely, S. C. Sustainable Hydrogels Based on Lignin-Methacrylate Copolymers with Enhanced Water Retention and Tunable Material Properties. *Biomacromolecules* **2018**, 19 (7), 2665–2672.
<https://doi.org/10.1021/acs.biomac.8b00282>.
- (90) El-Zawawy, W. K.; Ibrahim, M. M. Preparation and Characterization of Novel Polymer Hydrogel from Industrial Waste and Copolymerization of Poly(Vinyl Alcohol) and Polyacrylamide. *Journal of Applied Polymer Science* **2012**, 124 (5), 4362–4370. <https://doi.org/10.1002/app.35481>.
- (91) Ciolacu, D.; Oprea, A. M.; Anghel, N.; Cazacu, G.; Cazacu, M. New Cellulose–Lignin Hydrogels and Their Application in Controlled Release of Polyphenols. *Materials Science and Engineering: C* **2012**, 32 (3), 452–463.
<https://doi.org/10.1016/j.msec.2011.11.018>.
- (92) Kai, D.; Low, Z. W.; Liow, S. S.; Abdul Karim, A.; Ye, H.; Jin, G.; Li, K.; Loh, X. J. Development of Lignin Supramolecular Hydrogels with Mechanically Responsive and Self-Healing Properties-SUPPORTING INFORMATION. *ACS Sustainable Chem. Eng.* **2015**, 3 (9), 2160–2169.
<https://doi.org/10.1021/acssuschemeng.5b00405>.
- (93) You, X.; Wang, X.; Zhang, H. J.; Cui, K.; Zhang, A.; Wang, L.; Yadav, C.; Li, X. Supertough Lignin Hydrogels with Multienergy Dissipative Structures and

- Ultrahigh Antioxidative Activities. *ACS Appl. Mater. Interfaces* **2020**, acsami.0c10657. <https://doi.org/10.1021/acsami.0c10657>.
- (94) Cheng, L.; Deng, B.; Luo, W.; Nie, S.; Liu, X.; Yin, Y.; Liu, S.; Wu, Z.; Zhan, P.; Zhang, L.; Chen, J. PH-Responsive Lignin-Based Nanomicelles for Oral Drug Delivery. *J. Agric. Food Chem.* **2020**, *68* (18), 5249–5258. <https://doi.org/10.1021/acs.jafc.9b08171>.
- (95) Dai, L.; Ma, M.; Xu, J.; Si, C.; Wang, X.; Liu, Z.; Ni, Y. All-Lignin-Based Hydrogel with Fast PH-Stimuli Responsiveness for Mechanical Switching and Actuation. *Chem. Mater.* **2020**, acs.chemmater.0c01198. <https://doi.org/10.1021/acs.chemmater.0c01198>.
- (96) Chandna, S.; Thakur, N. S.; Kaur, R.; Bhaumik, J. Lignin–Bimetallic Nanoconjugate Doped PH-Responsive Hydrogels for Laser-Assisted Antimicrobial Photodynamic Therapy. *Biomacromolecules* **2020**, *21* (8), 3216–3230. <https://doi.org/10.1021/acs.biomac.0c00695>.
- (97) Tahari, N.; de Hoyos-Martinez, P. L.; Abderrabba, M.; Ayadi, S.; Labidi, J. Lignin - Montmorillonite Hydrogels as Toluene Adsorbent. *Colloids and Surfaces A: Physicochemical and Engineering Aspects* **2020**, *602*, 125108. <https://doi.org/10.1016/j.colsurfa.2020.125108>.
- (98) Zhang, L.; Lu, H.; Chu, J.; Ma, J.; Fan, Y.; Wang, Z.; Ni, Y. Lignin-Directed Control of Silver Nanoparticles with Tunable Size in Porous Lignocellulose Hydrogels and Their Application in Catalytic Reduction. *ACS Sustainable Chem. Eng.* **2020**, *8* (33), 12655–12663. <https://doi.org/10.1021/acssuschemeng.0c04298>.
- (99) Xu, J.; Xu, J. J.; Lin, Q.; Jiang, L.; Zhang, D.; Li, Z.; Ma, B.; Zhang, C.; Li, L.; Kai, D.; Yu, H.-D.; Loh, X. J. Lignin-Incorporated Nanogel Serving As an Antioxidant Biomaterial for Wound Healing. *ACS Appl. Bio Mater.* **2020**, acsabm.0c00858. <https://doi.org/10.1021/acsabm.0c00858>.
- (100) Andeme Ela, R. C.; Tajiri, M.; Newberry, N. K.; Heiden, P. A.; Ong, R. G. Double-Shell Lignin Nanocapsules Are a Stable Vehicle for Fungicide Encapsulation and Release. *ACS Sustainable Chem. Eng.* **2020**, acssuschemeng.0c06686. <https://doi.org/10.1021/acssuschemeng.0c06686>.
- (101) Bhattarai, N.; Gunn, J.; Zhang, M. Chitosan-Based Hydrogels for Controlled, Localized Drug Delivery. *Advanced Drug Delivery Reviews* **2010**, *62* (1), 83–99. <https://doi.org/10.1016/j.addr.2009.07.019>.
- (102) Zainal, S. H.; Mohd, N. H.; Suhaili, N.; Anuar, F. H.; Lazim, A. M.; Othaman, R. Preparation of Cellulose-Based Hydrogel: A Review. *Journal of Materials Research and Technology* **2021**, *10*, 935–952. <https://doi.org/10.1016/j.jmrt.2020.12.012>.
- (103) Parit, M.; Saha, P.; Davis, V. A.; Jiang, Z. Transparent and Homogenous Cellulose Nanocrystal/Lignin UV-Protection Films. *ACS Omega* **2018**, *3* (9), 10679–10691. <https://doi.org/10.1021/acsomega.8b01345>.
- (104) Sadeghifar, H.; Venditti, R.; Jur, J.; Gorga, R. E.; Pawlak, J. J. Cellulose-Lignin Biodegradable and Flexible UV Protection Film. *ACS Sustainable Chem. Eng.* **2017**, *5* (1), 625–631. <https://doi.org/10.1021/acssuschemeng.6b02003>.

- (105) Kai, D.; Tan, M. J.; Chee, P. L.; Chua, Y. K.; Yap, Y. L.; Loh, X. J. Towards Lignin-Based Functional Materials in a Sustainable World. *Green Chem.* **2016**, *18* (5), 1175–1200. <https://doi.org/10.1039/C5GC02616D>.
- (106) Crouvisier-Urien, K.; Bodart, P. R.; Winckler, P.; Raya, J.; Gougeon, R. D.; Cayot, P.; Domenek, S.; Debeaufort, F.; Karbowiak, T. Biobased Composite Films from Chitosan and Lignin: Antioxidant Activity Related to Structure and Moisture. *ACS Sustainable Chem. Eng.* **2016**, *4* (12), 6371–6381. <https://doi.org/10.1021/acssuschemeng.6b00956>.
- (107) Pouteau, C.; Dole, P.; Cathala, B.; Averous, L.; Boquillon, N. Antioxidant Properties of Lignin in Polypropylene. *Polymer Degradation and Stability* **2003**, *81* (1), 9–18. [https://doi.org/10.1016/S0141-3910\(03\)00057-0](https://doi.org/10.1016/S0141-3910(03)00057-0).
- (108) Dong, X.; Dong, M.; Lu, Y.; Turley, A.; Jin, T.; Wu, C. Antimicrobial and Antioxidant Activities of Lignin from Residue of Corn Stover to Ethanol Production. *Industrial Crops and Products* **2011**, *34* (3), 1629–1634. <https://doi.org/10.1016/j.indcrop.2011.06.002>.
- (109) Sunthornvarabhas, J.; Liengprayoon, S.; Suwonsichon, T. Antimicrobial Kinetic Activities of Lignin from Sugarcane Bagasse for Textile Product. *Industrial Crops and Products* **2017**, *109*, 857–861. <https://doi.org/10.1016/j.indcrop.2017.09.059>.
- (110) Duval, A.; Lawoko, M. A Review on Lignin-Based Polymeric, Micro- and Nano-Structured Materials. *Reactive and Functional Polymers* **2014**, *85*, 78–96. <https://doi.org/10.1016/j.reactfunctpolym.2014.09.017>.
- (111) Dutta, S.; Wu, K. C.-W.; Saha, B. Emerging Strategies for Breaking the 3D Amorphous Network of Lignin. *Catal. Sci. Technol.* **2014**, *4* (11), 3785–3799. <https://doi.org/10.1039/C4CY00701H>.
- (112) Wang, H.; Pu, Y.; Ragauskas, A.; Yang, B. From Lignin to Valuable Products—Strategies, Challenges, and Prospects. *Bioresource Technology* **2019**, *271*, 449–461. <https://doi.org/10.1016/j.biortech.2018.09.072>.
- (113) Adler, E. Lignin Chemistry? Past, Present and Future. *Wood Sci. Technol.* **1977**, *11* (3), 169–218. <https://doi.org/10.1007/BF00365615>.
- (114) Mandlekar, N.; Cayla, A.; Rault, F.; Giraud, S.; Salaün, F.; Malucelli, G.; Guan, J.-P. An Overview on the Use of Lignin and Its Derivatives in Fire Retardant Polymer Systems. In *Lignin - Trends and Applications*; Poletto, M., Ed.; InTech, 2018. <https://doi.org/10.5772/intechopen.72963>.
- (115) *Advances in Chemical, Bio and Environmental Engineering*; Ratan, J. K., Sahu, D., Pandhare, N. N., Bhavanam, A., Eds.; Environmental Science and Engineering; Springer International Publishing: Cham, 2022. <https://doi.org/10.1007/978-3-030-96554-9>.
- (116) Bajwa, D. S.; Pourhashem, G.; Ullah, A. H.; Bajwa, S. G. A Concise Review of Current Lignin Production, Applications, Products and Their Environmental Impact. *Industrial Crops and Products* **2019**, *139*, 111526. <https://doi.org/10.1016/j.indcrop.2019.111526>.
- (117) Brethauer, S.; Shahab, R. L.; Studer, M. H. Impacts of Biofilms on the Conversion of Cellulose. *Appl Microbiol Biotechnol* **2020**, *104* (12), 5201–5212. <https://doi.org/10.1007/s00253-020-10595-y>.

- (118) Klett, A. S.; Chappell, P. V.; Thies, M. C. Recovering Ultraclean Lignins of Controlled Molecular Weight from Kraft Black-Liquor Lignins. *Chemical Communications* **2015**, *51* (64), 12855–12858. <https://doi.org/10.1039/C5CC05341B>.
- (119) Arshanitsa, A.; Krumina, L.; Telysheva, G.; Dizhbite, T. Exploring the Application Potential of Incompletely Soluble Organosolv Lignin as a Macromonomer for Polyurethane Synthesis. *Industrial Crops and Products* **2016**, *92*, 1–12. <https://doi.org/10.1016/j.indcrop.2016.07.050>.
- (120) Kim, J.-Y.; Park, J.; Kim, U.-J.; Choi, J. W. Conversion of Lignin to Phenol-Rich Oil Fraction under Supercritical Alcohols in the Presence of Metal Catalysts. *Energy Fuels* **2015**, *29* (8), 5154–5163. <https://doi.org/10.1021/acs.energyfuels.5b01055>.
- (121) Lake, M. A.; Blackburn, J. C. PROCESS FOR RECOVERING LIGNIN. US 9260464 B2, February 16, 2016. <https://patents.google.com/patent/US9260464B2/>.
- (122) Holladay, J. E.; White, J. F.; Bozell, J. J.; Johnson, D. *Top Value-Added Chemicals from Biomass - Volume II—Results of Screening for Potential Candidates from Biorefinery Lignin*; PNNL-16983, 921839; 2007; p PNNL-16983, 921839. <https://doi.org/10.2172/921839>.
- (123) Asaworarit, P.; Daorattanachai, P.; Laosiripojana, W.; Sakdaronnarong, C.; Shotipruk, A.; Laosiripojana, N. Catalytic Depolymerization of Organosolv Lignin from Bagasse by Carbonaceous Solid Acids Derived from Hydrothermal of Lignocellulosic Compounds. *Chemical Engineering Journal* **2019**, *356*, 461–471. <https://doi.org/10.1016/j.cej.2018.09.048>.
- (124) Zhang, X.; Zhang, Q.; Long, J.; Xu, Y.; Wang, T.; Ma, L.; Li, Y. Phenolics Production through Catalytic Depolymerization of Alkali Lignin with Metal Chlorides. *BioResources* **2014**, *9* (2), 3347–3360. <https://doi.org/10.15376/biores.9.2.3347-3360>.
- (125) Liu, X.; Jiang, Z.; Feng, S.; Zhang, H.; Li, J.; Hu, C. Catalytic Depolymerization of Organosolv Lignin to Phenolic Monomers and Low Molecular Weight Oligomers. *Fuel* **2019**, *244*, 247–257. <https://doi.org/10.1016/j.fuel.2019.01.117>.
- (126) Liu, Q.; Wang, S.; Zheng, Y.; Luo, Z.; Cen, K. Mechanism Study of Wood Lignin Pyrolysis by Using TG–FTIR Analysis. *Journal of Analytical and Applied Pyrolysis* **2008**, *82* (1), 170–177. <https://doi.org/10.1016/j.jaap.2008.03.007>.
- (127) Kawamoto, H. Lignin Pyrolysis Reactions. *J Wood Sci* **2017**, *63* (2), 117–132. <https://doi.org/10.1007/s10086-016-1606-z>.
- (128) Yang, H.; Yan, R.; Chen, H.; Lee, D. H.; Zheng, C. Characteristics of Hemicellulose, Cellulose and Lignin Pyrolysis. *Fuel* **2007**, *86* (12–13), 1781–1788. <https://doi.org/10.1016/j.fuel.2006.12.013>.
- (129) Qu, W.; Xue, Y.; Gao, Y.; Rover, M.; Bai, X. Repolymerization of Pyrolytic Lignin for Producing Carbon Fiber with Improved Properties. *Biomass and Bioenergy* **2016**, *95*, 19–26. <https://doi.org/10.1016/j.biombioe.2016.09.013>.
- (130) Huang, C.; Ma, J.; Zhang, W.; Huang, G.; Yong, Q. Preparation of Lignosulfonates from Biorefinery Lignins by Sulfomethylation and Their Application as a Water

- Reducer for Concrete. *Polymers* **2018**, *10* (8), 841. <https://doi.org/10.3390/polym10080841>.
- (131) Jankowska, D.; Heck, T.; Schubert, M.; Yerlikaya, A.; Weymuth, C.; Rentsch, D.; Schober, I.; Richter, M. Enzymatic Synthesis of Lignin-Based Concrete Dispersing Agents. *ChemBioChem* **2018**, *19* (13), 1365–1369. <https://doi.org/10.1002/cbic.201800064>.
- (132) Wei, R.; Sakai, Y. Improving the Properties of Botanical Concrete Based on Waste Concrete, Wood, and Kraft Lignin Powder. *Powder Technology* **2022**, *397*, 117024. <https://doi.org/10.1016/j.powtec.2021.11.068>.
- (133) Kalliola, A.; Vehmas, T.; Liitiä, T.; Tamminen, T. Alkali-O₂ Oxidized Lignin – A Bio-Based Concrete Plasticizer. *Industrial Crops and Products* **2015**, *74*, 150–157. <https://doi.org/10.1016/j.indcrop.2015.04.056>.
- (134) Lin, Y.; Pang, Y.; Li, Z.; Zhou, M.; Lou, H.; Qiu, X. Thermo-Responsive Behavior of Enzymatic Hydrolysis Lignin in the Ethanol/Water Mixed Solvent and Its Application in the Controlled Release of Pesticides. *ACS Sustainable Chem. Eng.* **2021**, *9* (46), 15634–15640. <https://doi.org/10.1021/acssuschemeng.1c06061>.
- (135) Zhang, D.; Liu, G.; Jing, T.; Luo, J.; Wei, G.; Mu, W.; Liu, F. Lignin-Modified Electronegative Epoxy Resin Nanocarriers Effectively Deliver Pesticides against Plant Root-Knot Nematodes (*Meloidogyne Incognita*). *J. Agric. Food Chem.* **2020**, *68* (47), 13562–13572. <https://doi.org/10.1021/acs.jafc.0c01736>.
- (136) Gazzurelli, C.; Migliori, A.; Mazzeo, P. P.; Carcelli, M.; Pietarinen, S.; Leonardi, G.; Pandolfi, A.; Rogolino, D.; Pelagatti, P. Making Agriculture More Sustainable: An Environmentally Friendly Approach to the Synthesis of Lignin@Cu Pesticides. *ACS Sustainable Chem. Eng.* **2020**, *8* (39), 14886–14895. <https://doi.org/10.1021/acssuschemeng.0c04645>.
- (137) Xu, C.; Wang, D.; Zhang, S.; Guo, E.; Luo, H.; Zhang, Z.; Yu, H. Effect of Lignin Modifier on Engineering Performance of Bituminous Binder and Mixture. *Polymers* **2021**, *13* (7), 1083. <https://doi.org/10.3390/polym13071083>.
- (138) Xie, S.; Li, Q.; Karki, P.; Zhou, F.; Yuan, J. S. Lignin as Renewable and Superior Asphalt Binder Modifier. *ACS Sustainable Chem. Eng.* **2017**, *5* (4), 2817–2823. <https://doi.org/10.1021/acssuschemeng.6b03064>.
- (139) Batista, K. B.; Padilha, R. P. L.; Castro, T. O.; Silva, C. F. S. C.; Araújo, M. F. A. S.; Leite, L. F. M.; Pasa, V. M. D.; Lins, V. F. C. High-Temperature, Low-Temperature and Weathering Aging Performance of Lignin Modified Asphalt Binders. *Industrial Crops and Products* **2018**, *111*, 107–116. <https://doi.org/10.1016/j.indcrop.2017.10.010>.
- (140) Ang, A. F.; Ashaari, Z.; Lee, S. H.; Md Tahir, P.; Halis, R. Lignin-Based Copolymer Adhesives for Composite Wood Panels – A Review. *International Journal of Adhesion and Adhesives* **2019**, *95*, 102408. <https://doi.org/10.1016/j.ijadhadh.2019.102408>.
- (141) Henn, K. A.; Forssell, S.; Pietiläinen, A.; Forsman, N.; Smal, I.; Nousiainen, P.; Bangalore Ashok, R. P.; Oinas, P.; Österberg, M. Interfacial Catalysis and Lignin Nanoparticles for Strong Fire- and Water-Resistant Composite Adhesives. *Green Chem.* **2022**, *24* (17), 6487–6500. <https://doi.org/10.1039/D2GC01637K>.

- (142) Chen, X.; Xi, X.; Pizzi, A.; Fredon, E.; Du, G.; Gerardin, C.; Amirou, S. Oxidized Demethylated Lignin as a Bio-Based Adhesive for Wood Bonding. *The Journal of Adhesion* **2021**, *97* (9), 873–890. <https://doi.org/10.1080/00218464.2019.1710830>.
- (143) He, S.; Shi, G.; Xiao, H.; Sun, G.; Shi, Y.; Chen, G.; Dai, H.; Yuan, B.; Chen, X.; Yang, X. Self S-Doping Activated Carbon Derived from Lignin-Based Pitch for Removal of Gaseous Benzene. *Chemical Engineering Journal* **2021**, *410*, 128286. <https://doi.org/10.1016/j.cej.2020.128286>.
- (144) Zeng, L.; Lou, X.; Zhang, J.; Wu, C.; Liu, J.; Jia, C. Carbonaceous Mudstone and Lignin-Derived Activated Carbon and Its Application for Supercapacitor Electrode. *Surface and Coatings Technology* **2019**, *357*, 580–586. <https://doi.org/10.1016/j.surfcoat.2018.10.041>.
- (145) Wu, Q.; Ye, X.; Lv, Y.; Pei, R.; Wu, M.; Liu, M. Lignin-Based Magnetic Activated Carbon for p-Arsanilic Acid Removal: Applications and Absorption Mechanisms. *Chemosphere* **2020**, *258*, 127276. <https://doi.org/10.1016/j.chemosphere.2020.127276>.
- (146) Leskinen, T.; Witos, J.; Valle-Delgado, J. J.; Lintinen, K.; Kostianen, M.; Wiedmer, S. K.; Österberg, M.; Mattinen, M.-L. Adsorption of Proteins on Colloidal Lignin Particles for Advanced Biomaterials. *Biomacromolecules* **2017**, *18* (9), 2767–2776. <https://doi.org/10.1021/acs.biomac.7b00676>.
- (147) Wang, X.; Jiang, C.; Hou, B.; Wang, Y.; Hao, C.; Wu, J. Carbon Composite Lignin-Based Adsorbents for the Adsorption of Dyes. *Chemosphere* **2018**, *206*, 587–596. <https://doi.org/10.1016/j.chemosphere.2018.04.183>.
- (148) Wu, L.; Huang, S.; Zheng, J.; Qiu, Z.; Lin, X.; Qin, Y. Synthesis and Characterization of Biomass Lignin-Based PVA Super-Absorbent Hydrogel. *International Journal of Biological Macromolecules* **2019**, *140*, 538–545. <https://doi.org/10.1016/j.ijbiomac.2019.08.142>.
- (149) Yu, C.; Wang, F.; Zhang, C.; Fu, S.; Lucia, L. A. The Synthesis and Absorption Dynamics of a Lignin-Based Hydrogel for Remediation of Cationic Dye-Contaminated Effluent. *Reactive and Functional Polymers* **2016**, *106*, 137–142. <https://doi.org/10.1016/j.reactfunctpolym.2016.07.016>.
- (150) Liu, M.; Liu, Y.; Shen, J.; Zhang, S.; Liu, X.; Chen, X.; Ma, Y.; Ren, S.; Fang, G.; Li, S.; Tong Li, C.; Sun, T. Simultaneous Removal of Pb²⁺, Cu²⁺ and Cd²⁺ Ions from Wastewater Using Hierarchical Porous Polyacrylic Acid Grafted with Lignin. *Journal of Hazardous Materials* **2020**, *392*, 122208. <https://doi.org/10.1016/j.jhazmat.2020.122208>.
- (151) Yuan, H.; Peng, J.; Ren, T.; Luo, Q.; Luo, Y.; Zhang, N.; Huang, Y.; Guo, X.; Wu, Y. Novel Fluorescent Lignin-Based Hydrogel with Cellulose Nanofibers and Carbon Dots for Highly Efficient Adsorption and Detection of Cr(VI). *Science of The Total Environment* **2021**, *760*, 143395. <https://doi.org/10.1016/j.scitotenv.2020.143395>.
- (152) Morales, A.; Labidi, J.; Gullón, P. Effect of the Formulation Parameters on the Absorption Capacity of Smart Lignin-Hydrogels. *European Polymer Journal* **2020**, *129*, 109631. <https://doi.org/10.1016/j.eurpolymj.2020.109631>.

- (153) Parvathy, P. A.; Ayobami, A. V.; Raichur, A. M.; Sahoo, S. K. Methacrylated Alkali Lignin Grafted P(Nipam-Co-AAc) Copolymeric Hydrogels: Tuning the Mechanical and Stimuli-Responsive Properties. *International Journal of Biological Macromolecules* **2021**, *192*, 180–196. <https://doi.org/10.1016/j.ijbiomac.2021.09.183>.
- (154) Jin, C.; Song, W.; Liu, T.; Xin, J.; Hiscox, W. C.; Zhang, J.; Liu, G.; Kong, Z. Temperature and PH Responsive Hydrogels Using Methacrylated Lignosulfonate Cross-Linker: Synthesis, Characterization, and Properties. *ACS Sustainable Chem. Eng.* **2018**, *6* (2), 1763–1771. <https://doi.org/10.1021/acssuschemeng.7b03158>.
- (155) You, X.; Wang, X.; Zhang, H. J.; Cui, K.; Zhang, A.; Wang, L.; Yadav, C.; Li, X. Supertough Lignin Hydrogels with Multienergy Dissipative Structures and Ultrahigh Antioxidative Activities. *ACS Appl. Mater. Interfaces* **2020**, *12* (35), 39892–39901. <https://doi.org/10.1021/acscami.0c10657>.
- (156) Liu, T.; Ren, X.; Zhang, J.; Liu, J.; Ou, R.; Guo, C.; Yu, X.; Wang, Q.; Liu, Z. Highly Compressible Lignin Hydrogel Electrolytes via Double-Crosslinked Strategy for Superior Foldable Supercapacitors. *Journal of Power Sources* **2020**, *449*, 227532. <https://doi.org/10.1016/j.jpowsour.2019.227532>.
- (157) Cui, L.; An, Y.; Xu, H.; Jia, M.; Li, Y.; Jin, X. An All-Lignin-Based Flexible Supercapacitor Based on a Nitrogen-Doped Carbon Dot Functionalized Graphene Hydrogel. *New J. Chem.* **2021**, *45* (46), 21692–21700. <https://doi.org/10.1039/D1NJ04054E>.
- (158) Wang, D.; Yang, F.; Cong, L.; Feng, W.; Wang, C.; Chu, F.; Nan, J.; Chen, R. Lignin-Containing Hydrogel Matrices with Enhanced Adhesion and Toughness for All-Hydrogel Supercapacitors. *Chemical Engineering Journal* **2022**, *450*, 138025. <https://doi.org/10.1016/j.cej.2022.138025>.
- (159) Oveissi, F.; Naficy, S.; Le, T. Y. L.; Fletcher, D. F.; Dehghani, F. Tough and Processable Hydrogels Based on Lignin and Hydrophilic Polyurethane. *ACS Appl. Bio Mater.* **2018**. <https://doi.org/10.1021/acscabm.8b00546>.
- (160) Bian, H.; Wei, L.; Lin, C.; Ma, Q.; Dai, H.; Zhu, J. Y. Lignin-Containing Cellulose Nanofibril-Reinforced Polyvinyl Alcohol Hydrogels. *ACS Sustainable Chem. Eng.* **2018**, *6* (4), 4821–4828. <https://doi.org/10.1021/acssuschemeng.7b04172>.
- (161) Ciobanu, C.; Ungureanu, M.; Ignat, L.; Ungureanu, D.; Popa, V. I. Properties of Lignin–Polyurethane Films Prepared by Casting Method. *Industrial Crops and Products* **2004**, *20* (2), 231–241. <https://doi.org/10.1016/j.indcrop.2004.04.024>.
- (162) Wang, S.; Shuai, L.; Saha, B.; Vlachos, D. G.; Epps, T. H. From Tree to Tape: Direct Synthesis of Pressure Sensitive Adhesives from Depolymerized Raw Lignocellulosic Biomass. *ACS Cent. Sci.* **2018**, *4* (6), 701–708. <https://doi.org/10.1021/acscentsci.8b00140>.
- (163) Liu, H.; Chung, H. Lignin-Based Polymers via Graft Copolymerization. *Journal of Polymer Science Part A: Polymer Chemistry* **2017**, *55* (21), 3515–3528. <https://doi.org/10.1002/pola.28744>.
- (164) Liu, H.; Chung, H. Self-Healing Properties of Lignin-Containing Nanocomposite: Synthesis of Lignin-Graft-Poly(5-Acetylaminopentyl Acrylate) via RAFT and

- Click Chemistry. *Macromolecules* **2016**, *49* (19), 7246–7256.
<https://doi.org/10.1021/acs.macromol.6b01028>.
- (165) Shen, X.; Berton, P.; Shamshina, J. L.; Rogers, R. D. Preparation and Comparison of Bulk and Membrane Hydrogels Based on Kraft- and Ionic-Liquid-Isolated Lignins. *Green Chem.* **2016**, *18* (20), 5607–5620.
<https://doi.org/10.1039/C6GC01339B>.
- (166) Jin, C.; Zhang, X.; Xin, J.; Liu, G.; Wu, G.; Kong, Z.; Zhang, J. Clickable Synthesis of 1,2,4-Triazole Modified Lignin-Based Adsorbent for the Selective Removal of Cd(II). *ACS Sustainable Chem. Eng.* **2017**, *5* (5), 4086–4093.
<https://doi.org/10.1021/acssuschemeng.7b00072>.
- (167) Ge, Y.; Li, Z. Application of Lignin and Its Derivatives in Adsorption of Heavy Metal Ions in Water: A Review. *ACS Sustainable Chem. Eng.* **2018**, *6* (5), 7181–7192. <https://doi.org/10.1021/acssuschemeng.8b01345>.
- (168) Xu, W.; Wang, X.; Sandler, N.; Willför, S.; Xu, C. Three-Dimensional Printing of Wood-Derived Biopolymers: A Review Focused on Biomedical Applications. *ACS Sustainable Chem. Eng.* **2018**, *6* (5), 5663–5680.
<https://doi.org/10.1021/acssuschemeng.7b03924>.
- (169) Zhang, H.; Zhang, W.; Ming, H.; Pang, J.; Zhang, H.; Cao, G.; Yang, Y. Design Advanced Carbon Materials from Lignin-Based Interpenetrating Polymer Networks for High Performance Sodium-Ion Batteries. *Chemical Engineering Journal* **2018**, *341*, 280–288. <https://doi.org/10.1016/j.cej.2018.02.016>.
- (170) Passauer, L. Highly Swellable Lignin Hydrogels: Novel Materials with Interesting Properties. In *ACS Symposium Series*; Liebner, F., Rosenau, T., Eds.; American Chemical Society: Washington, DC, 2012; Vol. 1107, pp 211–228.
<https://doi.org/10.1021/bk-2012-1107.ch011>.
- (171) Park, S.; Kim, S. H.; Kim, J. H.; Yu, H.; Kim, H. J.; Yang, Y.-H.; Kim, H.; Kim, Y. H.; Ha, S. H.; Lee, S. H. Application of Cellulose/Lignin Hydrogel Beads as Novel Supports for Immobilizing Lipase. *Journal of Molecular Catalysis B: Enzymatic* **2015**, *119*, 33–39. <https://doi.org/10.1016/j.molcatb.2015.05.014>.
- (172) Emerson, J. A.; Garabedian, N. T.; Burris, D. L.; Furst, E. M.; Epps, T. H. Exploiting Feedstock Diversity To Tune the Chemical and Tribological Properties of Lignin-Inspired Polymer Coatings. *ACS Sustainable Chem. Eng.* **2018**, *6* (5), 6856–6866. <https://doi.org/10.1021/acssuschemeng.8b00667>.
- (173) Klett, A. S.; Payne, A. M.; Thies, M. C. Continuous-Flow Process for the Purification and Fractionation of Alkali and Organosolv Lignins. *ACS Sustainable Chem. Eng.* **2016**, *4* (12), 6689–6694.
<https://doi.org/10.1021/acssuschemeng.6b01560>.
- (174) Ding, J.; Klett, A. S.; Gamble, J. A.; Tindall, G. W.; Thies, M. C. Liquid–Liquid Equilibrium Compositions and Global Phase Behavior for the Lignin–Acetic Acid–Water System at 70 and 95 °C. *Fluid Phase Equilibria* **2018**, *461*, 8–14.
<https://doi.org/10.1016/j.fluid.2018.01.002>.
- (175) Thies, M. C.; Klett, A. S.; Bruce, D. A. SOLVENT AND RECOVERY PROCESS FOR LIGNIN. US 10053482 B2, August 21, 2018.
<https://patents.google.com/patent/US20160137680A1/en>.

- (176) Kai, D.; Low, Z. W.; Liow, S. S.; Abdul Karim, A.; Ye, H.; Jin, G.; Li, K.; Loh, X. J. Development of Lignin Supramolecular Hydrogels with Mechanically Responsive and Self-Healing Properties. *ACS Sustainable Chem. Eng.* **2015**, *3* (9), 2160–2169. <https://doi.org/10.1021/acssuschemeng.5b00405>.
- (177) Hill-West, J. L.; Chowdhury, S. M.; Slepian, M. J.; Hubbell, J. A. Inhibition of Thrombosis and Intimal Thickening by in Situ Photopolymerization of Thin Hydrogel Barriers. *Proceedings of the National Academy of Sciences* **1994**, *91* (13), 5967–5971. <https://doi.org/10.1073/pnas.91.13.5967>.
- (178) Sawhney, A. S.; Pathak, C. P.; Hubbell, J. A. Bioerodible Hydrogels Based on Photopolymerized Poly(Ethylene Glycol)-Co-Poly(.Alpha.-Hydroxy Acid) Diacrylate Macromers. *Macromolecules* **1993**, *26* (4), 581–587. <https://doi.org/10.1021/ma00056a005>.
- (179) Menard, K. *Dynamic Mechanical Analysis: A Practical Introduction*; CRC Press, 1999. <https://doi.org/10.1201/9781420049183>.
- (180) TA Instruments. Quantifying Polymer Crosslinking Density Using Rheology and DMA, 2020. <https://www.tainstruments.com/pdf/literature/RH102.pdf> (accessed 2021-06-21).
- (181) TA Instruments. RSA III Rheometrics System Analyzer - Rheometric Series User Manual, 2005.
- (182) Gluck-Hirsch, J. B.; Kokini, J. L. Determination of the Molecular Weight between Crosslinks of Waxy Maize Starches Using the Theory of Rubber Elasticity. *Journal of Rheology* **1997**, *41* (1), 129–140. <https://doi.org/10.1122/1.550804>.
- (183) Treloar, L. R. G. *The Physics of Rubber Elasticity: By L.R.G. Treloar*, 3rd ed.; Oxford classic texts in the physical sciences; Clarendon Press ; Oxford University Press: Oxford : New York, 2005.
- (184) Barszczewska-Rybarek, I. M.; Korytkowska-Wałach, A.; Kurcok, M.; Chladek, G.; Kasperski, J. DMA Analysis of the Structure of Crosslinked Poly(Methyl Methacrylate)s. *Acta of Bioengineering and Biomechanics; 01/2017; ISSN 1509-409X* **2017**. <https://doi.org/10.5277/ABB-00590-2016-01>.
- (185) Urayama, K.; Takigawa, T.; Masuda, T. Poisson's Ratio of Poly(Vinyl Alcohol) Gels. *Macromolecules* **1993**, *26* (12), 3092–3096. <https://doi.org/10.1021/ma00064a016>.
- (186) Chen, R.; Xu, X.; Yu, D.; Xiao, C.; Liu, M.; Huang, J.; Mao, T.; Zheng, C.; Wang, Z.; Wu, X. Highly Stretchable and Fatigue Resistant Hydrogels with Low Young's Modulus as Transparent and Flexible Strain Sensors. *J. Mater. Chem. C* **2018**, *6* (41), 11193–11201. <https://doi.org/10.1039/C8TC02583E>.
- (187) Chhetri, D. K.; Zhang, Z.; Neubauer, J. Measurement of Young's Modulus of Vocal Folds by Indentation. *Journal of Voice* **2011**, *25* (1), 1–7. <https://doi.org/10.1016/j.jvoice.2009.09.005>.
- (188) Ye, F.; Li, M.; Ke, D.; Wang, L.; Lu, Y. Ultrafast Self-Healing and Injectable Conductive Hydrogel for Strain and Pressure Sensors. *Adv. Mater. Technol.* **2019**, *4* (9), 1900346. <https://doi.org/10.1002/admt.201900346>.
- (189) Dimitriadis, E. K.; Horkay, F.; Maresca, J.; Kachar, B.; Chadwick, R. S. Determination of Elastic Moduli of Thin Layers of Soft Material Using the Atomic

- Force Microscope. *Biophysical Journal* **2002**, *82* (5), 2798–2810. [https://doi.org/10.1016/S0006-3495\(02\)75620-8](https://doi.org/10.1016/S0006-3495(02)75620-8).
- (190) Chan, E. P. Materials Properties (Gc, E) of Soft Materials from Contact Adhesion Testing (CAT). 4.
- (191) Sakai, M.; Shimizu, S. Indentation Rheometry for Glass-Forming Materials. *Journal of Non-Crystalline Solids* **2001**, *282* (2–3), 236–247. [https://doi.org/10.1016/S0022-3093\(01\)00316-7](https://doi.org/10.1016/S0022-3093(01)00316-7).
- (192) Wang, W.; Zhao, Y.; Bai, H.; Zhang, T.; Ibarra-Galvan, V.; Song, S. Methylene Blue Removal from Water Using the Hydrogel Beads of Poly(Vinyl Alcohol)-Sodium Alginate-Chitosan-Montmorillonite. *Carbohydrate Polymers* **2018**, *198*, 518–528. <https://doi.org/10.1016/j.carbpol.2018.06.124>.
- (193) Dou, X.; Li, P.; Zhang, D.; Feng, C.-L. C₂-Symmetric Benzene-Based Hydrogels with Unique Layered Structures for Controllable Organic Dye Adsorption. *Soft Matter* **2012**, *8* (11), 3231. <https://doi.org/10.1039/c2sm06927j>.
- (194) Pardo, A.; Garcia, H.; Ramirez, P.; Carrillo-Alvarado, M. A.; Krishna, K. S.; Dominguez, N.; Islam, M. T.; Wang, H.; Noveron, J. C. Self-Regenerating Photocatalytic Hydrogel for the Adsorption and Decomposition of Methylene Blue and Antibiotics in Water. *Environmental Technology & Innovation* **2018**, *11*, 321–327. <https://doi.org/10.1016/j.eti.2018.06.005>.
- (195) Dasgupta, J.; Singh, A.; Kumar, S.; Sikder, J.; Chakraborty, S.; Curcio, S.; Arafat, H. A. Poly (Sodium-4-Styrenesulfonate) Assisted Ultrafiltration for Methylene Blue Dye Removal from Simulated Wastewater: Optimization Using Response Surface Methodology. *Journal of Environmental Chemical Engineering* **2016**, *4* (2), 2008–2022. <https://doi.org/10.1016/j.jece.2016.03.033>.
- (196) Zaghbani, N.; Hafiane, A.; Dhahbi, M. Separation of Methylene Blue from Aqueous Solution by Micellar Enhanced Ultrafiltration. *Separation and Purification Technology* **2007**, *55* (1), 117–124. <https://doi.org/10.1016/j.seppur.2006.11.008>.
- (197) Bielska, M.; Szymanowski, J. Removal of Methylene Blue from Waste Water Using Micellar Enhanced Ultrafiltration. *Water Research* **2006**, *40* (5), 1027–1033. <https://doi.org/10.1016/j.watres.2005.12.027>.
- (198) Cavallo, A.; Madaghiele, M.; Masullo, U.; Lionetto, M. G.; Sannino, A. Photo-Crosslinked Poly(Ethylene Glycol) Diacrylate (PEGDA) Hydrogels from Low Molecular Weight Prepolymer: Swelling and Permeation Studies: ARTICLE. *J. Appl. Polym. Sci.* **2017**, *134* (2). <https://doi.org/10.1002/app.44380>.
- (199) Ehrenhofer, A.; Wallmersperger, T. Adjustable Fluid and Particle Permeation through Hydrogel Composite Membranes. *Journal of Intelligent Material Systems and Structures* **2018**, *29* (3), 310–322. <https://doi.org/10.1177/1045389X17704065>.
- (200) Fujiyabu, T.; Li, X.; Shibayama, M.; Chung, U.; Sakai, T. Permeation of Water through Hydrogels with Controlled Network Structure. *Macromolecules* **2017**, *50* (23), 9411–9416. <https://doi.org/10.1021/acs.macromol.7b01807>.

- (201) Offeddu, G. S.; Axpe, E.; Harley, B. A. C.; Oyen, M. L. Relationship between Permeability and Diffusivity in Polyethylene Glycol Hydrogels. *AIP Advances* **2018**, *8* (10), 105006. <https://doi.org/10.1063/1.5036999>.
- (202) Xiang, Y.; Mao, C.; Liu, X.; Cui, Z.; Jing, D.; Yang, X.; Liang, Y.; Li, Z.; Zhu, S.; Zheng, Y.; Yeung, K. W. K.; Zheng, D.; Wang, X.; Wu, S. Rapid and Superior Bacteria Killing of Carbon Quantum Dots/ZnO Decorated Injectable Folic Acid-Conjugated PDA Hydrogel through Dual-Light Triggered ROS and Membrane Permeability. *Small* **2019**, *15* (22), 1900322. <https://doi.org/10.1002/smll.201900322>.
- (203) Yazdi, M. K.; Vatanpour, V.; Taghizadeh, A.; Taghizadeh, M.; Ganjali, M. R.; Munir, M. T.; Habibzadeh, S.; Saeb, M. R.; Ghaedi, M. Hydrogel Membranes: A Review. *Materials Science and Engineering: C* **2020**, *114*, 111023. <https://doi.org/10.1016/j.msec.2020.111023>.
- (204) Deen, W. M. *Analysis of Transport Phenomena*; Topics in chemical engineering; Oxford University Press: New York, 1998.
- (205) Davis, E. M.; Kim, J.; Oleshko, V. P.; Page, K. A.; Soles, C. L. Uncovering the Structure of Nafion-SiO₂ Hybrid Ionomer Membranes for Prospective Large-Scale Energy Storage Devices. *Adv. Funct. Mater.* **2015**, *25* (26), 4064–4075. <https://doi.org/10.1002/adfm.201501116>.
- (206) Rohrbach, K.; Li, Y.; Zhu, H.; Liu, Z.; Dai, J.; Andreasen, J.; Hu, L. A Cellulose Based Hydrophilic, Oleophobic Hydrated Filter for Water/Oil Separation. *Chem. Commun.* **2014**, *50* (87), 13296–13299. <https://doi.org/10.1039/C4CC04817B>.
- (207) Zhu, Y.; Zheng, Y.; Wang, F.; Wang, A. Monolithic Supermacroporous Hydrogel Prepared from High Internal Phase Emulsions (HIPEs) for Fast Removal of Cu²⁺ and Pb²⁺. *Chemical Engineering Journal* **2016**, *284*, 422–430. <https://doi.org/10.1016/j.cej.2015.08.157>.
- (208) Li, N.; Bai, R. Copper Adsorption on Chitosan–Cellulose Hydrogel Beads: Behaviors and Mechanisms. *Separation and Purification Technology* **2005**, *42* (3), 237–247. <https://doi.org/10.1016/j.seppur.2004.08.002>.
- (209) Cheng, X.; Jin, Y.; Sun, T.; Qi, R.; Fan, B.; Li, H. Oxidation- and Thermo-Responsive Poly(N-Isopropylacrylamide-Co-2-Hydroxyethyl Acrylate) Hydrogels Cross-Linked via Diselenides for Controlled Drug Delivery. *RSC Advances* **2015**, *5* (6), 4162–4170. <https://doi.org/10.1039/C4RA13500H>.
- (210) Das, A.; Mehndiratta, M.; Chattopadhyay, P.; Ray, A. R. Prolonged Zero-Order BSA Release from PH-Sensitive Hydrogels of Poly(AAc- Co -DMAPMA) Having Rich Nano through Micro Scale Morphology. *Journal of Applied Polymer Science* **2010**, *115* (1), 393–403. <https://doi.org/10.1002/app.30968>.
- (211) Klett, A. S.; Payne, A. M.; Phongprecha, T.; Hodge, D. B.; Thies, M. C. Benign Fractionation of Lignin with CO₂-Expanded Solvents of Acetic Acid + Water. *Ind. Eng. Chem. Res.* **2017**, *56* (34), 9778–9782. <https://doi.org/10.1021/acs.iecr.7b02272>.
- (212) Thakur, V. K.; Thakur, M. K. Recent Advances in Green Hydrogels from Lignin: A Review. *International Journal of Biological Macromolecules* **2015**, *72* (Supplement C), 834–847. <https://doi.org/10.1016/j.ijbiomac.2014.09.044>.

- (213) O'Dea, R. M.; Willie, J. A.; Epps, T. H. 100th Anniversary of Macromolecular Science Viewpoint: Polymers from Lignocellulosic Biomass. Current Challenges and Future Opportunities. *ACS Macro Lett.* **2020**, *9*, 476–493. <https://doi.org/10.1021/acsmacrolett.0c00024>.
- (214) Ganewatta, M. S.; Lokupitiya, H. N.; Tang, C. Lignin Biopolymers in the Age of Controlled Polymerization. *Polymers* **2019**, *11* (7), 1176. <https://doi.org/10.3390/polym11071176>.
- (215) Upton, B. M.; Kasko, A. M. Strategies for the Conversion of Lignin to High-Value Polymeric Materials: Review and Perspective. *Chem. Rev.* **2016**, *116* (4), 2275–2306. <https://doi.org/10.1021/acs.chemrev.5b00345>.
- (216) Thakur, V. K.; Thakur, M. K.; Raghavan, P.; Kessler, M. R. Progress in Green Polymer Composites from Lignin for Multifunctional Applications: A Review. *ACS Sustainable Chem. Eng.* **2014**, *2* (5), 1072–1092. <https://doi.org/10.1021/sc500087z>.
- (217) Xu, Y.; You, F.; Sun, H.; Shao, L. Realizing Mussel-Inspired Polydopamine Selective Layer with Strong Solvent Resistance in Nanofiltration toward Sustainable Reclamation. *ACS Sustainable Chem. Eng.* **2017**, *5* (6), 5520–5528. <https://doi.org/10.1021/acssuschemeng.7b00871>.
- (218) Holmberg, A. L.; Nguyen, N. A.; Karavolias, M. G.; Reno, K. H.; Wool, R. P.; Epps, T. H. Softwood Lignin-Based Methacrylate Polymers with Tunable Thermal and Viscoelastic Properties. *Macromolecules* **2016**, *49* (4), 1286–1295. <https://doi.org/10.1021/acs.macromol.5b02316>.
- (219) Lindström, T. The Colloidal Behaviour of Kraft Lignin. *Colloid and Polymer Science* **1979**, *257* (3), 277–285. <https://doi.org/10.1007/BF01382370>.
- (220) Lindström, T.; Westman, L. The Colloidal Behaviour of Kraft Lignin III. Swelling Behaviour and Mechanical Properties of Kraft Lignin Gels. *Colloid and Polymer Science* **1980**, *258* (4), 390–397. <https://doi.org/10.1007/BF01480830>.
- (221) Lindström, T.; Westman, L. The Colloidal Behaviour of Kraft Lignin. *Colloid and Polymer Science* **1982**, *260* (6), 594–598. <https://doi.org/10.1007/BF01422591>.
- (222) Larrañeta, E.; Imízcoz, M.; Toh, J. X.; Irwin, N. J.; Ripolin, A.; Perminova, A.; Domínguez-Robles, J.; Rodríguez, A.; Donnelly, R. F. Synthesis and Characterization of Lignin Hydrogels for Potential Applications as Drug Eluting Antimicrobial Coatings for Medical Materials. *ACS Sustainable Chem. Eng.* **2018**, *6* (7), 9037–9046. <https://doi.org/10.1021/acssuschemeng.8b01371>.
- (223) Kai, D.; Low, Z. W.; Liow, S. S.; Abdul Karim, A.; Ye, H.; Jin, G.; Li, K.; Loh, X. J. Development of Lignin Supramolecular Hydrogels with Mechanically Responsive and Self-Healing Properties. *ACS Sustainable Chem. Eng.* **2015**, *3* (9), 2160–2169. <https://doi.org/10.1021/acssuschemeng.5b00405>.
- (224) Rajan, K.; Mann, J. K.; English, E.; Harper, D. P.; Carrier, D. J.; Rials, T. G.; Labbé, N.; Chmely, S. C. Sustainable Hydrogels Based on Lignin-Methacrylate Copolymers with Enhanced Water Retention and Tunable Material Properties. *Biomacromolecules* **2018**, *19* (7), 2665–2672. <https://doi.org/10.1021/acs.biomac.8b00282>.

- (225) Passauer, L. Highly Swellable Lignin Hydrogels: Novel Materials with Interesting Properties. In *Functional Materials from Renewable Sources*; ACS Symposium Series; American Chemical Society, 2012; Vol. 1107, pp 211–228. <https://doi.org/10.1021/bk-2012-1107.ch011>.
- (226) Peñaranda A., J. E.; Sabino, M. A. Effect of the Presence of Lignin or Peat in IPN Hydrogels on the Sorption of Heavy Metals. *Polymer Bulletin* **2010**, *65* (5), 495–508. <https://doi.org/10.1007/s00289-010-0264-3>.
- (227) Rudzinski, W. E.; Dave, A. M.; Vaishnav, U. H.; Kumbar, S. G.; Kulkarni, A. R.; Aminabhavi, T. M. Hydrogels as Controlled Release Devices in Agriculture. *Designed Monomers and Polymers* **2002**, *5* (1), 39–65. <https://doi.org/10.1163/156855502760151580>.
- (228) Ciolacu, D.; Oprea, A. M.; Anghel, N.; Cazacu, G.; Cazacu, M. New Cellulose–Lignin Hydrogels and Their Application in Controlled Release of Polyphenols. *Materials Science and Engineering: C* **2012**, *32* (3), 452–463. <https://doi.org/10.1016/j.msec.2011.11.018>.
- (229) Sathawong, S.; Sridach, W.; Techato, K. Lignin: Isolation and Preparing the Lignin Based Hydrogel. *Journal of Environmental Chemical Engineering* **2018**, *6* (5), 5879–5888. <https://doi.org/10.1016/j.jece.2018.05.008>.
- (230) Fernández-Pérez, M.; Villafranca-Sánchez, M.; Flores-Céspedes, F.; Daza-Fernández, I. Ethylcellulose and Lignin as Bearer Polymers in Controlled Release Formulations of Chloridazon. *Carbohydrate Polymers* **2011**, *83* (4), 1672–1679. <https://doi.org/10.1016/j.carbpol.2010.10.024>.
- (231) Domínguez-Robles, J.; Peresin, M. S.; Tamminen, T.; Rodríguez, A.; Larrañeta, E.; Jääskeläinen, A.-S. Lignin-Based Hydrogels with “Super-Swelling” Capacities for Dye Removal. *International Journal of Biological Macromolecules* **2018**, *115*, 1249–1259. <https://doi.org/10.1016/j.ijbiomac.2018.04.044>.
- (232) Joshi, N.; Suman, K.; Joshi, Y. M. Rheological Behavior of Aqueous Poly(Vinyl Alcohol) Solution during a Freeze–Thaw Gelation Process. *Macromolecules* **2020**, *53* (9), 3452–3463. <https://doi.org/10.1021/acs.macromol.0c00488>.
- (233) Tavakoli, J.; Gascooke, J.; Xie, N.; Tang, B. Z.; Tang, Y. Enlightening Freeze–Thaw Process of Physically Cross-Linked Poly(Vinyl Alcohol) Hydrogels by Aggregation-Induced Emission Fluorogens. *ACS Appl. Polym. Mater.* **2019**, *1* (6), 1390–1398. <https://doi.org/10.1021/acsapm.9b00173>.
- (234) Stauffer, S. R.; Peppast, N. A. Poly (Vinyl Alcohol) Hydrogels Prepared by Freezing-Thawing Cyclic Processing. *Polymer* **1992**, *33* (18), 3932–3936.
- (235) Hassan, C. M.; Stewart, J. E.; Peppas, N. A. Diffusional Characteristics of Freeze/Thawed Poly (Vinyl Alcohol) Hydrogels: Applications to Protein Controlled Release from Multilaminate Devices. *European Journal of Pharmaceutics and Biopharmaceutics* **2000**, *49* (2), 161–165.
- (236) Lian, Z.; Ye, L. Effect of PEO on the Network Structure of PVA Hydrogels Prepared by Freezing/Thawing Method. *Journal of Applied Polymer Science* **2013**, *128* (5), 3325–3329. <https://doi.org/10.1002/app.38544>.
- (237) Xiao, W.; He, J.; Nichol, J. W.; Wang, L.; Hutson, C. B.; Wang, B.; Du, Y.; Fan, H.; Khademhosseini, A. Synthesis and Characterization of Photocrosslinkable

- Gelatin and Silk Fibroin Interpenetrating Polymer Network Hydrogels. *Acta Biomaterialia* **2011**, 7 (6), 2384–2393.
<https://doi.org/10.1016/j.actbio.2011.01.016>.
- (238) Lee, S. J.; Kim, S. S.; Lee, Y. M. Interpenetrating Polymer Network Hydrogels Based on Poly(Ethylene Glycol) Macromer and Chitosan. *Carbohydrate Polymers* **2000**, 41 (2), 197–205. [https://doi.org/10.1016/S0144-8617\(99\)00088-0](https://doi.org/10.1016/S0144-8617(99)00088-0).
- (239) Myung, D.; Koh, W.; Ko, J.; Hu, Y.; Carrasco, M.; Noolandi, J.; Ta, C. N.; Frank, C. W. Biomimetic Strain Hardening in Interpenetrating Polymer Network Hydrogels. *Polymer* **2007**, 48 (18), 5376–5387.
<https://doi.org/10.1016/j.polymer.2007.06.070>.
- (240) Kim, S. J.; Park, S. J.; Kim, S. I. Swelling Behavior of Interpenetrating Polymer Network Hydrogels Composed of Poly(Vinyl Alcohol) and Chitosan. *Reactive and Functional Polymers* **2003**, 55 (1), 53–59. [https://doi.org/10.1016/S1381-5148\(02\)00214-6](https://doi.org/10.1016/S1381-5148(02)00214-6).
- (241) Silvaroli, A. J.; Heyl, T. R.; Qiang, Z.; Beebe, J. M.; Ahn, D.; Mangold, S.; Shull, K. R.; Wang, M. Tough, Transparent, Photocurable Hybrid Elastomers. *ACS Appl. Mater. Interfaces* **2020**, 12 (39), 44125–44136.
<https://doi.org/10.1021/acsami.0c11643>.
- (242) Nakajima, T.; Furukawa, H.; Tanaka, Y.; Kurokawa, T.; Osada, Y.; Gong, J. P. True Chemical Structure of Double Network Hydrogels. *Macromolecules* **2009**, 42 (6), 2184–2189. <https://doi.org/10.1021/ma802148p>.
- (243) Sperling, L. H. Interpenetrating Polymer Networks: An Overview. In *Interpenetrating Polymer Networks*; Klemperer, D., Sperling, L. H., Utracki, L. A., Eds.; Advances in Chemistry; American Chemical Society: Washington, DC, 1994; Vol. 239, pp 3–38. <https://doi.org/10.1021/ba-1994-0239.ch001>.
- (244) Velez, J.; Thies, M. C. Liquid Lignin from the SLRP™ Process: The Effect of Processing Conditions and Black-Liquor Properties. *Journal of Wood Chemistry and Technology* **2016**, 36 (1), 27–41.
<https://doi.org/10.1080/02773813.2015.1039545>.
- (245) Ghaffar, S. H.; Fan, M. Structural Analysis for Lignin Characteristics in Biomass Straw. *Biomass and Bioenergy* **2013**, 57, 264–279.
<https://doi.org/10.1016/j.biombioe.2013.07.015>.
- (246) Johnson, K. L.; Kendall, K.; Roberts, A. D. Surface Energy and the Contact of Elastic Solids. *Proceedings of the Royal Society A: Mathematical, Physical and Engineering Sciences* **1971**, 324 (1558), 301–313.
<https://doi.org/10.1098/rspa.1971.0141>.
- (247) Rashid, T.; Kait, C. F.; Regupathi, I.; Murugesan, T. Dissolution of Kraft Lignin Using Protic Ionic Liquids and Characterization. *Industrial Crops and Products* **2016**, 84, 284–293. <https://doi.org/10.1016/j.indcrop.2016.02.017>.
- (248) Son, K.; Lee, J. Synthesis and Characterization of Poly(Ethylene Glycol) Based Thermo-Responsive Hydrogels for Cell Sheet Engineering. *Materials* **2016**, 9 (10), 854. <https://doi.org/10.3390/ma9100854>.

- (249) Kalami, S.; Arefmanesh, M.; Master, E.; Nejad, M. Replacing 100% of Phenol in Phenolic Adhesive Formulations with Lignin: ARTICLE. *J. Appl. Polym. Sci.* **2017**, *134* (30), 45124. <https://doi.org/10.1002/app.45124>.
- (250) Zhao, R.; Wang, Y.; Li, X.; Sun, B.; Wang, C. Synthesis of β -Cyclodextrin-Based Electrospun Nanofiber Membranes for Highly Efficient Adsorption and Separation of Methylene Blue. *ACS Appl. Mater. Interfaces* **2015**, *7* (48), 26649–26657. <https://doi.org/10.1021/acsami.5b08403>.
- (251) Peppas, N. A.; Merrill, E. W. Poly(Vinyl Alcohol) Hydrogels: Reinforcement of Radiation-Crosslinked Networks by Crystallization. *J. Polym. Sci. Polym. Chem. Ed.* **1976**, *14* (2), 441–457. <https://doi.org/10.1002/pol.1976.170140215>.
- (252) Sakurada, I.; Nakajima, A.; Fujiwara, H. Vapor Pressures of Polymer Solutions. II. Vapor Pressure of the Poly(Vinyl Alcohol)-Water System. *J. Polym. Sci.* **1959**, *35* (129), 497–505. <https://doi.org/10.1002/pol.1959.1203512916>.
- (253) Pu, Y.; Cao, S.; Ragauskas, A. J. Application of Quantitative ^{31}P NMR in Biomass Lignin and Biofuel Precursors Characterization. *Energy Environ. Sci.* **2011**, *4* (9), 3154. <https://doi.org/10.1039/c1ee01201k>.
- (254) Argyropoulos, D. Quantitative Phosphorus-31 NMR Analysis of Lignins, a New Tool for the Lignin Chemist. *J. of Wood Chem. & Tech.* **1994**, *14* (1), 45–63. <https://doi.org/10.1080/02773819408003085>.
- (255) Safou-Tchiana, R.; Barhé, T. A.; Soulonganga, P.; Akagah, A. G.; Jeso, B. D. A Comparative Study of the Syringyl, Guaiacyl and Hydroxyl Groups Units Distribution in Some African Tropical Hardwoods' Lignin by Py-GC/MS and Spectroscopic Techniques. **2017**, 12.
- (256) Milotskyi, R.; Szabó, L.; Takahashi, K.; Bliard, C. Chemical Modification of Plasticized Lignins Using Reactive Extrusion. *Front. Chem.* **2019**, *7*, 633. <https://doi.org/10.3389/fchem.2019.00633>.
- (257) Sannigrahi, P.; Pu, Y.; Ragauskas, A. Cellulosic Biorefineries—Unleashing Lignin Opportunities. *Current Opinion in Environmental Sustainability* **2010**, *2* (5–6), 383–393. <https://doi.org/10.1016/j.cosust.2010.09.004>.
- (258) Senyurt, A. F.; Wei, H.; Hoyle, C. E.; Piland, S. G.; Gould, T. E. Ternary Thiol–Ene/Acrylate Photopolymers: Effect of Acrylate Structure on Mechanical Properties. *Macromolecules* **2007**, *40* (14), 4901–4909. <https://doi.org/10.1021/ma062534b>.
- (259) Ye, S.; Cramer, N. B.; Bowman, C. N. Relationship between Glass Transition Temperature and Polymerization Temperature for Cross-Linked Photopolymers. *Macromolecules* **2011**, *44* (3), 490–494. <https://doi.org/10.1021/ma101296j>.
- (260) Jones, B. H.; Alam, T. M.; Lee, S.; Celina, M. C.; Allers, J. P.; Park, S.; Chen, L.; Martinez, E. J.; Unangst, J. L. Curing Behavior, Chain Dynamics, and Microstructure of High Tg Thiol-Acrylate Networks with Systematically Varied Network Heterogeneity. *Polymer* **2020**, *205*, 122783. <https://doi.org/10.1016/j.polymer.2020.122783>.
- (261) Njuguna, D. G.; Schönherr, H. Xanthan Gum Hydrogels as High-Capacity Adsorbents for Dye Removal. *ACS Appl. Polym. Mater.* **2021**, *3* (6), 3142–3152. <https://doi.org/10.1021/acsapm.1c00343>.

- (262) Dai, L.; Ma, M.; Xu, J.; Si, C.; Wang, X.; Liu, Z.; Ni, Y. All-Lignin-Based Hydrogel with Fast PH-Stimuli Responsiveness for Mechanical Switching and Actuation. *Chem. Mater.* **2020**, *32* (10), 4324–4330. <https://doi.org/10.1021/acs.chemmater.0c01198>.
- (263) Saito, T.; Brown, R. H.; Hunt, M. A.; Pickel, D. L.; Pickel, J. M.; Messman, J. M.; Baker, F. S.; Keller, M.; Naskar, A. K. Turning Renewable Resources into Value-Added Polymer: Development of Lignin-Based Thermoplastic. *Green Chem.* **2012**, *14* (12), 3295. <https://doi.org/10.1039/c2gc35933b>.
- (264) Gioia, C.; Lo Re, G.; Lawoko, M.; Berglund, L. Tunable Thermosetting Epoxies Based on Fractionated and Well-Characterized Lignins. *J. Am. Chem. Soc.* **2018**, *140* (11), 4054–4061. <https://doi.org/10.1021/jacs.7b13620>.
- (265) Cao, Q.; Wu, Q.; Dai, L.; Shen, X.; Si, C. A Well-Defined Lignin-Based Filler for Tuning the Mechanical Properties of Polymethyl Methacrylate. *Green Chem.* **2021**, *23* (6), 2329–2335. <https://doi.org/10.1039/D1GC00249J>.
- (266) Cao, Q.; Wu, Q.; Dai, L.; Li, C.; Zhong, Y.; Yu, F.; Li, R.; Si, C. Size-Controlled Lignin Nanoparticles for Tuning the Mechanical Properties of Poly(Vinyl Alcohol). *Industrial Crops and Products* **2021**, *172*, 114012. <https://doi.org/10.1016/j.indcrop.2021.114012>.
- (267) Kulas, D. G.; Thies, M. C.; Shonnard, D. R. Techno-Economic Analysis and Life Cycle Assessment of Waste Lignin Fractionation and Valorization Using the ALPHA Process. *ACS Sustainable Chem. Eng.* **2021**, *9* (15), 5388–5395. <https://doi.org/10.1021/acssuschemeng.1c00267>.
- (268) Bethel, K.; Buck, A.; Tindall, G.; Thies, M. C.; Davis, E. M. Fabrication of Physically Crosslinked Lignin–PVA Hydrogels Containing High Concentrations of Fractionated and Cleaned Lignins. *MRS Communications* **2022**. <https://doi.org/10.1557/s43579-022-00219-z>.
- (269) Gregorich, N.; Ding, J.; Thies, M. C.; Davis, E. M. Novel Composite Hydrogels Containing Fractionated, Purified Lignins for Aqueous-Based Separations. *J. Mater. Chem. A* **2021**, *9* (2), 1025–1038. <https://doi.org/10.1039/D0TA09046H>.
- (270) Jin, J.; Ding, J.; Klett, A.; Thies, M. C.; Ogale, A. A. Carbon Fibers Derived from Fractionated–Solvated Lignin Precursors for Enhanced Mechanical Performance. *ACS Sustainable Chem. Eng.* **2018**, *6* (11), 14135–14142. <https://doi.org/10.1021/acssuschemeng.8b02697>.
- (271) Jawerth, M. E.; Brett, C. J.; Terrier, C.; Larsson, P. T.; Lawoko, M.; Roth, S. V.; Lundmark, S.; Johansson, M. Mechanical and Morphological Properties of Lignin-Based Thermosets. *ACS Appl. Polym. Mater.* **2020**, *2* (2), 668–676. <https://doi.org/10.1021/acsapm.9b01007>.
- (272) Wang, Y.-Y.; Li, M.; Wyman, C. E.; Cai, C. M.; Ragauskas, A. J. Fast Fractionation of Technical Lignins by Organic Cosolvents. *ACS Sustainable Chem. Eng.* **2018**, *6* (5), 6064–6072. <https://doi.org/10.1021/acssuschemeng.7b04546>.
- (273) Chen, J.; Shen, F.; Lyu, G.; Yang, G.; Lu, N.; Hu, C. STRUCTURAL CHARACTERIZATION OF LIGNIN. *Cellulose Chem. Technol.* **2018**, *52* (5–6), 371–380.

- (274) Adjaoud, A.; Dieden, R.; Verge, P. Sustainable Esterification of a Soda Lignin with Phloretic Acid. *Polymers* **2021**, *13* (4), 637. <https://doi.org/10.3390/polym13040637>.
- (275) Yang, F.; Zhao, J.; Koshut, W. J.; Watt, J.; Riboh, J. C.; Gall, K.; Wiley, B. J. A Synthetic Hydrogel Composite with the Mechanical Behavior and Durability of Cartilage. *Adv. Funct. Mater.* **2020**, *30* (36), 2003451. <https://doi.org/10.1002/adfm.202003451>.
- (276) Ye, D.; Chang, C.; Zhang, L. High-Strength and Tough Cellulose Hydrogels Chemically Dual Cross-Linked by Using Low- and High-Molecular-Weight Cross-Linkers. *Biomacromolecules* **2019**, *20* (5), 1989–1995. <https://doi.org/10.1021/acs.biomac.9b00204>.
- (277) Ma, F.; Pang, X.; Tang, B. Alginate/Chondroitin Sulfate Based Hybrid Hydrogel with Different Molecular Weight and Its Capacity to Regulate Chondrocytes Activity. *Carbohydrate Polymers* **2019**, *206*, 229–237. <https://doi.org/10.1016/j.carbpol.2018.10.109>.
- (278) Hájovská, P.; Chytil, M.; Kalina, M. Rheological Study of Albumin and Hyaluronan-Albumin Hydrogels: Effect of Concentration, Ionic Strength, PH and Molecular Weight. *International Journal of Biological Macromolecules* **2020**, *161*, 738–745. <https://doi.org/10.1016/j.ijbiomac.2020.06.063>.
- (279) Hosseini, M. S.; Nabid, M. R. Synthesis of Chemically Cross-Linked Hydrogel Films Based on Basil Seed (*Ocimum Basilicum* L.) Mucilage for Wound Dressing Drug Delivery Applications. *International Journal of Biological Macromolecules* **2020**, *163*, 336–347. <https://doi.org/10.1016/j.ijbiomac.2020.06.252>.
- (280) Münster, L.; Capáková, Z.; Fišera, M.; Kuřitka, I.; Vícha, J. Biocompatible Dialdehyde Cellulose/Poly(Vinyl Alcohol) Hydrogels with Tunable Properties. *Carbohydrate Polymers* **2019**, *218*, 333–342. <https://doi.org/10.1016/j.carbpol.2019.04.091>.
- (281) Petridis, L.; Schulz, R.; Smith, J. C. Simulation Analysis of the Temperature Dependence of Lignin Structure and Dynamics. *J. Am. Chem. Soc.* **2011**, *133* (50), 20277–20287. <https://doi.org/10.1021/ja206839u>.
- (282) Li, J.; Mooney, D. J. Designing Hydrogels for Controlled Drug Delivery. *Nat Rev Mater* **2016**, *1* (12), 16071. <https://doi.org/10.1038/natrevmats.2016.71>.
- (283) Kopač, T.; Ručigaj, A.; Krajnc, M. The Mutual Effect of the Crosslinker and Biopolymer Concentration on the Desired Hydrogel Properties. *International Journal of Biological Macromolecules* **2020**, *159*, 557–569. <https://doi.org/10.1016/j.ijbiomac.2020.05.088>.